Ministry of Higher Education and Scientific Research
وزارة التعليم العالي والبحث العلمي

Badji Mokhtar Annaba University
Université Badji Mokhtar – Annaba
Faculty of Technology
Electromechanical Department

جامعة باجي مختار – عنابـــــــــة
كلية التكنولوجيا
قســـــــم: الكهروميكانيك

Thesis

Presented to obtain the diploma of

Doctorate

Specialty : Industrial maintenance

Field : Electromechanics

By :
BOUDIAF Rabah

Theme :

Fault diagnosis for energy conversion systems

Thesis defended on Nov 13, 2025 ahead the jury composed of:

N°	Full name	Degree	Institution	Quality
01	CHEGHIB Hocine	Prof	Badji Mokhtar -Annaba University	President
02	HADJADJ AOUL Elias	Prof	Badji Mokhtar -Annaba University	Rapporteur
03	OUADA Mehdi	MCA	Badji Mokhtar -Annaba University	Examiner
04	DEFDAF Mabrouk	MCA	Mohamed Boudiaf- M'Sila University	Examiner
05	CHERIF Bilal Djamal Eddine	MCA	Mohamed Boudiaf- M'Sila University	Examiner

Acknowledgements

"In moments of darkness and despair, I am thankful to God for providing me with the inner strength to keep going and the bravery to turn obstacles into opportunities"

I would like to express my gratitude and sincere thanks to Mr. HADJADJ AOUL Elias, professor at Badji-Mokhtar University - Annaba, for the time he dedicated to me throughout this thesis, for his great scientific expertise, for his advice, his always constructive remarks, and his remarkable human qualities.

I would like to express my heartfelt thanks to the members of the defense jury of this doctoral thesis, namely: Mr. CHEGHIB Hocine, Professor at Badji Mokhtar University, Annaba, for agreeing to chair the defense jury.

Mr. OUADA Mehdi, Senior Lecturer -A- at Badji Mokhtar University, Annaba, for agreeing to evaluate this work.

Mr. DEFDAF Mabrouk, Senior Lecturer -A- at the University of Mohamed Boudiaf- M'Sila, for agreeing to evaluate this work.

Mr. CHERIF Bilal Djamal Eddine, Senior Lecturer -A- at the University of Mohamed Boudiaf- M'Sila, for agreeing to evaluate this work.

My heartfelt thanks go to my family, my parents, my friends who have always supported and encouraged me throughout my long studies.

BOUDIAF Rabah.

Dedication

I dedicate this modest work.

To my mother with all my affection.

To my father with all my gratitude.

To my family.

To all my friends.

Abstract

This thesis delves into the complex dynamics of energy conversion systems, with a focused exploration of induction motors due to their crucial role in various industrial applications. Central to this study is the enhancement of fault diagnosis techniques aimed at improving the reliability and efficiency of these motors. Employing advanced signal processing and artificial intelligence, the research innovatively applies Continuous Wavelet Transform to analyse vibration signals for precise identification of fault characteristics in time-frequency representations. This method highlights subtle anomalies often missed by traditional diagnostic approaches. Additionally, the thesis utilises Convolutional Neural Networks, specifically the efficient SqueezeNet architecture, to classify these faults based on features extracted from scalograms. This integration of sophisticated signal processing with cutting-edge machine learning technologies provides robust solutions for the real-time detection and classification of induction motor faults, thereby enhancing system reliability and operational efficiency. By advancing diagnostic capabilities, this research contributes significantly to the sustainability and efficiency of energy conversion systems, positioning these advanced diagnostic technologies at the forefront of industrial applications and maintenance strategies. The findings promise to redefine maintenance protocols and improve the longevity and performance of energy systems, ensuring they meet modern demands for energy efficiency and reliability.

Keywords: Energy Conversion Systems; Induction Motors; Fault Diagnosis; Continuous Wavelet Transform; Convolutional Neural Networks;

الملخص

تغوص هذه الأطروحة في الديناميكيات المعقدة لأنظمة تحويل الطاقة، مع التركيز بشكل خاص على محركات الحث نظرًا لدورها الحاسم في مجموعة متنوعة من التطبيقات الصناعية. يركز هذا البحث بشكل أساسي على تحسين تقنيات تشخيص الأعطال التي تهدف إلى تعزيز الاعتمادية والكفاءة لهذه المحركات. من خلال استخدام معالجة الإشارات المتقدمة والذكاء الاصطناعي، يطبق البحث بشكل مبتكر تحويل الموجة المستمرة لتحليل إشارات الاهتزاز للتعرف بدقة على خصائص الأعطال في التمثيلات الزمنية-الترددية. تسلط هذه الطريقة الضوء على الشذوذات الدقيقة التي غالبًا ما تُغفل بواسطة الطرق التشخيصية التقليدية. بالإضافة إلى ذلك، تستخدم الأطروحة شبكات الخلايا العصبية التلافيفية، وبشكل خاص هندسة سكويز نت الفعالة، لتصنيف هذه الأعطال استنادًا إلى الميزات المستخرجة من السكالوجرامات. يوفر هذا الدمج بين معالجة الإشارات المعقدة وتقنيات التعلم الآلي المتقدمة حلولاً متينة للكشف الفوري وتصنيف أعطال محركات الحث، مما يعزز الاعتمادية وكفاءة التشغيل للنظام. من خلال تقدم القدرات التشخيصية، يساهم هذا البحث بشكل كبير في استدامة وكفاءة أنظمة تحويل الطاقة، مما يجعل هذه التقنيات التشخيصية المتقدمة في طليعة التطبيقات الصناعية واستراتيجيات الصيانة. تَعِد النتائج بإعادة تعريف بروتوكولات الصيانة وتحسين طول العمر وأداء أنظمة الطاقة، مما يضمن استيفاءها للمتطلبات الحديثة لكفاءة الطاقة والاعتمادية.

الكلمات المفتاحية: أنظمة تحويل الطاقة؛ محركات الحث؛ تشخيص الأعطال؛ تحويل الموجة المستمرة؛ شبكات الخلايا العصبية التلافيفية .

Résumé

Cette thèse explore les dynamiques complexes des systèmes de conversion d'énergie, avec une exploration ciblée des moteurs à induction en raison de leur rôle crucial dans diverses applications industrielles. Au cœur de cette étude se trouve l'amélioration des techniques de diagnostic de pannes visant à améliorer la fiabilité et l'efficacité de ces moteurs. En utilisant des techniques avancées de traitement du signal et de l'intelligence artificielle, la recherche applique de manière innovante la Transformée en Ondelettes Continue pour analyser les signaux de vibration afin d'identifier précisément les caractéristiques des pannes dans des représentations temps-fréquence. Cette méthode met en évidence des anomalies subtiles souvent manquées par les approches diagnostiques traditionnelles. De plus, la thèse utilise des Réseaux de Neurones à Convolution, spécifiquement l'architecture SqueezeNet efficace, pour classer ces pannes basées sur les caractéristiques extraites des scalogrammes. Cette intégration de traitement du signal sophistiqué avec des technologies d'apprentissage machine de pointe fournit des solutions robustes pour la détection et la classification en temps réel des pannes des moteurs à induction, améliorant ainsi la fiabilité du système et l'efficacité opérationnelle. En faisant avancer les capacités diagnostiques, cette recherche contribue de manière significative à la durabilité et à l'efficacité des systèmes de conversion d'énergie, positionnant ces technologies diagnostiques avancées à l'avant-garde des applications industrielles et des stratégies de maintenance. Les résultats promettent de redéfinir les protocoles de maintenance et d'améliorer la longévité et la performance des systèmes énergétiques, garantissant qu'ils répondent aux demandes modernes en matière d'efficacité et de fiabilité énergétique.

Mots-clés : Systèmes de Conversion d’Énergie ; Moteurs à Induction ; Diagnostic de Pannes; Transformée en Ondelettes Continue ; Réseaux de Neurones à Convolution

Table of contents

LIST OF FIGURES

LIST OF TABLES

List of symbols

Ω_s	Angular speed
ω	The pulsation of the alternating currents
p	The number of pole pairs
f	The frequency of the alternating current.
ϕ	Phase shift
φ	The flux of the magnetic field
s	The slip
S	Apparent power
PF	The power factor
P_{fS}	The inductive magnetic field causes losses in the iron
P_{em}	Electromagnetic power
P_{JR}	The rotor Joule effect losses
P_m	Mechanical power
P_w	Rotational losses
P_1	Electrical power input in watts $[W]$
V_L	Voltage between two phases in volts $[V]$
I_L	Line current in amperes $[A]$
ϕ	Phase shift angle between current and voltage in degrees [°]
P_{JS}	Joule effect losses in the stator in watts $[W]$
R	Resistance between two phase terminals in ohms [Ω]
I^2	Line current in square amperes $[A_2]$
R'	Resistance of a winding in ohms [Ω]
I^2	Line current in square amperes $[A_2]$
R''	Resistance of a winding in ohms [Ω]
J^2	Current in a winding in square amperes $[A_2]$
T_{em}	Electromagnetic torque
T_u	A useful torque
η	The efficiency
P_u	The useful power
U	The effective supply voltage

Φ_s	The stator flux
f_{brb}	Frequency of the effect of a broken bar
f_{unb}	Frequency of eccentricity or unbalance
f_s	Supply frequency
N_R	Number of rotor notches
f_{sc}	Short circuit frequency,
f_i	The frequency of the inner race
f_o	The frequency of the outer race
n_b	Number of rolling elements
D_b	Rolling element diameter
D_c	Distance from the centre of the rolling elements
θ	Contact angle of the rolling element with the cage

List of abbreviations

PWM	Pulse Width Modulation
MCSA	Motor Current Signature Analysis
FEA	Finite Element Analysis
AI	Artificiel Intelligence
AE	Acoustic Emission
Ku	Kurtosis
SK	Skewness
DFT	Discrete Fourier Transform
CFT	Continuous Fourier Transform
F_r	Rotation Frequency
f_r	The Rotational Frequency of the Bearing
F_b	The Belt Rotation Frequency
HT	The Hilbert Transform
STFT	Sliding Window Fourier Transform
WT	The Wavelet Transform
CWT	The Continuous Wavelet Transform
DWT	The Discrete Wavelet Transform
DT-CWT	The Discrete-Time Continuous Wavelet Transform
RMS	Root Mean Square
SVM	Support Vector Machine
RBF	Radial Basis Function
OVO	One Versus One
OVA	One-Versus-All method
MCSVM	Multi-Class Support Vector Machine
DAG-SVMs	Directed Acyclic Graph Support Vector Machines
ANN	Artificial Neural Network
MLP	Multilayer Perceptrons
PNN	Probabilistic Neural Networks
DL	Deep Learning
CNNs	Convolutional Neural Networks
CL	Convolution Layer

SL	The Subsampling Layer
FL	The Fully Connected Layer
MODWT	Maximal Overlap Discrete Wavelet Transform
ASD	Adjustable Speed Drive
PDM	Predictive Maintenance
LSTM	Long Short-Term Memory Networks
DBNs	Deep Belief Networks
AEs	Autoencoders
LRP	layer-wise Relevance Propagation
TBF	Time-Between-Failure
RUL	Remaining Useful Life
FFT	Fast Fourier Transform
MFPT	Machine Failure Prevention Technology
ORF	Outer-Race-Fault
IRF	Inner-Race-Fault
BPFI	Ball Pass Frequency Inner Race

General Introduction

The role of energy conversion systems is crucial in converting energy, whether it be from natural or artificial sources, into mechanical or electrical power that may be used. There are two main types of energy sources that these devices can collect: renewable and non-renewable. Renewable energy comes from natural, sustainable sources like solar and wind power, which are gaining popularity because of the little damage they do to the environment [1]. Although fossil fuels are efficient and produce a lot of energy, they are finite and have a major impact on environmental deterioration, which is why they are usually associated with non-renewable sources. Induction motors play a crucial role in these energy conversion systems, particularly for renewable energy applications. The operational efficiency of these motors is excellent in transforming mechanical energy into electrical energy or vice versa, and their robustness makes them reliable and long-lasting. Additionally, their cost-effectiveness guarantees that energy conversion systems remain financially viable. Induction motors guarantee a mechanically and economically optimised conversion of raw energy to power, which in turn contributes to efficient power generation [56].

Thanks to developments in industrial maintenance and more advanced industrial automation systems, asynchronous induction motors are now much more capable of handling a wide range of tasks, and they find use in many different industries. These motors have evolved into essential parts of many different types of industrial gear, serving as the brains of anything from basic mechanical drives to elaborate assembly lines. These motors are replacing more conventional direct current motors in many settings due to their low cost, high efficiency, and durability [162], [164].

However, despite their widespread use and inherent advantages, induction motors can face various operational challenges and failures caused by mechanical stresses, electrical anomalies, and environmental factors. The importance of these motors in industrial operations necessitates a focus on their reliability, as any period of inactivity can result in substantial disruptions and financial setbacks. This situation highlights the importance of utilising advanced diagnostic and predictive maintenance techniques to proactively detect potential failures and minimise their effects [39].

This thesis addresses the urgent need for enhanced reliability and operational efficiency in asynchronous induction motors through the development and implementation of innovative

diagnostic techniques. The research focuses on the integration of cutting-edge signal processing algorithms and artificial intelligence to develop a comprehensive diagnostic framework. This framework is designed to detect, diagnose, and predict failures in induction motors, thereby facilitating timely interventions that can prevent costly downtimes and extend the motors' operational life [65].

The manuscript of the thesis is organized into four chapters:

The first chapter provides an overview of energy conversion systems, highlighting both renewable and non-renewable sources. It discusses several types of energy conversions, including mechanical to electrical and chemical to electrical, emphasising their efficiency and scalability. This chapter further digs into the global adoption of these technologies, including a statistical study of their technological impacts and contributions to sustainable energy solutions.

The second chapter's focus shifts to conducting a thorough fault analysis of induction motors. The present study aims to explore various types of faults that could potentially affect these motors, including issues related to the rotor and stator. Additionally, it seeks to examine the diagnostic techniques used for their identification. The present chapter delves into the fundamental principles that underlie these flaws, elucidates the prevalent symptoms that serve as indicators of their existence, and examines the potential ramifications on motor function. We commonly use methodologies to predict the operational efficiency of motors during faults, thereby improving the predictive maintenance capabilities of motor systems.

The third chapter explores advanced signal processing methods and artificial intelligence for diagnosing faults in induction motors. The chapter evaluates the effectiveness of integrating thermal imaging, acoustic signals, and advanced machine learning algorithms like support vector machines (SVM) and neural networks in fault detection and diagnosis.

The fourth and final chapter presents practical applications and experimental setups designed in the laboratory to test the discussed diagnostic techniques on actual induction motors. The experiments include the use of vibration analysis, FFT, DWT, and convolutional neural networks for detailed fault classification. The chapter concludes with a thorough analysis and interpretation of the experimental results, validating the effectiveness of the diagnostic methods.

The thesis concludes with a general summary that synthesizes the key findings from all chapters, highlighting the practical implications of the research and suggesting directions for future research in energy conversion systems and induction motor diagnostic

Chapter 1 State of the Art in Energy Conversion Systems

1.1 Introduction

Energy conversion plays a crucial role in our complex society, serving as the key element that enables the smooth transition of different types of energy to meet our daily power needs. "The Essence of Energy Conversion" establishes the foundation for our investigation, gradually uncovering the underlying essence of energy conversion. We explore the fundamental concepts that drive this revolutionary process, ranging from the intricate movements of electrons to the action of gears and turbines [1].

A systematic understanding is crucial as we embark on our journey into the realm of energy conversion. In "Principles of Classifying Energy Systems," an exploration is conducted into the frameworks and methodologies utilized for the purpose of categorizing the diverse range of energy conversion systems. The Principles of Energy Conversion Mechanisms: Unraveling the Categorization and Comprehension of Mechanical, Electrical, Thermal, and Kinetic Energy. The purpose of this chapter is to establish a foundation for a structured investigation into renewable and non-renewable sources, innovative systems, and, specifically, the induction motor [2].

1.2 Classification of energy conversion systems

Energy conversion systems can be classified in a number of ways, depending on:
The type of energy they convert:

- Mechanical to electrical (e.g., generators),
- Electrical to mechanical (e.g., motors),
- Chemical to electrical (e.g., batteries),
- Thermal to electrical (e.g., solar panels),
- Solar to thermal (e.g., solar thermal collectors),
- Nuclear to electrical (e.g., nuclear power plants) [1].

The source of the energy they convert:

- Renewable energy sources (e.g., solar, wind, hydro, geothermal, biomass) [1], [3],
- Non-renewable energy sources (e.g., fossil fuels, nuclear) [4].

The efficiency of the system:

- High efficiency (e.g., fuel cells),
- Low efficiency (e.g., incandescent light bulbs).

The scale of the system:

- Large-scale (e.g., power plants),
- Small-scale (e.g., solar panels on a rooftop).

The best type of energy conversion system for a particular application will depend on a number of factors, such as the availability of energy sources, the required power output, the cost, and the environmental impact.

1.3 Renewable energy sources

1.3.1 Hydraulic energy

Hydropower is currently the leading renewable source of electricity. The world's installed worldwide in 2004 was estimated at 715 GW, or around 19% of the world's electrical capacity. Nearly 15% of all electricity installed in Europe is of hydroelectric origin [2].

Hydroelectric power generation harnesses the mechanical (kinetic and potential) energy of water. The principle used to generate electricity using the force of water is the same as for water mills of antiquity. Instead of activating a wheel, the force of the water activates a turbine that drives an alternator and produces electricity [1], [2].

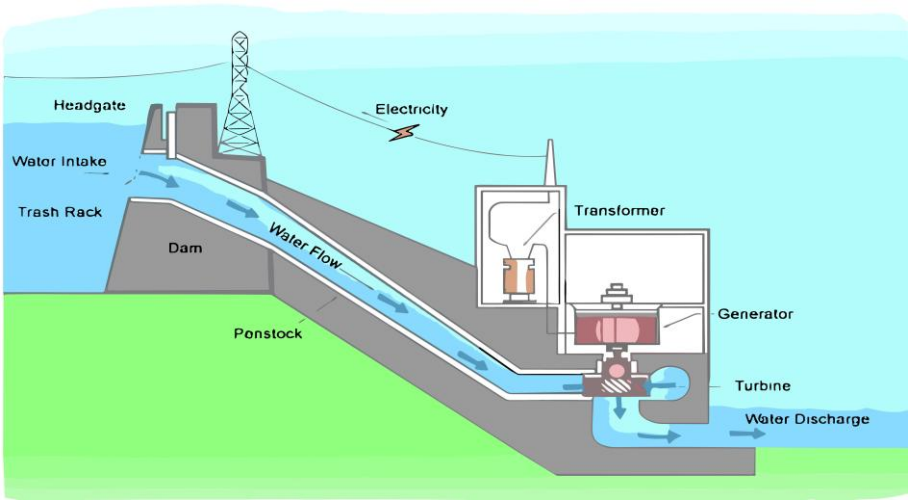

Figure 1.1 *Hydroelectric power system.*

1.3.2 Biomass energy

Biomass is divided into four categories: dry biomass (wood, agricultural waste, etc.), biogas, solid renewable household waste and wet biomass (bioethanol, biodiesel, vegetable oil, etc.). In 2010, biomass accounted for 7.5% of the energy produced.

We should achieve a 15% share by 2024. The heat produced by combustion will heat a tank of water, which then produces steam in the same way as a pressure cooker. This steam is then released at high pressure, enabling a turbine connected to an alternator to turn. It is this alternator that produces the electricity. Biomass power plants are particularly interesting because they can allow electricity to be produced from elements that we no longer need [5].

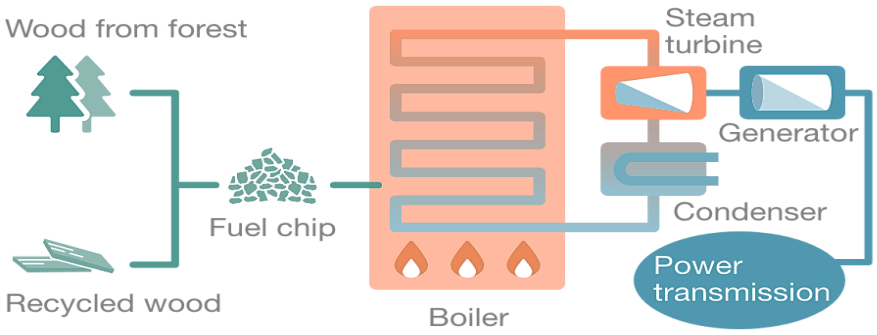

Figure 1.2 *Biomass power generation* [6].

1.3.3 Geothermal energy

Geothermal energy refers to the conversion of heat from the Earth into usable energy. Traditionally, geothermal energy has been divided into three categories based on the accessible temperature level for use:

- High-energy geothermal energy
- Low-energy geothermal energy.
- Very low-energy geothermal energy

To use this underground energy, cold water is sent underground. This cold water heats up. It is then pumped up and brought back to the surface where it is used either to produce electricity in a power station, or directly as hot water in homes (hot water for showers, radiators, etc…) [6].

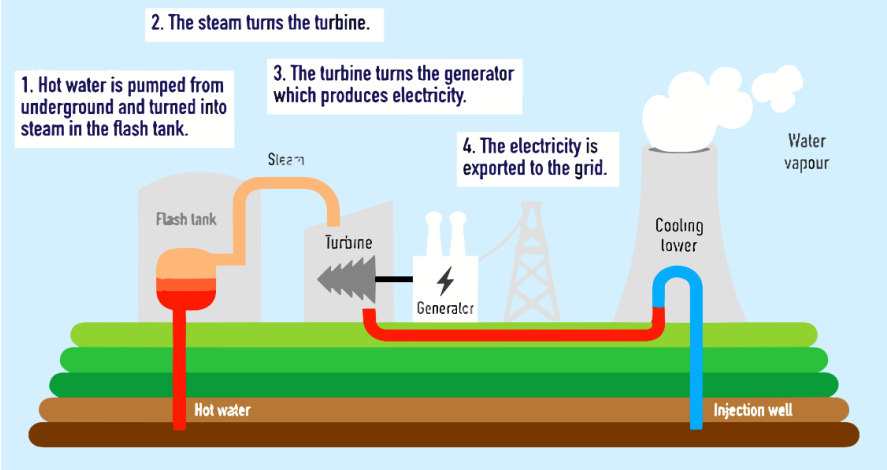

Figure 1.3 *Geothermal power generation* [7].

1.3.4 Solar energy

The sun emits 8400 times the energy humans need annually, making it a practically infinite energy source. An instantaneous power of 1 $\frac{kWp}{m^2}$ is received over the full spectrum, from ultraviolet to infrared. Deserts get more solar energy in 6 hours than humans do in a year. Agriculture, photosynthesis, drying, and heating are the main direct uses of solar energy. This energy is abundant over the Earth's surface, and despite severe attenuation in the atmosphere, a lot reaches the ground. For temperate regions, 1000 $\frac{W}{m^2}$ is typical, and up to 1400 $\frac{W}{m^2}$ is possible with mild dust or water pollution [3].

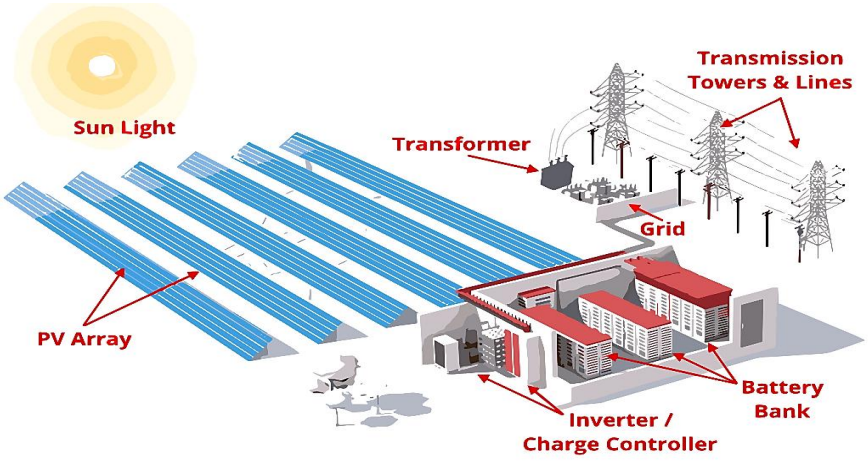

Figure 1.4 *Solar power plant* [8].

1.3.5 Wind energy

The wind resource comes from the movement of air masses, which is indirectly due to the Earth's sunshine. By heating certain areas of the planet and cooling others, a pressure difference is created, and the air masses are constantly on the move. Although this form of energy has been exploited since ancient times, it has long been forgotten, but over the last 30 years or so, it has experienced an unprecedented boom, due in particular to the first oil crises. On a global scale, wind energy has been growing at a rate of 30% a year for the last ten years or so. The machine consists of three blades (generally) carried by a rotor and installed at the top of a vertical mast [1]. This assembly is attached to a nacelle housing a generator. An electric motor steers the upper part so that it always faces into the wind. The blades convert the wind's kinetic energy into mechanical energy. The wind turns the blades at between 10 and 25 revolutions per minute. The speed at which the blades rotate depends on their size. The larger the blades, the slower they turn [9].

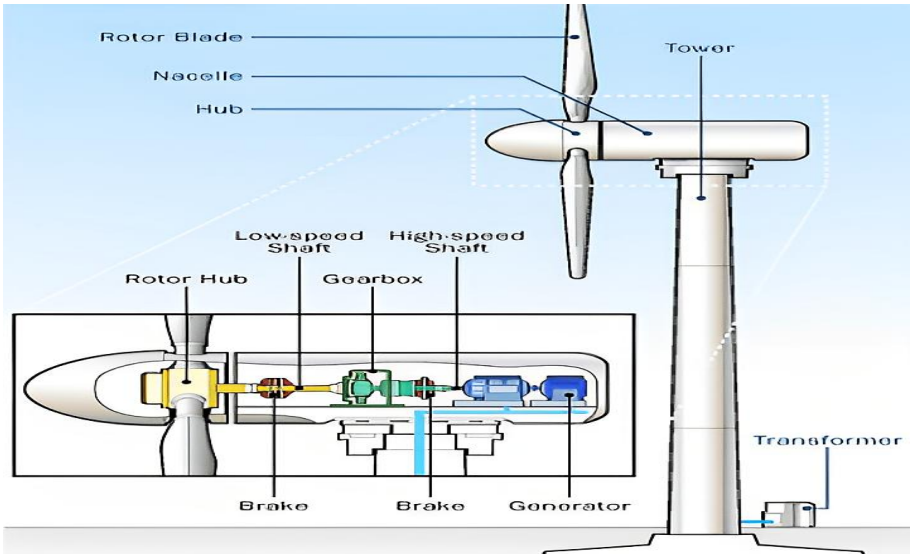

Figure 1.5 *Wind power generation* [10].

1.4 Non-Renewable Energy Sources

1.4.1 Fossil fuel power plants

Fossil fuel power plants have a substantial impact on worldwide electricity production since they use the combustion of coal, oil, or natural gas to generate energy. Coal-fired power plants, which have historically been widespread, create electricity by the combustion of coal, resulting in the production of steam that powers turbines. Although these plants are dependable, they significantly contribute to environmental problems by releasing considerable quantities of carbon dioxide and contaminants. Natural gas power plants use the burning of natural gas to produce electricity, with combined cycle plants providing improved efficiency. These power plants are seen as cleaner options. Oil-fired power plants, while less prevalent, use heavy-fuel oil for the purpose of generating electricity. Although fossil fuel power stations have significant historical significance, they are under growing scrutiny as a result of environmental concerns. This has led to a transition towards cleaner and more sustainable energy sources, such as renewables. The purpose of this shift is to tackle climate change and diminish the

environmental consequences linked to conventional energy production relying on fossil fuels [11].

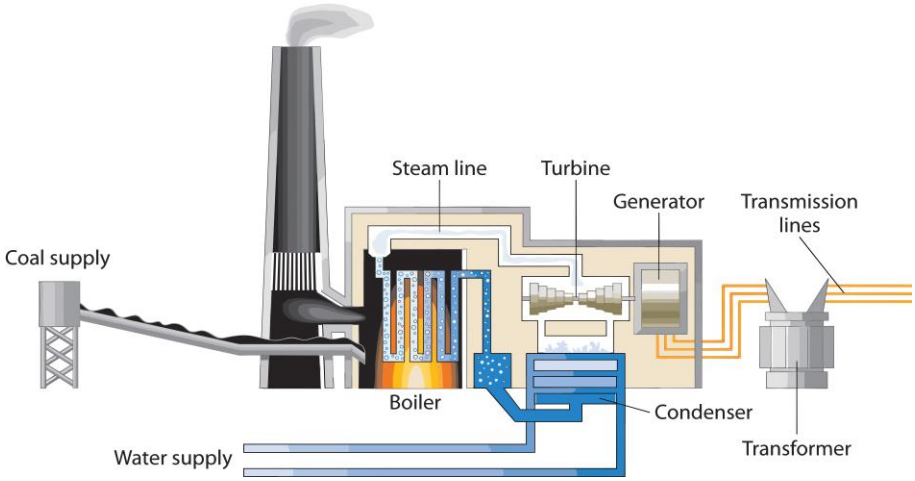

Figure 1.6 *Fossil fuel power plants* [12].

1.4.2 Nuclear power plants

Nuclear power plants employ uranium-235 or plutonium-239 to create large amounts of electricity. In these facilities, nuclear fission in huge atomic nuclei generates thermal energy that powers steam turbines that generate electricity. Nuclear power emits fewer greenhouse gases, making it a greener energy alternative. This device generates enormous power from small amounts of nuclear fuel because of its high energy density. Despite these advantages, nuclear accidents like Chernobyl and Fukushima raise concerns. The dangers of nuclear proliferation, radioactive waste management, and high initial costs should be considered while analysing nuclear power's role in global energy. The complex trade-off between nuclear energy's benefits and risks is being studied to improve safety, reduce environmental impact, and develop new reactor technologies [4].

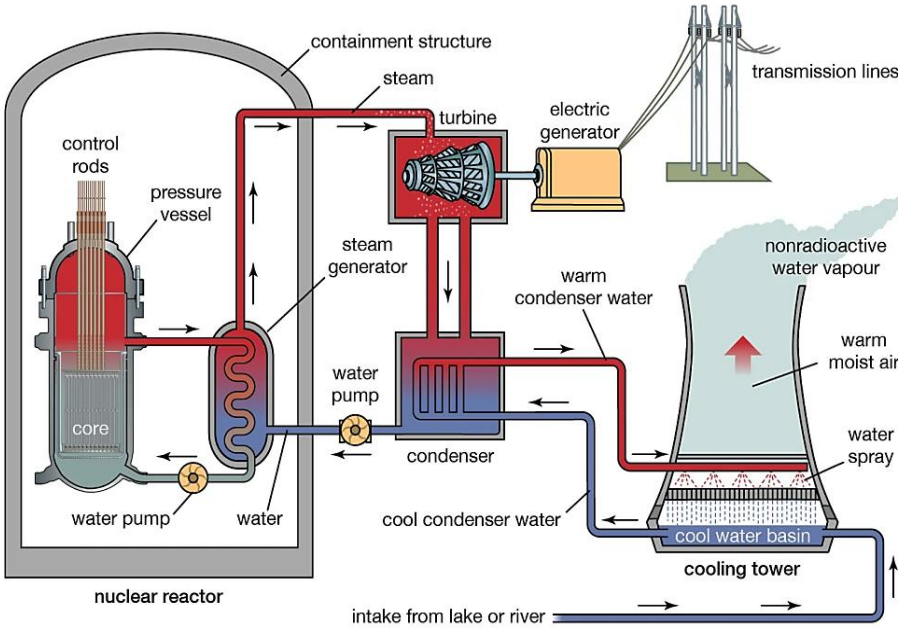

Figure 1.7 *Nuclear power plant* [13].

1.5 Other energy conversion systems

1.5.1 Fuel cells

The fuel cell, a remarkable technological innovation, serves as a device that harnesses the power of chemical reactions to produce electrical energy. In the realm of fuel cell technology, it is a well-established fact that each and every fuel cell is equipped with a pair of electrodes, known as the anode and cathode, respectively. The electrochemical reactions responsible for the generation of electrical energy occur specifically at the electrodes [14].

In the realm of fuel cell technology, it is imperative to acknowledge that each and every fuel cell is equipped with a vital component known as an electrolyte. This electrolyte, acting as a conduit, facilitates the transportation of electrically charged particles from one electrode to its counterpart. Furthermore, an additional crucial element, namely a catalyst, assumes a pivotal role in expediting the reactions transpiring at the electrodes [15].

1.5.2 Batteries

The Significance of Batteries in Modern Society: Powering Essential Devices and Infrastructures The generation of electricity by small devices: an inquiry. Exploring the captivating realm of batteries: An in-depth analysis [16].

The conversion of chemical energy into electrical energy is the primary function of a battery. The composition of a battery typically includes one or multiple electrochemical cells, which encompass an anode serving as the negative terminal, a cathode functioning as the positive terminal, and an electrolyte. The production of electricity is achieved through the collaborative functioning of various components, which engage in a sequence of chemical reactions [17].

The Environmental Impact of Battery Disposal: A Critical Examination of Batteries' Role in Society The release of harmful chemicals into the land and water can be attributed to improper disposal practices. The responsible disposal of batteries is crucial, and this can be achieved by recycling them at designated collection points [16].

The continuous evolution of battery technology is driven by researchers who are dedicated to enhancing energy density, lifespan, and safety through the exploration of novel materials and designs. Advancements in battery technology have the potential to significantly enhance efficiency and sustainability in the future [18].

1.5.3 Electric motors

Electric motors are essential elements of contemporary technology, propelling a wide range of devices, from industrial equipment to domestic appliances. Due to their high efficiency and adaptability, they play a vital role in a wide range of applications. Let us examine the realm of electric motors and investigate the reasons why the induction motor has dominance in several scenario [19], [20].

Multiple variations of electric motors are available, each with distinct merits and drawbacks. Here are a few of the most prevalent:

- Alternating current (AC) motors: These motors are driven by alternating current (AC). In general, AC motors are more efficient and need less maintenance compared to DC motors [19].
- DC motors use direct current (DC) as its power source: These devices provide enhanced speed regulation and are often used in compact appliances [21].

- Brushed motors use brushes to establish contact with the commutator, facilitating the transmission of current to the rotor. Although they are reasonably priced, they want frequent upkeep [21].
- Brushless motors use electronic controllers to remove the need for brushes. Brushless motors exhibit higher efficiency and need lower maintenance compared to brushed motors [22].
- Induction motors are AC motors that operate based on the principle of electromagnetic induction. They are renowned for their simple design, sturdy construction, and exceptional effectiveness [20], [23].
- Synchronous motors are AC motors that maintain a consistent speed that is synced with the AC power source. They have a high level of efficiency and are often used in industrial settings [24], [25].

1.6 The Heart of the Matter: Induction Motors

Induction motors are crucial components in energy conversion systems and are fundamental to a wide range of industrial applications. These electromechanical devices are often used for their high efficiency, durability, and adaptability in turning electrical energy into mechanical power [20], [26].

An induction motor operates via the interaction between a spinning magnetic field and a conducting rotor, resulting in the induction of currents and the generation of torque. Induction motors play a substantial role in the entire energy landscape due to their widespread use in operating pumps, fans, compressors, and other vital gear. The significance of preserving the health and dependability of induction motors has been widely acknowledged by researchers and professionals [27]. This is because the failure of these motors may result in operational interruptions and significant energy inefficiencies.

1.6.1 Induction motor components

From a mechanical standpoint, it is noteworthy to highlight that the three-phase induction motor comprises three discrete components:

- The stator, also referred to as the stationary component, is an integral part of the motor that remains fixed in its position.
- The rotor, also known as the rotating component, is a fundamental element of the motor.
- The bearings, which are integral mechanical components, serve the crucial purpose of providing support to the shaft ends of the rotor. This support enables the rotor to attain a certain level of freedom, allowing it to rotate smoothly and efficiently [19], [20], [23].

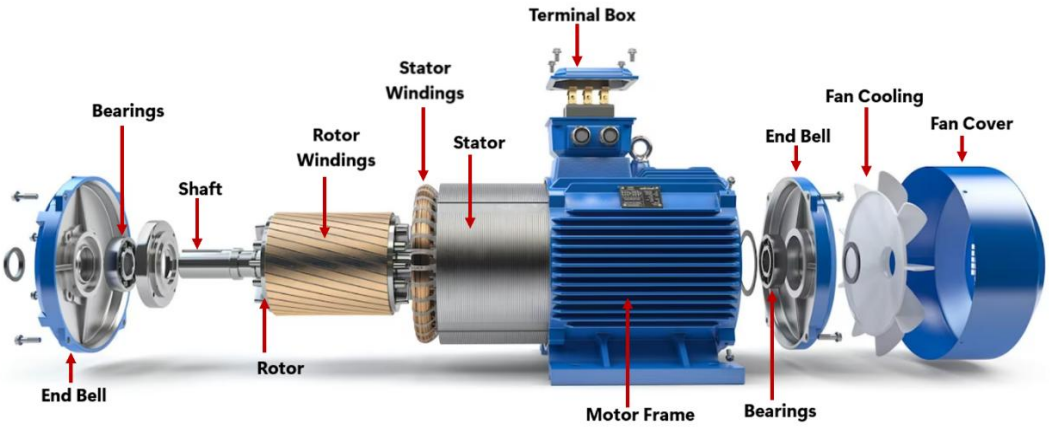

Figure 1.8 *Components of an induction squirrel-cage motor.*

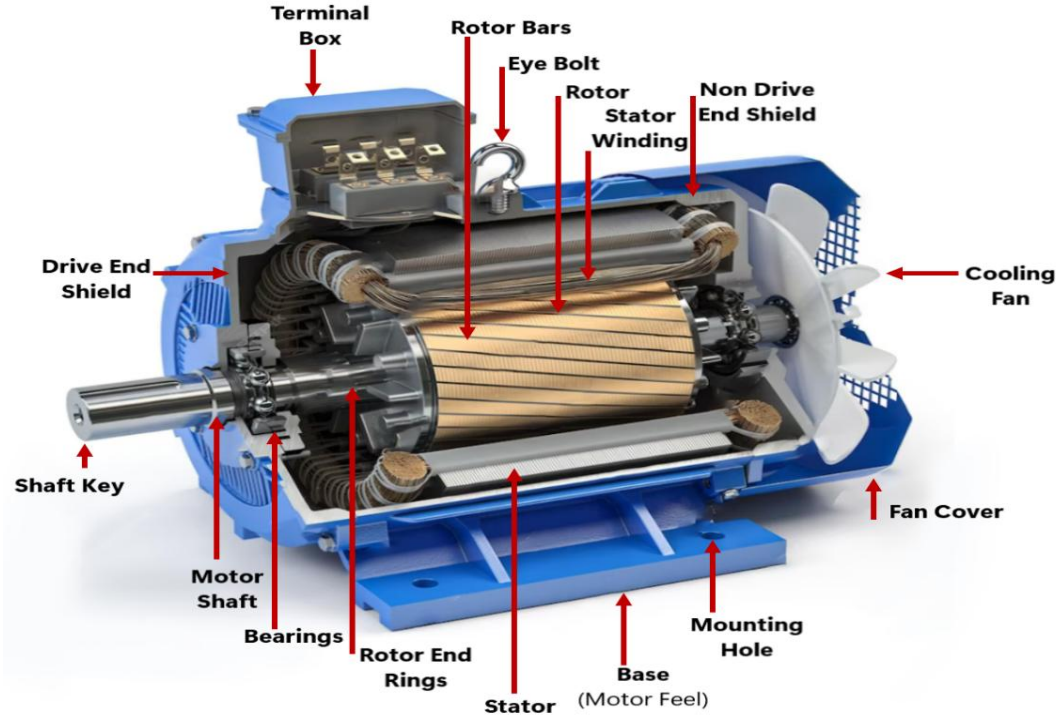

Figure 1.9 *Components of an induction squirrel-cage motor (Cross section).*

1.6.1.1 The stator

The stator of an induction motor is composed of laminated steel sheets that house the stator windings. In the case of small motors, it is observed that the sheets are subjected to a singular cutting process, resulting in a single piece. Conversely, larger machines undergo a division process, wherein the sheets are partitioned into distinct sections. In order to mitigate the effects of eddy currents [28], it is customary to apply a layer of varnish to the surface of the object in question. The stator windings are carefully placed within specifically allocated slots to fulfil their intended function. The windings have the potential to be arranged in various configurations, including but not limited to nested, corrugated, or concentric patterns. The diagram presented in Figure 1.8 provides a visual representation of the various compositions found within the stator of an asynchronous machine [19], [20], [23].

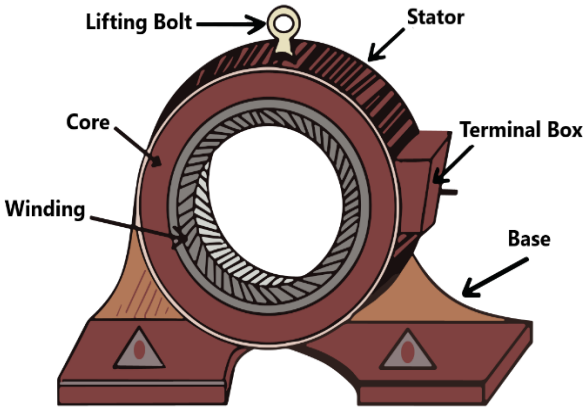

Figure 1.10 *Three-phase IM Stator.*

Figure 1.11 *Real image of Three-phase IM Stator.*

The stator is the inductor of the asynchronous motor: it is in the stator that the field coils described above are located and where the magnetic field is generated. It is connected to the three-phase electrical network. Note that an induction motor stator is manufactured in exactly the same way as a synchronous alternator stator [29]. In the three-phase case, the stator is made up of three phases through which three-phase alternating currents flow, and each phase may involve several pairs of poles. The stator currents create the magnetic field rotating at the angular speed Ω_s, called the synchronous speed, and given by:

$$\Omega_s = \frac{\omega}{p} \qquad 1.1$$

where ω is the pulsation of the alternating currents and p is the number of pole pairs. The synchronous angular velocity Ω_s can be expressed as the number of revolutions per unit of time [30]. Its value ns is then given by the relation:

$$n_s = \frac{\Omega_s}{2\pi} = \frac{f}{p} \qquad 1.2$$

where f is the frequency of the alternating current.

1.6.1.2 The rotor

The rotor of an induction motor is not connected to any power supply [29]. It is made up of short-circuited conductors through which induced currents flow: rotor currents. These conductors can be a set of windings (wound rotor) or a squirrel cage Figure 1.13.

There are two types of rotors for induction motor:

- Wound rotors, which are constructed similarly to the stator winding. The rotor phases are accessible using brush rings on the machine shaft, which enables the utilization of specific characteristics of this rotor type, such as starting, braking, and speed variation of the motor by inserting resistance,

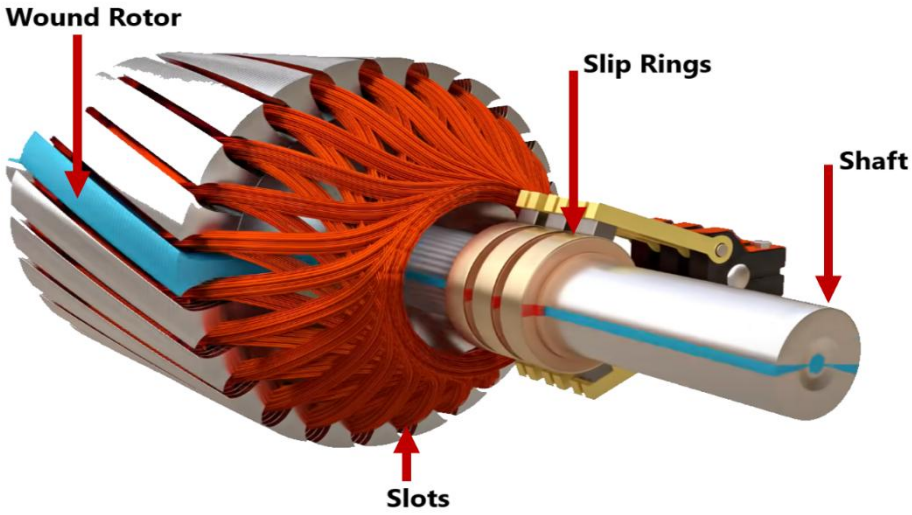

Figure 1.12 *Three-phase IM Wound Rotor* [22].

- Meanwhile, squirrel-cage rotors have windings made up of copper bars for large motors or aluminium bars for low-power motors.

The squirrel cage rotor holds its name from its shape. It is made up of conductive bars, often in aluminium. The ends of these bars are joined by two equally conductive rings. In our practical work, we will study the case of a squirrel-cage induction motor. This is the rotor most commonly used in asynchronous motors [20].

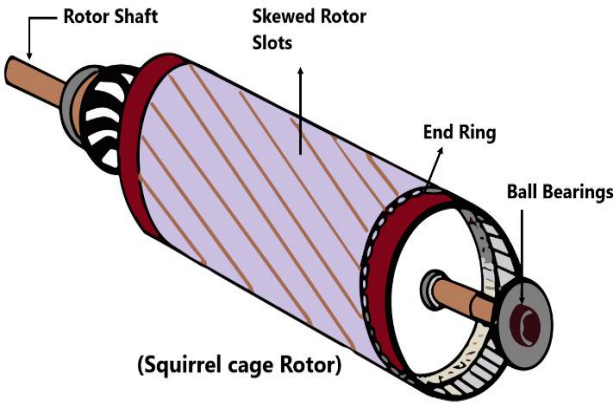

Figure 1.13 *Three-phase IM Squirrel cage Rotor.*

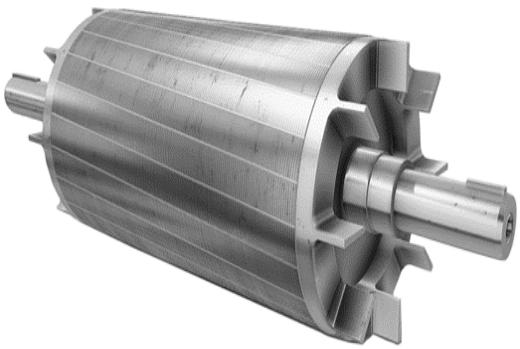

Figure 1.14 *Photo of Three-phase IM Squirrel cage Rotor.*

1.6.1.3 Bearing

The components responsible for supporting and facilitating the rotation of the rotor shaft consist of flanges and rolling element bearings, which are affixed to the shaft through a hot-pressing process. The attachment of cast iron flanges to the stator housing is accomplished through the utilization of either bolts or clamping rods, as depicted in Figure 1.8 The squirrel-cage induction motor is the resultant Product [19], [20], [23].

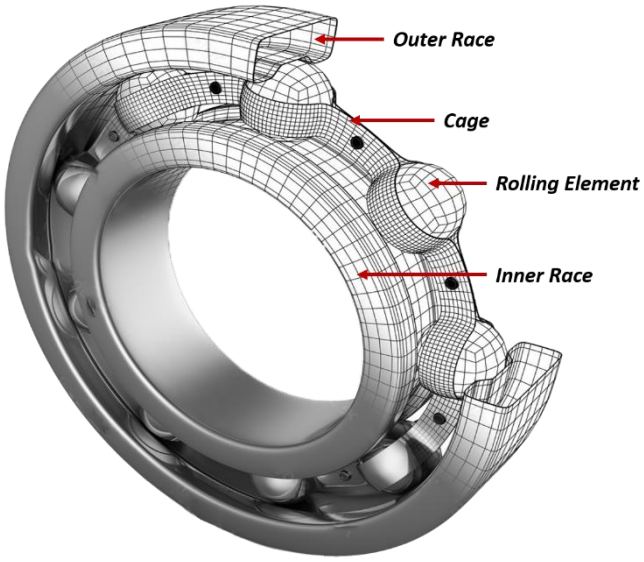

Figure 1.15 *Typical Rolling element Bearing Structure.*

1.6.2 Working principle of induction motor

We saw in the case of a synchronous alternator that a magnetic field rotating on coils offset by 120° degrees creates a balanced three-phase system of electromotive forces. The asynchronous motor uses the opposite phenomenon, the injection of a three-phase current to create a rotating field [31].

Figure 1.16 shows a schematic diagram of how the induction motor works. Sinusoidal currents of pulsation ω are injected into coils offset by 120° degrees in space, by $\frac{2\pi}{3}$ rad, with a phase shift ϕ of $\frac{2\pi}{3}$. This creates three elementary components of the magnetic field, which are themselves sinusoidal and of pulsation ω. The alternating variation of these three components creates a rotating magnetic field within the coils. The speed of rotation of this magnetic field is called the synchronism speed. It is a function of ω and the number of pairs of coils used to create the field [19], [23].

If a conductor is placed in the middle of the coils, it will be subject to variations in the flux φ of the magnetic field, since it is passing through a rotating, and therefore variable.

Under the effect of Faraday's law [32], an induced electromotive force then appears, creating induced currents. Note that this electromotive force can only exist if:

$$\frac{d\phi}{dt} \neq 0 \qquad 1.3$$

These currents are responsible for the appearance of a pair of Laplace forces which tend to set the conductor in motion in order to oppose the variation in flux, according to Lenz's law: the conductor then starts to turn in an attempt to follow the magnetic field [19], [23].

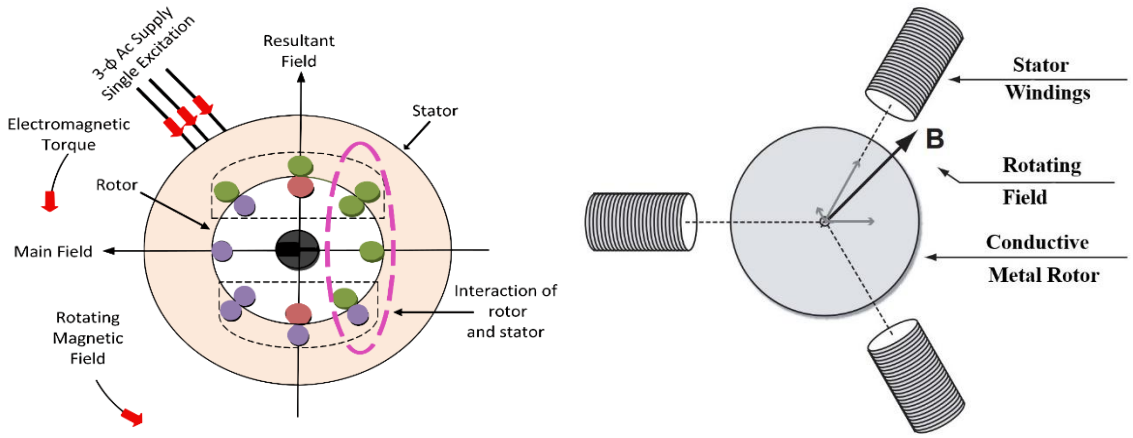

Figure 1.16 *Working principal of induction motor* [20].

1.6.2.1 Slip

The motor is said to be asynchronous because it is impossible for the rotor to reach the same speed as the stator field: the rotor always lags behind the stator currents. This is intuitively understandable, as the rotating field must first give rise to the rotor currents before interacting with them. If the rotor were able to rotate at the same speed as the rotating magnetic field, all the conductors making up the rotor would be immersed in a magnetic flux which, for them, would become constant: Faraday's relation (**1.1**) would no longer be verified. As a result, the rotor currents would not be induced and could not produce torque: the motor's rotor would no longer be driven [19], [23].

The difference in speed between the rotor and the stator field is called the slip [33], and we will refer to it as s. Slip depends on the motor's mechanical load: the more torque the motor has to deliver, the more the rotor will slip. It is conceivable that a rotor with a higher load would have more difficulty following the magnetic field. The slip is defined by the synchronism and rotor speeds according to the relationship:

$$s = \frac{\Omega_s - \Omega}{\Omega_s} = \frac{n_s - n}{n_s} \qquad 1.4$$

1.6.2.2 Operation at empty

The concept of no-load operation refers to the condition in which a device or system operates without any external load or resistance [34].

The no-load regime is when the engine is not carrying a load. As a result, there is no slip and the motor rotates at synchronous speed.

At no load: $s \approx 0$ so $n_m = n_{sync}$ and $T_u = T_0$

The power factor under no-load has a very low value ($PF < 0.2$), yet the current drawn stays at a high level (P: active power is modest and S: apparent power is big). The phenomenon described is often known as reactive or magnetizing current, which is used to generate the magnetic field.

1.6.2.3 On-load operation

The present state of the motor is one where it is loaded, specifically referring to the condition that the motor shaft imparts motion to a resistive load that acts in opposition to the rotational movement of the rotor [34]. In steady state: $T_u = T_l$

1.6.2.4 The Mechanical Characteristic: $T_u = f(n')$

The operating point is located at the intersection of the motor's mechanical characteristic and the curve characterising the load's resistive torque. the curve that characterises the load's resistive torque. The mechanical characteristic of the motor in is a straight line. Two points are all you need to draw it. The first is given by the study of a specific operating case, the second is deduced from the no-load test. In this test, the useful torque is zero, and is associated with a rotation frequency considered to be equal to the synchronism frequency [20], [35].

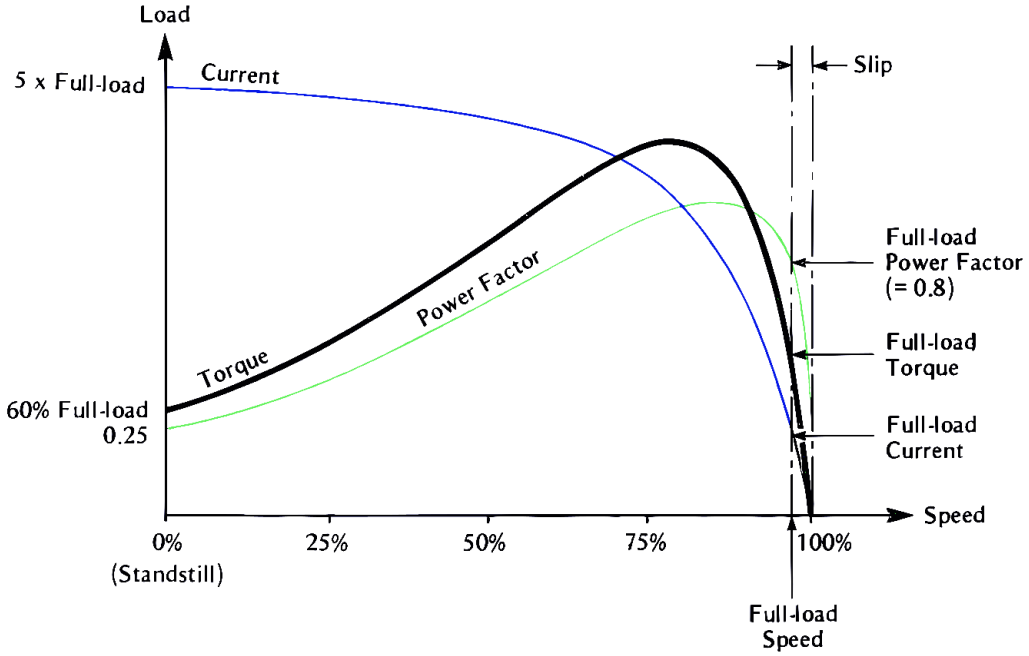

Figure 1.17 *The speed-torque curve of an induction motor* [36].

1.6.3 Power Stages in an Induction Motor

Induction motors convert electrical energy to mechanical energy in phases. Each step has energy losses, lowering system efficiency. Understanding these phases and losses is crucial to optimizing motor performance and reducing energy usage [37].

The balance of power and losses in an induction motor is shown in Figure 1.18. The induction motor absorbs active three-phase electrical power P_1 from the mains.

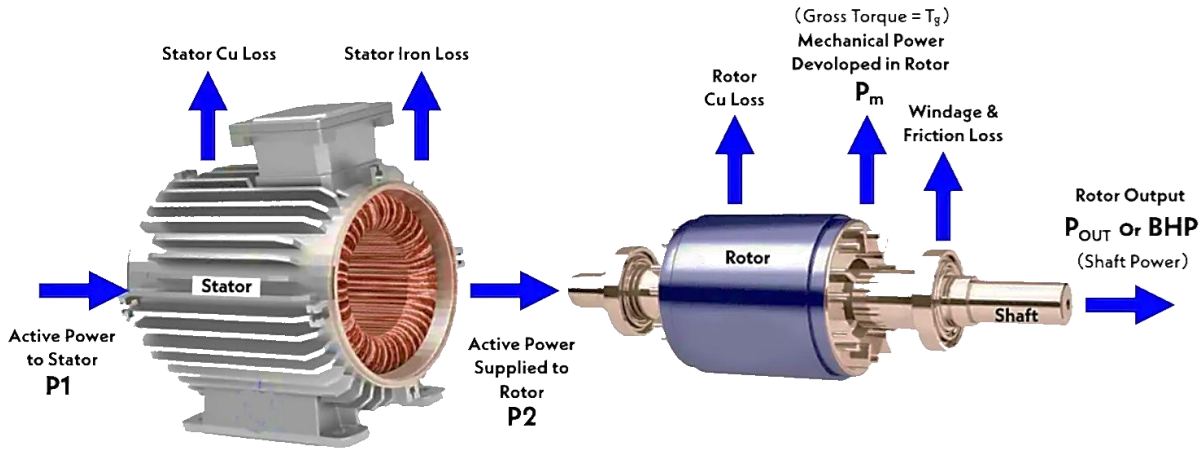

Figure 1.18 *Power Stages and losses in Induction motor* [37].

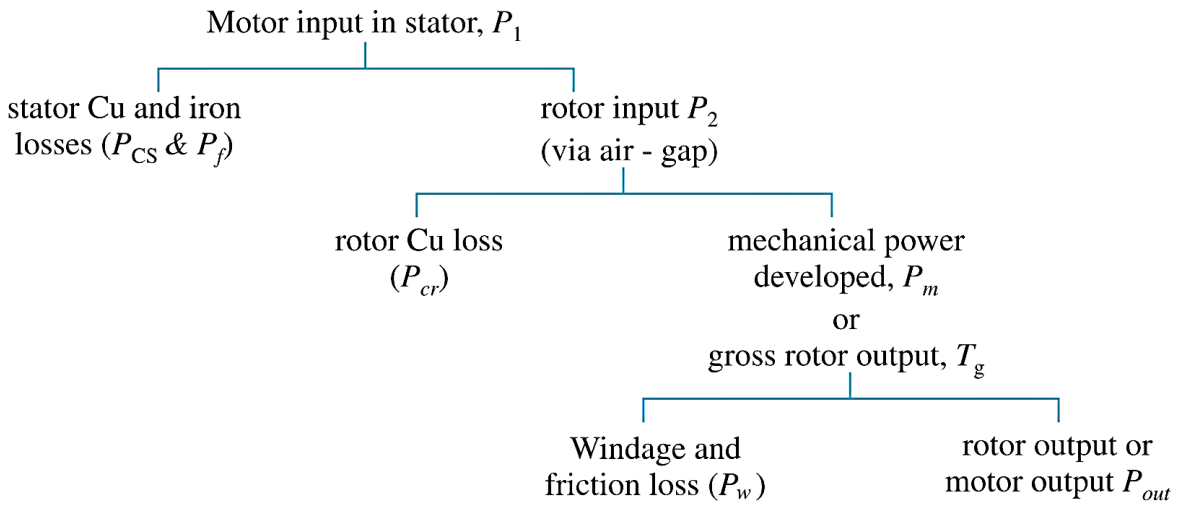

Figure 1.19 *Diagram of Power Stages in Induction motor* [38].

The part P_{JS} of this power (P_1) is dissipated by the Joule effect in the stator windings. Subsequently, the inductive magnetic field causes losses in the iron P_{fS}, by hysteresis and eddy current. The rest of the power P_2 is transmitted to the rotor through the air gap. Most of this power is then used to produce electromagnetic power P_{em}, while the presence of an induced current in the rotor causes Joule effect losses P_{JR} [19], [39].

The electromagnetic power supplied by the stator is responsible for setting the rotor in motion, which produces the useful mechanical power P_m which is then transmitted to the load via a transmission shaft or a drive belt. However, as the rotor moves, some of the power is lost through various friction mechanisms, known as rotational losses P_w [19].

In the following, we give the various relationships for calculating the losses and powers involved in the asynchronous motor, where these can be calculated.

1.6.3.1 Input Power (P_1)

The power absorbed by an induction motor is active electrical power. When the motor is connected to a three-phase network, P_1 satisfies the relationship:

$$P_1 = \sqrt{3}.V_L.I_L.cos\,\phi \quad 1.5$$

P_1 : Electrical power input in watts, $[W]$
V_L : Voltage between two phases in volts, $[V]$
I_L : Line current in amperes, $[A]$
ϕ : Phase shift angle between current and voltage in degrees. [°]

Part of the absorbed power is dissipated in stator joule losses (P_{JS}) and iron losses in the stator (P_{fS}), the rest of the transmitted power (P_2) passes through the air gap and is therefore electromagnetic power (P_{em}) [19], [23], [39].

1.6.3.1.1 Stator joule losses (P_{JS})

- **Case 1: The resistance R is given between two phase terminals**

$$P_{JS} = \frac{3}{2}R.I^2 \quad 1.6$$

P_{JS} : Joule effect losses in the stator in watts. $[W]$
R : Resistance **between two phase terminals** in ohms. [Ω]
I^2 : Line current in square amperes. $[A_2]$

- **2nd case: Resistance R' is that of a winding**
  a-Star connection: the resistance between two terminals R is related to the resistance of each winding r by the relationship: $R' = 2r$

$$P_{JS} = \frac{3}{2}R'.I^2 \quad 1.7$$

P_{JS} : Joule effect losses in the stator in watts. $[W]$
R' : Resistance of a winding in ohms [Ω]
I^2 : Line current in square amperes. $[A_2]$

b- Triangular coupling: this relationship becomes: $R'' = \frac{2}{3}r$

$$P_{JS} = \frac{3}{2}R''.J^2 \quad 1.8$$

P_{JS} : Joule effect losses in the stator in watts. $[W]$
R'' : Resistance of a winding in ohms [Ω]
J^2 : Current in a winding in square amperes. $[A_2]$

1.6.3.1.2 Losses iron

Iron losses are a function of magnetic flux. They therefore only depend on the supply voltage and the frequency of the stator currents. Under operating conditions, these quantities do not vary and, consequently, iron losses can be considered **constant whatever the** motor **load** [19], [23], [37].

In practice, iron losses are measured during a **no-load test**, at the same time as rotational losses.

1.6.3.1.3 The power transmitted in the air gap P_2

The power transmitted to the rotor through the air gap P_2 is the part of the power absorbed that is not lost in the stator windings and in the iron. Also:

$$P_2 = P_1 - (P_{JS} + P_{fS}) \quad 1.9$$

1.6.3.1.4 Rotor Joule losses P_{JR}

Joule losses at the rotor are a function of the power transmitted to it. It can also be shown that they are also a function of slip. The quantities P_{JR} and P_2 are linked by the relationship:

$$P_{JR} = s - P_2 \quad 1.10$$

1.6.3.1.5 Electromagnetic power P_{em} and electromagnetic torque T_{em}

The electromagnetic power P_{em} transmitted to the rotor is equal to:

$$P_{em} = P_2 - P_{JR} = (1 - s) - P_2 \quad 1.11$$

The rotor, rotating at speed Ω , is subjected to an electromagnetic torque T_{em} and therefore receives an electromagnetic power equal to:

$$P_{em} = T_{em} - \Omega \quad 1.12$$

By injecting equation (1.11) into (1.12), we can show that:

$$T_{em} = \frac{P_{em}}{\Omega} = \frac{P_2}{\Omega_s} \quad 1.13$$

1.6.3.1.6 Mechanical losses rotational

Rotational losses depend solely on motor speed. As we saw earlier, the motor speed varies relatively little with the load, the stall speed being relatively close to the synchronous speed. In an asynchronous motor, the rotational losses will therefore be considered to be **constant**, and determined using a **no-load test** [19], [23], [37].

1.6.3.1.7 Mechanical power and useful torque P_u and T_u

The rotor develops a useful torque T_u at speed Ω. It then delivers the useful power P_u such that:

$$P_u = T_u . \Omega \quad 1.14$$

1.6.3.1.8 Performance

The efficiency η of the induction motor is the ratio between the mechanical power it supplies and the electrical power it absorbs, so that:

$$\eta = \frac{P_u}{P_1} \quad 1.15$$

Using the loss chain, we can also write:

$$\eta = \frac{P_1 - losses}{P_1} = \frac{P_1 - P_{JS} - P_{fS} - P_{JR}}{P_1} \quad 1.16$$

1.6.4 Advantages and disadvantages of the Induction motor

Induction motor have many advantages and some disadvantages:

Table 1.1 *Advantages and disadvantages of IM.*

Advantages	Disadvantages
– Low purchase cost – Low maintenance costs – Simple structure – Robust and easy to build	– Variable speed (variable speed drive required) – The speed depends on the load

1.6.5 Induction Motor Carcass, Shaft, and Bearing Design and Operation

The carcass functions as a structural framework, serving as a covering and offering defence against the surrounding external conditions. The shaft serves as a gearbox component. The structure consists of a centre section that provides support for the rotor body, as well as a shaft extension that is connected to one side of a coupling [19].

Typically, it is constructed from cast or forged steel. The dimensions of the object are determined by several forces, such as centrifugal force, radial magnetic attraction, and tangential forces caused by centrifugal forces. Additionally, torsional forces, such as electromagnetic torque during both permanent and temporary operation, also play a role in determining the dimensions. It is supported by one or several bearings. These bearings provide support to the rotor and guarantee unhindered rotation. The second bearing is designed to allow for the thermal expansion of the shaft [20], [23].

To prevent the occurrence of currents in the shaft caused by imbalances in the reluctances of the magnetic circuit, one of the bearings is equipped with electrical insulation [40]. Typically, they are roller bearings designed for machines with low to moderate power. Many machines are equipped with a converter to both regulate the speed of electric motors and convert energy [41]. Static converters are often used with electrical devices in many industrial operations, such as pumping and lifting.

This enables the provision of variable-frequency voltages and currents to the motors, which are used for control purposes.

1.6.6 Induction motor power supply constitution

In the case of asynchronous motors, the speed of rotation of the rotor depends on the stator frequency f_s (frequency of the motor supply voltage) and the frequency of the rotor currents (i.e., the load). A static converter is used to vary the amplitude and frequency of the supply voltage and, therefore, the speed of the machine.

Several control strategies can be used. Scalar controls [21] a simplified version of which ensures a constant $\frac{U}{f_s}$ ratio (with f_s, the frequency of the stator currents, and U, the effective supply voltage), and flux vector controls [21], [42]. The following diagram shows the general structure used for speed variation.

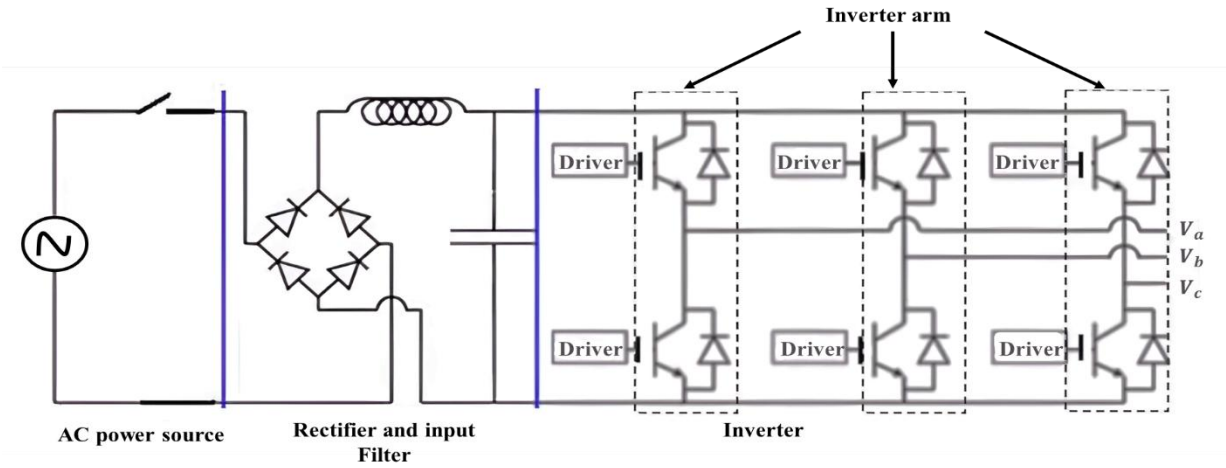

Figure 1.20 *Motor power supply structure for variable speed control* [43].

The various components making up the power supply chain are:

- **AC power source**

The AC electrical source is generally obtained from the three-phase electrical network.

- **Rectifier**

Transforms AC voltage into DC voltage.

- **Filtering**

It eliminates ripple phenomena in the voltage at the output of the rectifier. This filter, combined with the rectifier bridge, forms a DC voltage source used to supply the DC bus at the inverter input [42].

- **Inverter**

It transforms a DC voltage into an AC voltage of variable amplitude and frequency. In our application, the ratio $\frac{U}{f_s}$ is maintained constant because we want to maintain the motor's steady-state performance, i.e., have maximum torque available at all times, whatever the speed. To achieve this, the stator flux Φ_s must be kept constant, which means that, as a first approximation, $\frac{U}{f_s}$ must be kept constant up to the rated speed [36], [41]. It generates a succession of voltage pulses, achieved via switch control. Figure 1.20 shows an inverter with three half-bridges (or arms), which is the most common structure because it offers an interesting compromise between cost and performance [36], [42].

The most common control for this type of inverter is pulse width modulation (PWM). Pulse width modulation is a chopping technique used to generate arbitrary current shapes. In our case, they will be quasi-sinusoidal. The inverter will generate variable-frequency voltages or currents rich in harmonics [36], [41]. These cause additional losses (iron and joule) on top of the 'normal' losses we would have if the voltages and currents were sinusoidal. The increased

temperature rise due to these additional losses and the voltage stresses are likely to shorten the motor's life [31], [37].

All these constraints increase the risk of failure. Many faults can occur in electric drives. They fall into three categories: faults occurring in the electrical machine (bearing faults, bar breakage), those occurring in the drive chain (load fault, coupling), and those occurring in the power supply (power supply imbalance, converter fault) [44]. These faults are linked because they can interact. In the following sections, we will look at the various faults affecting the converter and the motor [45], [46].

1.7 Conclusion

In this foundational chapter, we delved into the essence of energy conversion, recognising its pivotal role in meeting our daily power needs. The exploration began with an understanding of the fundamental concepts driving this revolutionary process, encompassing the intricate movements of electrons as well as the actions of gears and turbines.

A systematic approach was then employed to classify energy conversion systems, providing a comprehensive framework for our investigation. The chapter outlined the principles guiding the categorization and comprehension of mechanical, electrical, thermal, and kinetic energy systems. This categorization is essential for navigating the diverse landscape of energy sources and conversion mechanisms.

Renewable and non-renewable energy sources were explored, highlighting the significance of sustainability in our energy landscape. Furthermore, we acknowledged the existence of other innovative energy conversion systems beyond traditional classifications.

The focal point of our attention in this chapter was the induction motor. Recognized as the heart of the matter, the induction motor holds a crucial role in energy conversion systems. As we transition to the next chapter, "Fault Analysis of Induction Motor," we aim to deepen our understanding of this vital component and unravel the intricacies of potential issues and faults that may impact its performance. This exploration is essential for ensuring the reliability and efficiency of energy conversion systems, laying the groundwork for a comprehensive study in the subsequent chapters.

Chapter 2 Fault Analysis of induction motor

2.1 Introduction

Induction motors, known for their sturdy construction and unmatched adaptability, are the hardworking mainstays of contemporary industrial operations. They provide energy to several machinery, including conveyor belts, pumps, compressors, and various other essential equipment. Nevertheless, like to any mechanical apparatus, these relentless labourers are susceptible to malfunctions. Malfunctions may have wide-ranging repercussions, including decreased output, expensive periods of inactivity, safety risks, and possible harm to linked machinery. Fault analysis is essential for guaranteeing the efficient and dependable functioning of induction motors [23], [47].

This chapter explores the important field of fault analysis, emphasising its tremendous importance in protecting the essential gear that powers our industries. In this analysis, we will examine the several categories of malfunctions that may afflict induction motors, their effects on both operational efficiency and safety, and the necessary methods used to effectively identify and analyse them. By comprehending the language of motor faults, we acquire the ability to react prior to their detrimental impact on operations, guaranteeing prolonged lifespans, enhanced performance, and a more secure industrial environment.

2.2 Faults: Origins and Consequences

Through the examination of the structure and functioning of an asynchronous motor, it becomes apparent that the components most susceptible to malfunctions are the bearings, stator windings, rotor bars, and shaft. Faults arise due to the lack of homogeneity in the air gap between the inner surface of the stator and the outer surface of the rotor. Various studies have been conducted to examine the dependability, efficiency, and occurrence of defects in motors [48], [49].

The statistical research on motor defects is mentioned in references [50], [51]. One aspect of this research was determining the proportion of certain defects in relation to the overall number of faults.

An initial investigation was conducted on several motors used in industrial settings. Table 2.1 displays the prevailing flaws and their corresponding statistical frequencies. The second investigation is conducted using the motor manufacturer's report as its foundation. According to their study, the primary malfunctions of the motor are listed in Table 2.1 [50], [52].

Table 2.1 *Details on motor problems and failures* [44].

Classification of defects	Number of problems/ failures				
	Induction motor	Synchronous motor	Wound-rotor	motor DC	All total motors
Bearing	152	2	10	2	166
Winding	75	16	6	-	97
Brushes or slip ring	-	6	8	2	16
Shaft	19	-	-	-	19
Rotor	8	1	4	-	13
External device	10	7	1	-	18
An additional	40	9	-	2	51

2.2.1 Main faults of induction motors

Induction machines play an important role in all industrial sectors. widely used because of its robustness and low purchase and maintenance costs [23].

Despite all these qualities, it can be affected by a certain number of failures. These have various origins, whether electrical, mechanical, or even magnetic.

Induction motor faults can be summarised in the following diagram:

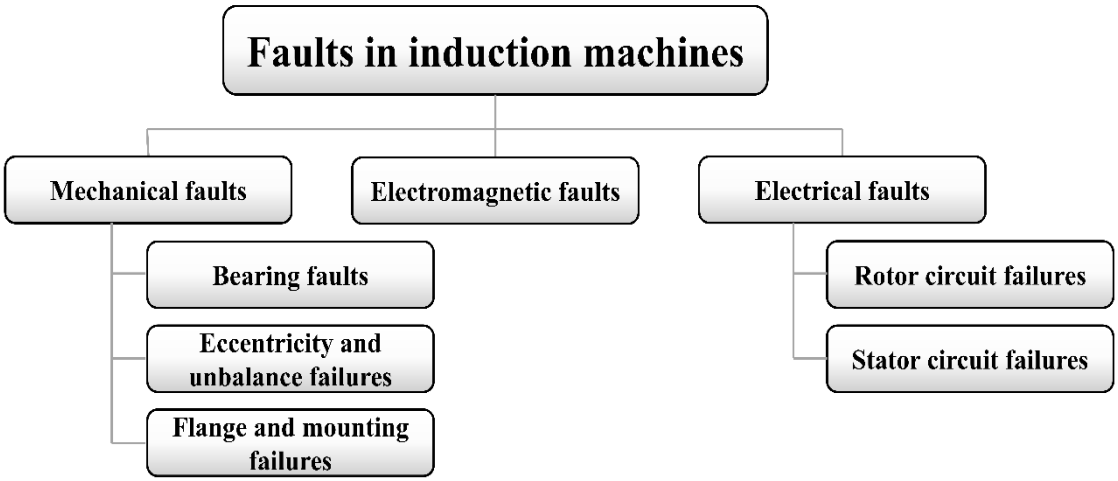

Figure 2.1 *diagram summarising induction machine failure types* [53].

2.2.1.1 Causes of defects

The asynchronous machine can have different types of faults, which can be classified as follows [54], [55]:

- Stator faults result from a fault in one or more stator phase windings or from poor connection of the stator windings.
- Rotor faults: breakage of rotor cage bars; breakage of short-circuit ring junctions.
- Static and/or dynamic irregularities in the air gap can result in a friction band between the rotor and stator, causing serious damage to the stator and its windings.
- Defects in motor bearings.

These multiple failures of the asynchronous machine can be predictable or untimely, mechanical or electrical and their causes are very varied.

For the purposes of a summary presentation, these faults can be classified into two main families. Figures (2.2) and (2.3) group these causes together [24], [25], [56].

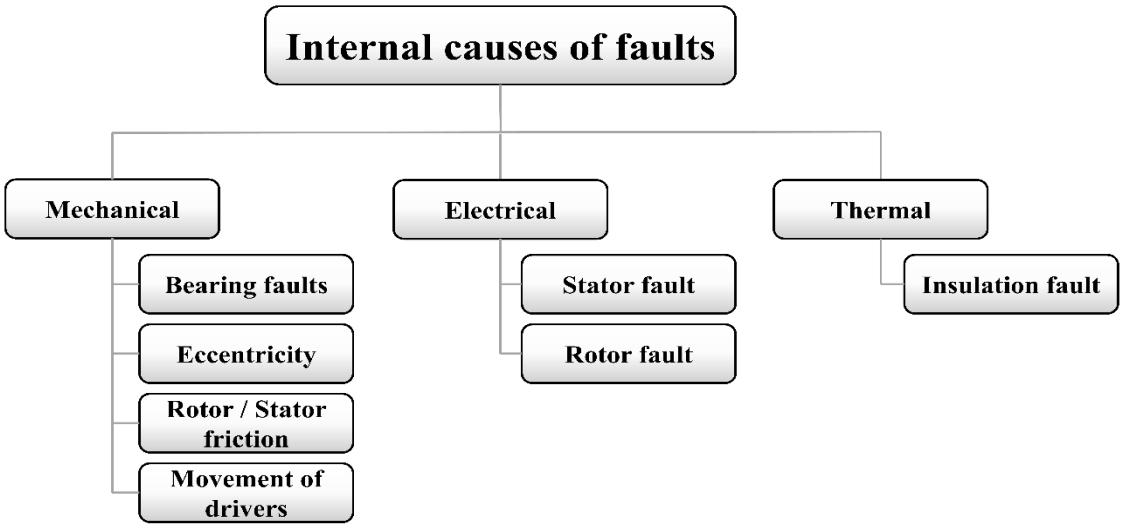

Figure 2.2 *Internal causes of faults in the three-phase asynchronous machine* [53].

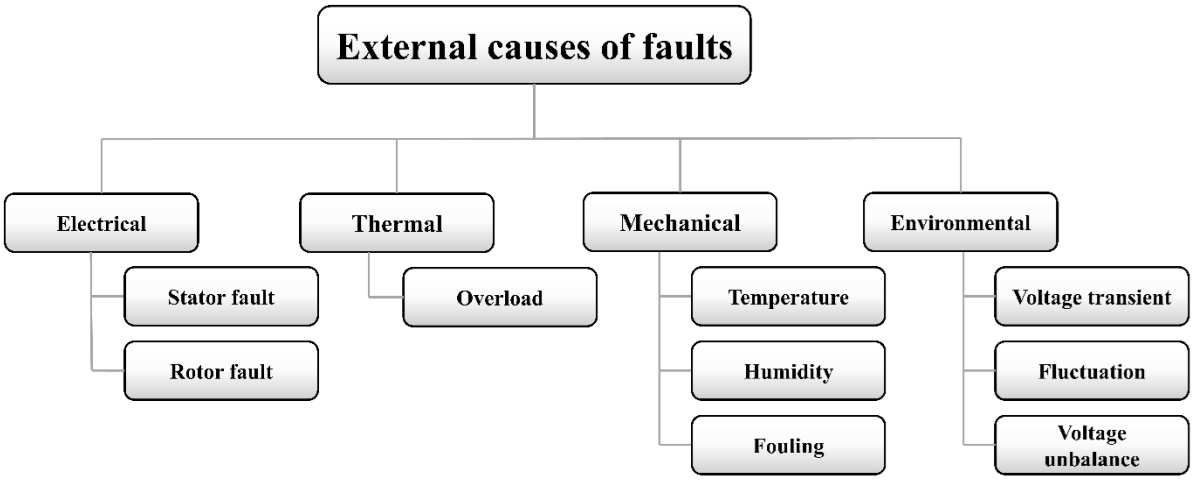

Figure 2.3 *External causes of faults in the three-phase asynchronous machine* [53].

2.2.1.2 Statistical studies of faults in medium-power three-phase induction motors

Over the last few decades, a series of statistical studies have been carried out on the breakdowns that can be attributed to induction machines.

In 1988, a German industrial systems insurance company [39] classified the breakdowns of medium-power induction machines (from 50 KW to 200 KW) as follows:

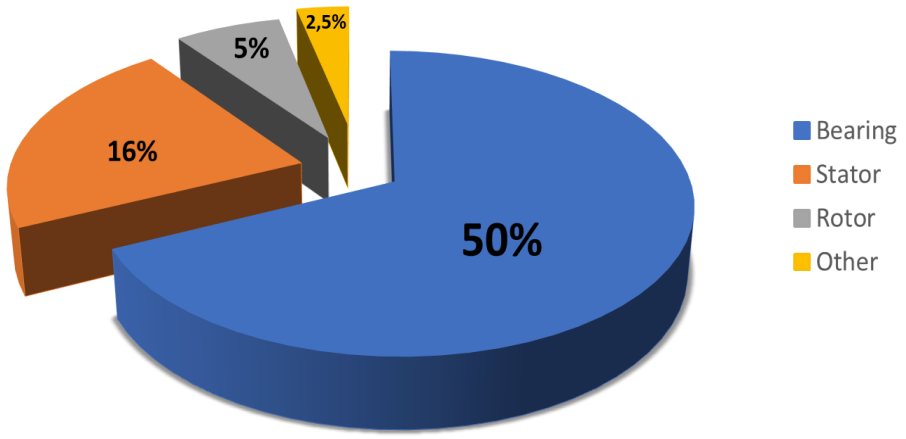

Figure 2.4 *Breakdown of failures according to the German industrial systems insurance company for medium-power motors* [39].

The same study shows that between 1973 and 1988; stator failures fell from 78% to 60% and rotor failures from 12% to 22%. This variation is reflected in the increased use of insulation during this period. The breakdown of the various faults is as follows:

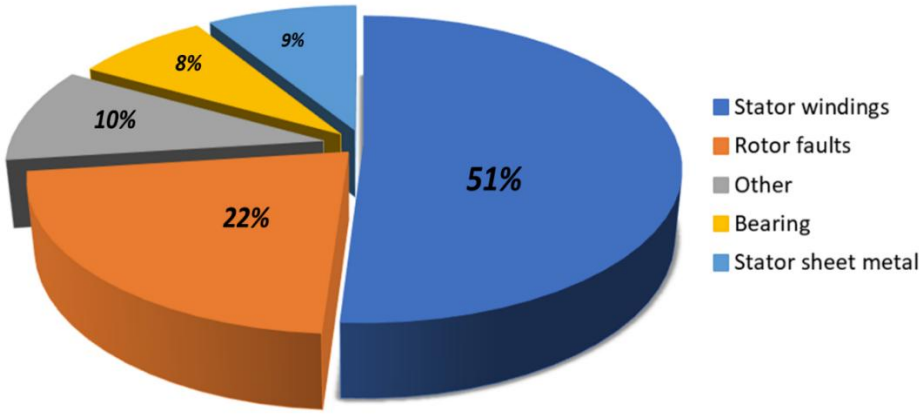

Figure 2.5 *Breakdown of failures according to the German industrial systems insurance company for low-power motors* [39].

For high-power induction motors (100 kW to 1 MW), the statistical study by Thorsen and Dalva [46] gave the following results:

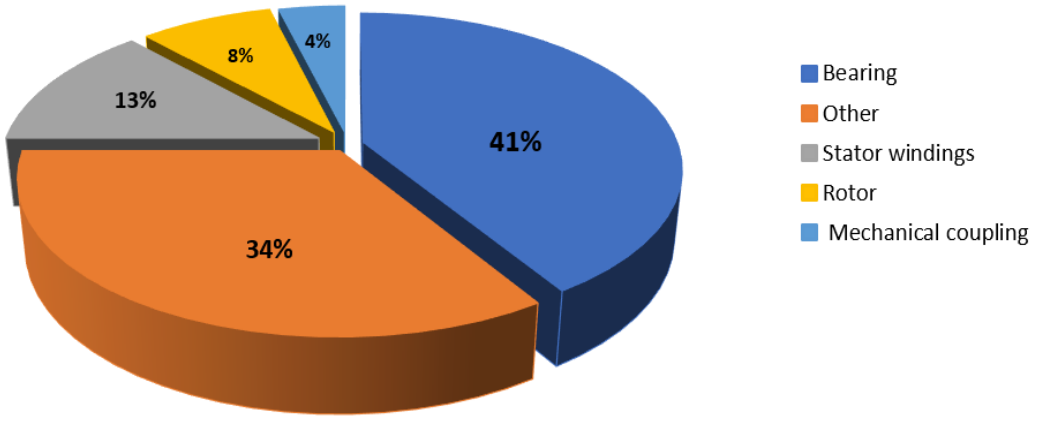

Figure 2.6 *Breakdown of high-power induction motor failures by Thorsen* [46].

And for the same power range, the Thomson study [57] in 1999 confirmed the results of previous studies.

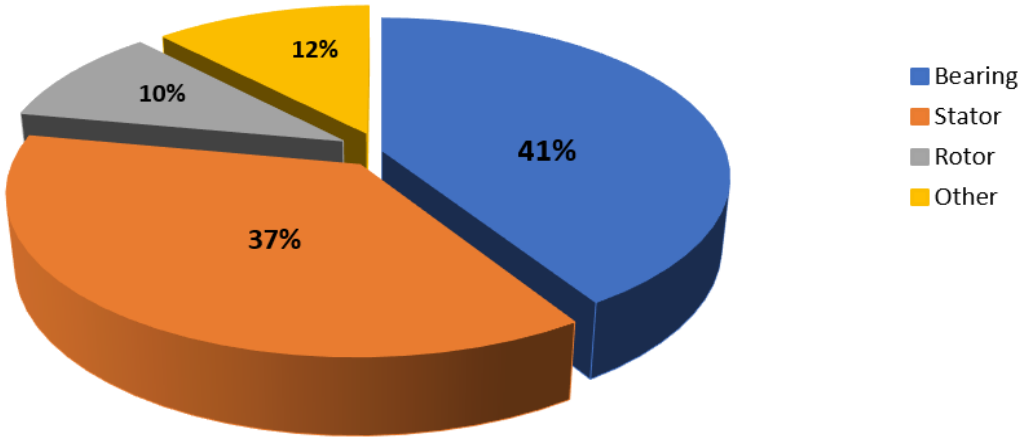

Figure 2.7 *Breakdown of high-power induction motor breakdowns in 1999 [57].*

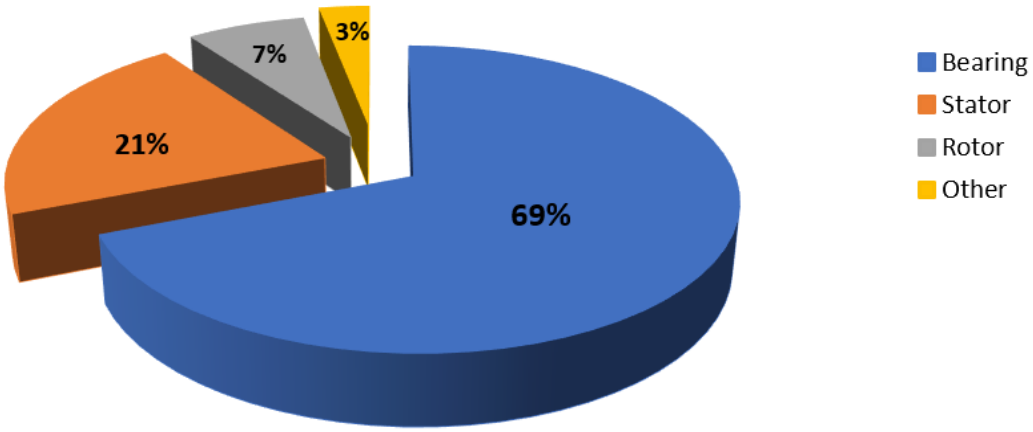

Figure 2.8 *Breakdown of high-power induction motor breakdowns in 2008 [58].*

It can be seen that over the last decade, the distribution of breakdowns has changed thanks to the development of manufacturing techniques for these machines.

Statistically, it is difficult to give an exact breakdown of electrical machine failures since the recording of breakdowns and faults is not automatic in all operating fleets and maintenance workshops [58]. But the most frequent source of failure is the bearings.

According to Thorsen and Dalva [46], the failure rate for motors used outdoors, where the environment is damp (in land and sea factories, for example), can be 2.5 times greater than the failure rate for motors used indoors.

As well as the power range of induction motors, for example we find that the rate of mechanical failures due to bearings is very high in high-power machines (from 100 kW to 1 MW), whereas stator and rotor faults are most common in medium-power machines (from 50 kW to 200 kW) [44], [45], [46].

2.3 Rotor Broken Bar

A rotor broken bar problem in induction motors occurs when there is physical damage to one or more bars in the rotor, resulting in major operating difficulties. This problem might occur as a result of mechanical strain, flaws in the manufacturing process, or prolonged working circumstances leading to excessive heat generation [59].

It is essential to identify this malfunction, which is characterised by increased vibration and noise, imbalanced magnetic fields, and torque pulsations. Methods such as current signature analysis, vibration analysis, and motor current signature analysis (MCSA) are used for detection. The problem has detrimental impacts on motor performance, such as decreased efficiency, heightened heat production, and higher mechanical strain [60].

Advanced analytical techniques, such as finite element analysis (FEA) and thermal analysis, provide more profound insights. Maintenance plans include the practice of regularly monitoring equipment to foresee any issues, with the potential remedy of either replacing or rewinding the motor. Additionally, mitigation necessitates the careful adjustment of the rotor once it has been repaired. Real-world case studies provide a practical framework, while future trends include the use of sophisticated sensor technologies and machine learning to improve the identification and avoidance of faults [61].

To summarise, a thorough examination of the rotor broken bar problem involves using many disciplines to successfully identify, reduce, and upkeep induction motors. Figure 2.9 depicts the rotor and the components of a damaged rotor bar.

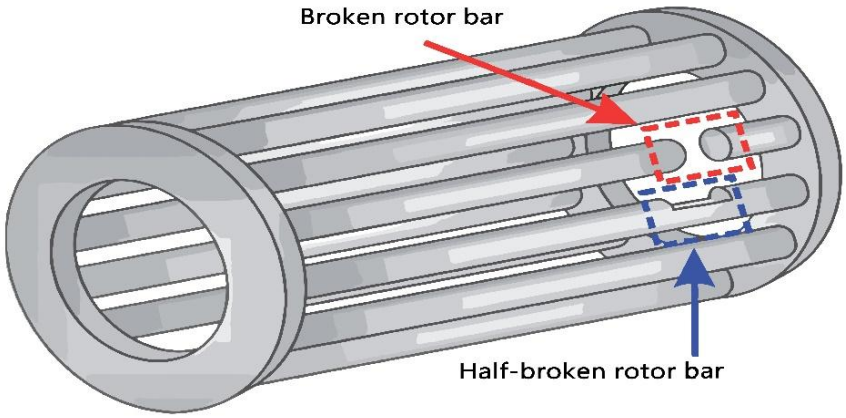

Figure 2.9 *broken rotor bar structure* [62].

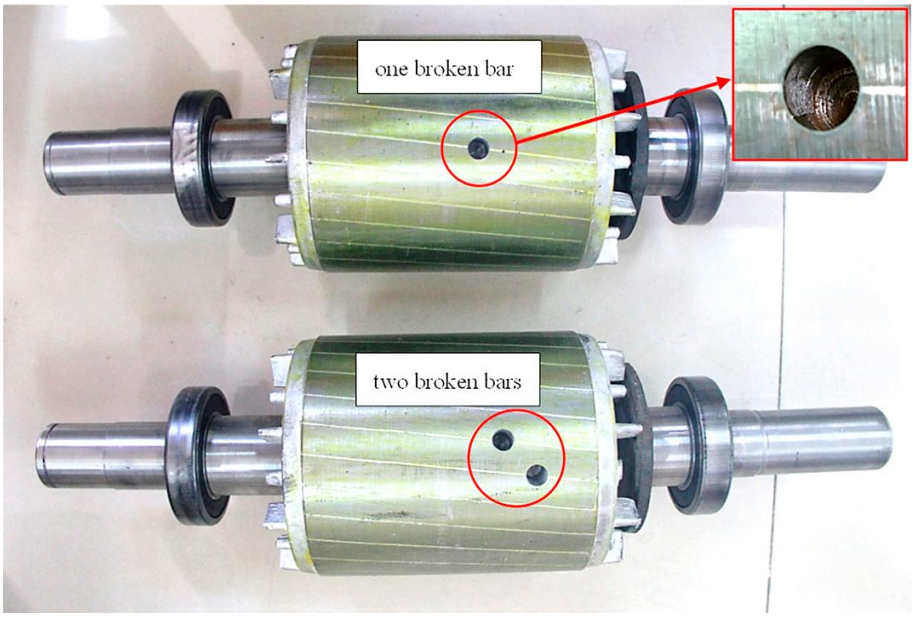

Figure 2.10 *Real image of broken rotor bars [63].*

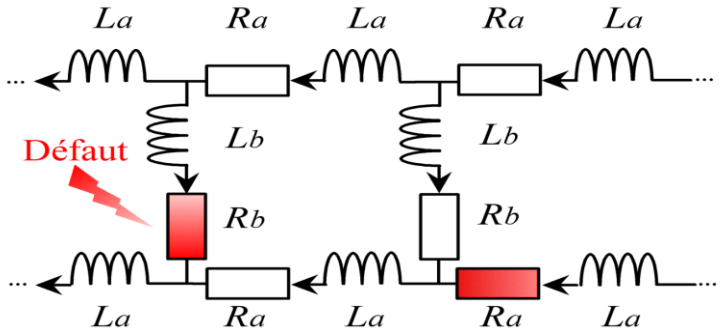

Figure 2.11 *The squirrel cage [64].*

The effect of a broken bar increases rapidly with the number of broken bars. The model differs for the simulation because the rank of the matrix relating to the rotor is no longer constant [44], [45]. Nevertheless, the frequencies generated, around the fundamental frequency of the power supply, by a bar or ring portion fault are:

$$f_{brb} = f(1 \pm 2ks) \qquad 2.1$$

With: $k = 1, 2, 3 \ldots \ldots K \in N$; where these harmonics are directly linked to the interaction between the rotating field and the asymmetry introduced by the broken bar [45].

On the other hand, space harmonics also interfere with frequencies whose relationship is:

$$f_b = \left\{\left(\frac{k}{p}\right)(1 - s) \pm s\right\} f \qquad 2.2$$

With $k = 1, 2, 3 \ldots \ldots K \in N$, p being the even number of poles [44], [45].

2.4 Mass Unbalance Fault

Factors including manufacturing variations, wear and tear, foreign object ingress, and irregular coatings or insulation on the rotor contribute to mass disequilibrium in an induction

motor. An adverse consequence of this imbalance may be increased vibrations, decreased efficiency, and possible harm to the motor and connected apparatus. Methods such as visual inspection, vibration analysis, and current analysis are utilised to detect mass imbalance. In order to correct the imbalance, dynamic balancing, static balancing, and trim balancing are frequently utilised methods, frequently in the course of maintenance or production. Preventive measures consist of routine maintenance, manufacturing quality control, and installation balancing. Software tools, balancing devices, and vibration analysers are examples of balancing apparatus and tools that assist in the detection and correction of mass unbalance. If an induction motor in a case study displays elevated levels of vibrations and noise, a comprehensive examination may uncover a mass unbalance concern that can be resolved by deactivating the motor and employing specialised equipment to conduct dynamic balancing. In summary, it is essential to rectify mass unbalance in order to ensure the continued optimal operation and durability of induction motors across a wide range of industrial applications [65].

2.4.1 Overview of Rotor Mass Unbalance

Rotor mass unbalance is a common problem in induction motors, either caused by manufacturing flaws or arising after a long period of operation. The imbalance may be ascribed to asymmetrical changes in mass around the rotor's axis of rotation, internal misalignment, or shaft bending, resulting in a misalignment between the center of gravity and the axis of rotation. Severe rotor eccentricity may cause imbalanced electromagnetic forces, which can lead to contact between the rotor and stator. This contact gradually wears away the rotor material, a phenomenon known as mass subtraction. This procedure worsens the defect of rotor mass imbalance, as seen in Figure 2.12. Effectively resolving these difficulties is essential for preserving the efficiency and dependability of the induction motor system [66], [67].

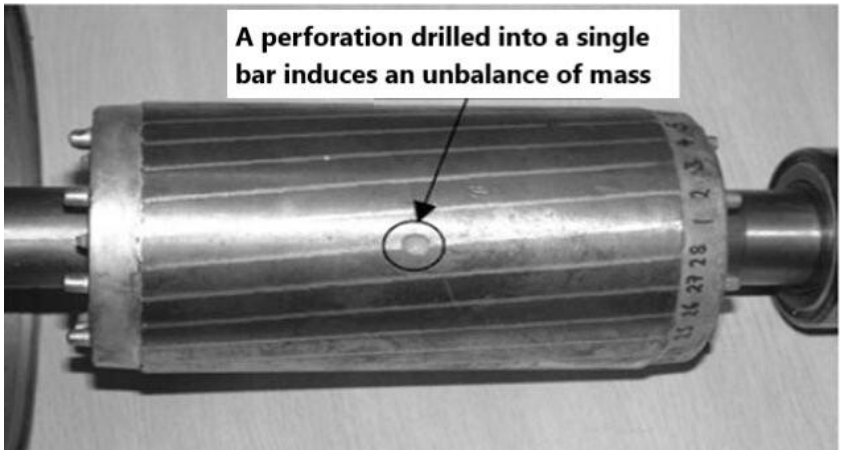

Figure 2.12 *mass unbalanced rotor* [68].

2.4.2 Unbalanced Static Mass Rotor

In the field of induction motors, the existence of an unbalanced stationary rotor mass is a significant issue. This problem occurs when there is an imbalanced distribution of mass in the rotor, usually due to manufacturing inconsistencies or anomalies that remain even after extended usage. The imbalance may arise due to asymmetrical additions or subtractions of mass around the rotor's axis of rotation. Furthermore, the presence of internal misalignment or

shaft bending may result in a mismatch between the center of gravity of the rotor and its center of rotation, thereby causing a static mass imbalance. Severe eccentricity may cause imbalanced electromagnetic forces that result in the rotor rubbing against the stator [69]. This rubbing can cause the rotor material to wear out, which worsens the static mass unbalance defect. Figure 2.13 depicts the attributes of this problem, emphasising the need for vigilant surveillance and remedial actions to guarantee the best possible functioning and durability of the induction motor system.

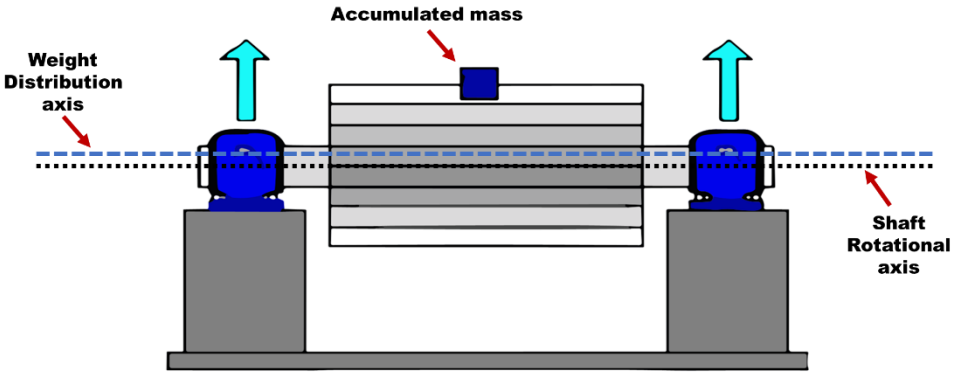

Figure 2.13 *the static mass unbalance defect.*

2.4.3 Two Unbalanced Rotors

The information is shown in Figure 2.14. If this malfunction occurs, the rotational axis of the shaft and the weight distribution axis of the rotor intersect exactly in the middle of the rotor [67].

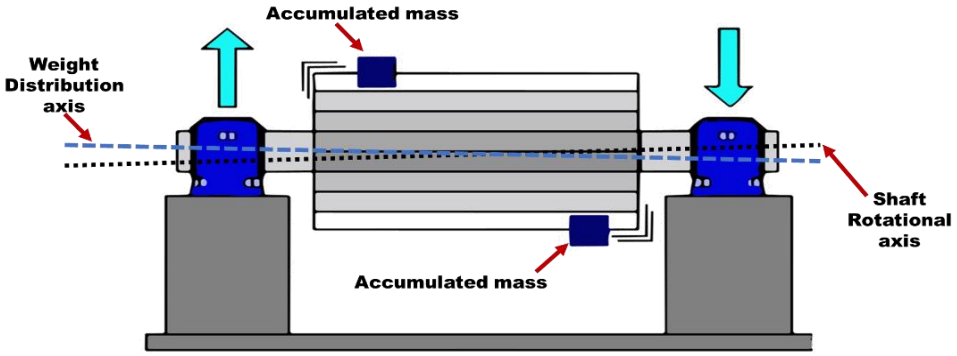

Figure 2.14 *Two Unbalanced Rotors.*

2.4.4 Dynamic unbalanced rotor

Figure 2.15 shows an example of this. When this problem develops, the shaft's axis of rotation and the axis of rotor weight distribution do not coincide. The distributions of rotor weight do not match. This is the result of a combination of coupling and static imbalance [70], [71].

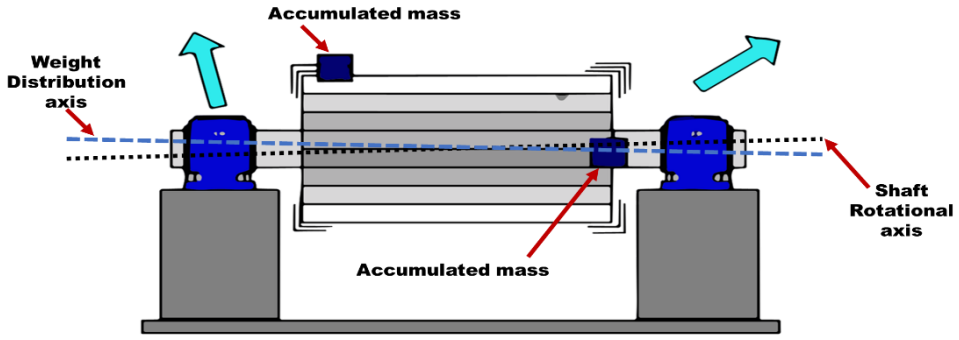

Figure 2.15 *Dynamic unbalanced.*

2.4.5 The Impact of Rotor Mass Unbalance

The presence of eccentricity is manifested by the creation of harmonics in the spectrum at frequencies close to the fundamental, are given by the relation below [72] and [73] :

$$f_{unb} = \left\{1 \pm n\left(\frac{1-s}{p}\right)\right\} f_s \qquad 2.3$$

Where:

f_{unb} = Rotor Mass Unbalance frequency,

$n = 1,2,3,\ldots, n \in N$,

s = The slip,

p = Number of pole pairs,

f_s = Supply frequency.

The advantage of this relationship is that it does not require precise knowledge of the asynchronous machine, as it does not include any terms related to its design.

A second approach is to use an expression linking the broken bar fault to those of mass unbalance and rotor notches. In this way, an equation in compact form reveals the frequency harmonics relating to these faults, many of which depend on the number of pole pairs [19].

$$f_{unb} = \left\{(k.N_R \pm n_d)\left(\frac{1-s}{p}\right) \pm n_{\omega s}\right\} f_s \qquad 2.4$$

Where:

f_{unb} = Rotor mass unbalance frequency,

$k = 1,2,3,\ldots, k \in N$,

N_R = Number of rotor notches,

$n_d \in N$,

s = The slip,

p = Number of pole pairs,

$n_{\omega s} = 1,3,5,\ldots,n_{\omega s} \in N,$

f_s = Supply frequency.

In the case of static mass unbalance, $n_d = 0$, whereas for dynamic unbalanced, n_d can take the following values: 1,2,3... (n_d is known as the "order of unbalance"). The coefficient $n_{\omega s}$ represents the time harmonic related to the supply of the asynchronous motor.

2.5 Stator Faults

For the stator circuit, failures are mainly due to a problem [74] :

- Thermal (overload....),
- Electrical (dielectric....),
- Mechanical (winding....),
- Environmental (aggression....).

The most recurrent faults, located in the stator, can be defined as follows:

- Insulation fault,
- short-circuit between windings of same phase (turn-to-turn short circuit),
- short-circuit between coils of same phase (coil-to-coil short circuit),
- short-circuit between phases (phase-to-phase short circuit),
- short-circuit between phase and ground (phase-to-ground short circuit),
- Magnetic circuit fault.

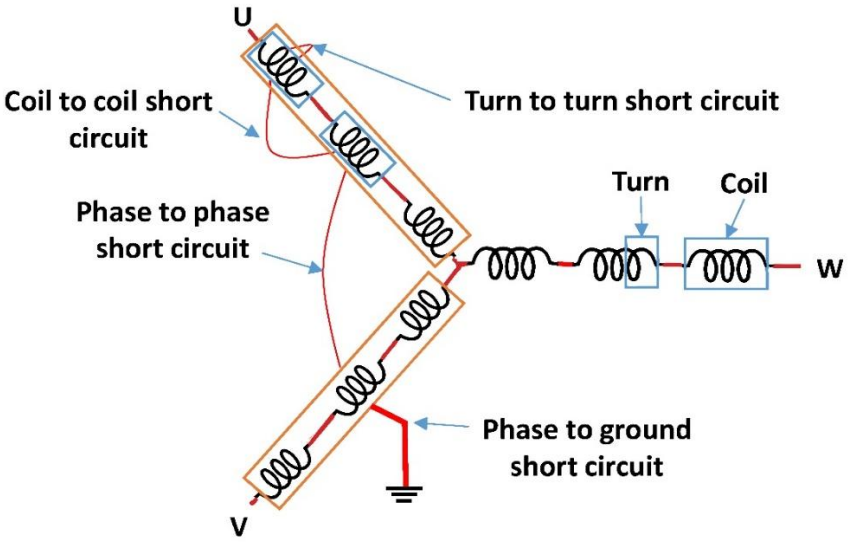

Figure 2.16 *Different three-phase IM stator faults* [75].

2.5.1 Insulation faults in a winding

Damage to the insulation in the windings can cause short circuits. The various losses (Joule, iron, mechanical, etc.) generate thermal phenomena, resulting in an increase in the temperature of the various motor components. However, insulation materials have temperature, voltage and mechanical limits. As a result, if the working environment of an insulation material

exceeds one of these limits, the material will degrade prematurely or accelerate and will eventually no longer perform its function. In this case, a short-circuit may occur in the winding concerned [44], [47], [68].

The various causes of this type of defect are:

- degradation of the insulation during manufacture,
- winding voltage above the limit of the insulation material,
- high current in the winding due to a short-circuit, converter fault or overload. This leads to a rise in temperature, prematurely damaging the insulation material,
- mechanical vibrations,
- the natural ageing of insulating materials. All insulating materials have a limited lifespan; even during 'normal' use, the insulation will naturally degrade,
- operation in a severe environment [74].

2.5.2 Short-circuit between windings

An occurrence of a short-circuit inside the same phase windings is a rather common electrical issue. This defect is caused by one or more insulation faults in the winding involved [75]. The result is an elevation in stator currents inside the impacted phase. A minor fluctuation in amplitude on the other phases alters the power factor and amplifies the currents in the rotor circuit. As a consequence, the temperature of the windings rises, leading to faster deterioration of the insulation. This might result in a chain fault, characterised by the occurrence of a second short-circuit. Conversely, the machine's average electromagnetic torque stays relatively constant, with the exception of an increase in oscillations that is directly proportional to the defect.

Figure 2.17 *short-circuit between the windings.*

Studies have shown that the stator current has an enriched spectrum due to the creation of a short-circuit between several turns in the stator [75], [76]. The frequencies are given by:

$$f_{sc} = \left\{\frac{n}{p}(1-s) \pm k\right\} f_s \qquad 2.5$$

Where:

f_{sc} = Short circuit frequency,

$n = 1,2,3,\ldots, n \in N$,

p = Number of pole pairs,

s = The slip,

$k = 1,3,5,\ldots, k \in N$,

f_s = Supply frequency.

2.6 Single Phasing

Single phasing in induction motors occurs when one of the three power supply phases to the motor is lost or interrupted. This may have adverse impacts on the motor's performance and may result in a range of problems, such as motor damage and harm to linked equipment [77]. Now, we will examine the factors that lead to single phasing in induction motors, the consequences of this issue, the actions that may be taken to prevent it, and the techniques used to diagnose it.

2.6.1 Causes of Single Phasing:

- **Power Supply problems :**
  - Malfunctioning contactors or relays inside the motor control circuit.
  - Malfunction of a single phase in the primary power source.
- **Loose Connections :**
  - Unsecured or eroded connections in the motor or control circuit might lead to a loss of phase.
- **Mechanical Failure :**
  - Breakage or loosening of conductors within the motor winding.
- **Overloading :**
  - Excessive load on the motor can lead to overheating and eventual failure of one phase.

2.6.2 Impact on Motor Performance:

- **Imbalance :**
  - The absence of one phase results in an asymmetry in the motor's magnetic field, resulting in decreased efficiency and torque.
- **Overheating :**
  - may occur when there is an excessive flow of current in the remaining phases, which has the potential to harm the insulation of the motor.
- **Vibration and Noise :**
  - Irregular forces exerted on the rotor might result in heightened levels of vibration and noise throughout the operation.
- **Diminished Efficiency :**
  - The motor functions with diminished efficiency, which impacts the overall performance of the system.

2.7 Crawling

The phenomenon of crawling, which refers to the operation of an induction motor at a lower speed than planned, has been a subject of interest for researchers for many years owing to its negative effects on performance and efficiency [40]. Multiple variables contribute to this unfavourable behaviour. Crawling mostly occurs due to the generation of harmonic currents in the rotor bars, namely the seventh harmonic. The harmonics in question interact with the spinning magnetic field, resulting in a torque that counteracts the intended direction of the

motor. This hampers the motor's ability to synchronise and achieve its maximum speed. This may arise from design decisions, such as using stator and rotor slot numbers that do not match, resulting in an uneven air-gap flow and intensifying the impact of harmonic effects. In addition, external variables such as insufficient power supply or high load may diminish the primary torque, hence enabling harmonics to have a more significant impact and cause crawling [44].

The ramifications of crawling are many. The primary consequence is a substantial decrease in power generation, since the motor functions much below its capacity to supply energy. Moreover, crawling intensifies mechanical deterioration. Elevated levels of vibrations and torque pulsations exert excessive strain on components, resulting in faster deterioration of bearings and, in certain cases, probable collapse of electrical insulation. Ultimately, crawling leads to diminished effectiveness, since the inherent energy losses become more noticeable at slower working speeds. Crawling may provide a significant operational obstacle in applications that need accurate control and seamless operation [78].

It is important to do further study on techniques to mitigate crawling. Active areas of inquiry include exploring design improvements to reduce harmonic production, using improved control algorithms to mitigate torque variations, and creating diagnostic procedures for early identification. Gaining comprehension and successfully addressing the issue of crawling would result in improved efficiency, dependability, and predictability of induction motor operations in many industrial settings.

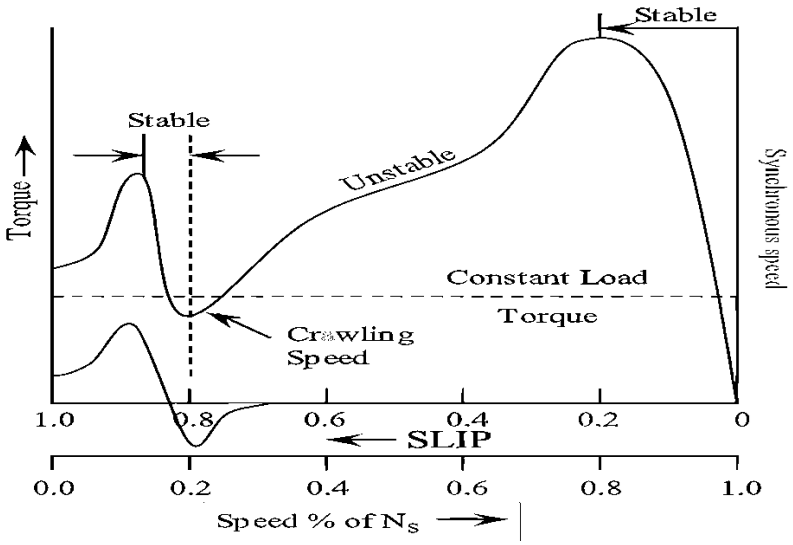

Figure 2.18 *the torque and speed curve of an induction motor* [44].

The graph illustrates that the motor's torque is highest at low speeds and thereafter diminishes as the speed escalates. This is a common attribute of induction motors. The curve also indicates the presence of two unstable operating areas for the motor: very low speeds (crawling) and extremely high speeds (cogging).

Crawling is the result of the magnetic field in the stator interacting with the current in the rotor. At low velocities, the magnetic field has the ability to attract the rotor, even in cases when there is insufficient torque to surpass the load. This might result in motor vibration and noise. Cogging arises from the non-uniform dispersion of the magnetic field inside the motor.

At high velocities, the rotor may get trapped inside one of the low points of the magnetic field. This might result in abrupt and erratic movements of the motor. To mitigate crawling and cogging, one may use a motor with increased torque or utilise a variable speed drive to regulate the motor's velocity [78].

2.8 Bearing Faults

The bearing is a crucial component in almost all rotational machinery. The main benefit of this design is its ability to minimise the friction caused by shaft rotation, efficiently distribute loads to stationary bearings, and provide support for radial loads. The shaft transmits loads to stationary bearings and provides support for both radial and axial stresses. Additionally, it may be used to guarantee accurate placement of the shaft and rectify any misalignment. Therefore, the majority of rotating machines are furnished with bearings to uphold the load and uphold the gaps between the stationary and revolving components of the machines [79]. Bearings, which are of utmost significance, are identified by the Institute of Electrical and Electronics Engineers (IEEE) as the components with the highest probability of failure in an electrical machine [46], [80].

2.8.1 Bearing Geometry

A rolling bearing is a geometries composed of raceways separated by a cage and two concentric rings, the inner and outer rings, respectively, that compose its body. The purpose of this enclosure, which is positioned between the rings, is to prevent the elements from rubbing against one another and thus reduce friction (see Figure 2.19). As required by the application, rolling elements might consist of needles, spheres, or rollers [81]. Specific attributes pertain to the radial and axial loads that can be borne by each bearing type, as well as its maximum allowable motion and misalignment. A lateral cover known as a flange encircles the space between the inner and outer rings on certain bearings.

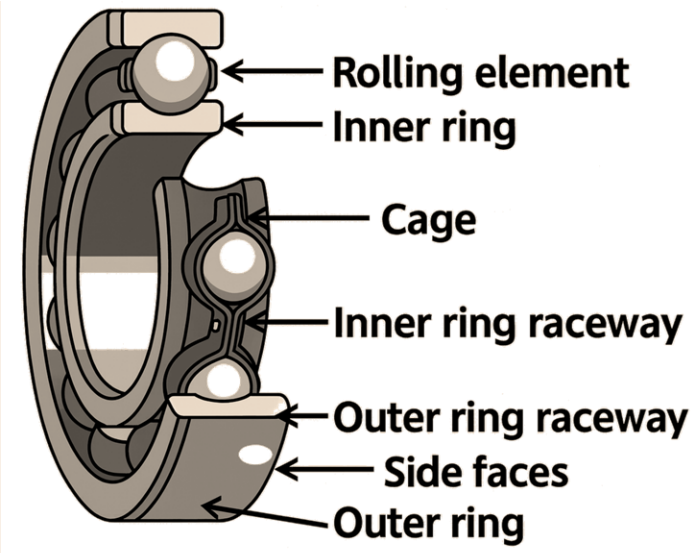

Figure 2.19 *Diagram of the construction of a rolling bearing* [82].

2.8.2 Defects in bearings

A theoretical model for calculating bearing life is often supplied by manufacturers. However, the contribution of numerous factors deviates from normal operating conditions, causing premature deterioration and modifying the predicted operating life. Various machine condition monitoring techniques based on acoustics [83], [84], [85], [86], ultrasound [87], [88], temperature, current [89], [90], [91], electrostatics [92], [93], [94], forces, and vibration [95], [96], [97], [98] can estimate the condition of the machine. However, monitoring vibration and acoustic emission levels is most commonly used to detect bearing faults and estimate the residual life of rotating machines [81].

In most cases, bearing faults start with a local loss of material on a matt surface (inner and outer ring, rolling elements) [99].

2.8.3 Bearing-related fault frequencies

The relationship between rolling element-bearing vibrations and the stator current spectrum is based on the fact that all eccentricities interfere with the field in the air gap of the asynchronous machine. A rolling element bearing fault is manifested by the continuous repetition of faulty contact with both the outer and inner bearing cages.

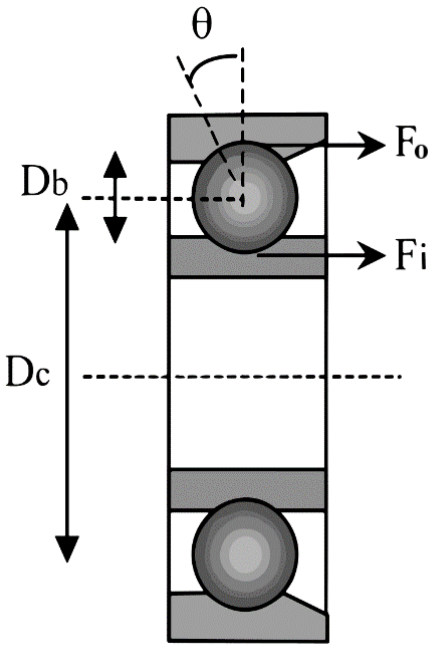

Figure 2.20 *The rolling element bearing.*

The frequency of repetition will be for the inner and outer cages:

$$\begin{cases} f_i = \frac{n_b}{2} * f_r \left\{1 + \frac{D_b}{D_c} cos\,\theta\right\} \\ f_o = \frac{n_b}{2} * f_r \left\{1 - \frac{D_b}{D_c} cos\,\theta\right\} \end{cases} \quad 2.6$$

The current spectrum is then described by:

$$f_{i,o} = f_s \pm n\frac{n_b}{2} * f_r \left\{1 \pm \frac{D_b}{D_c} cos\,\theta\right\} \quad 2.7$$

This expression contains data specific to rolling element bearings.

s = slip,

f_s = power frequency,

f_r = mechanical rotation frequency,

n = 1,2,3, . . ., $n \in$ N,

n_b = number of rolling elements,

D_b = rolling element diameter,

D_c = distance from the centre of the rolling elements,

θ = contact angle of the rolling element with the cage.

Assuming that the number of rolling elements is usually between 6 and 12, two commonly encountered relationships are:

$$\begin{cases} f_i = 0{,}4 * n_b * f_r \\ f_o = 0{,}6 * n_b * f_r \end{cases} \quad 2.8$$

So, the current spectrum will be enriched by:

$$f_{i,o} = f_s \pm n * f_{\{o,i\}} \quad 2.9$$

2.9 Other Faults

2.9.1 Mechanical Shaft Failure

The shaft of the machine may show a crack due to the use of the wrong material during construction. In the short or long term, this crack can lead to a clean fracture of the shaft, causing the asynchronous machine to stop irreparably. Corrosive environments can also weaken the robustness of the machine shaft. For example, humidity can cause microcracks and lead to the complete destruction of the machine [28], [100].

Static, dynamic, or mixed eccentricity can induce considerable stress on the motor shaft, leading to additional fatigue. A vibration analysis, an ultrasound analysis, Frequency analysis of absorbed currents or simply a visual analysis of the machine shaft can detect this type of failure.

2.9.2 Misalignment

Misalignment is a more common problem than unbalance, and the reason is quite simple. Despite the use of self-aligning bearings and flexible couplings, it is difficult to align two shafts and their bearings to ensure that there is no force that can cause vibration [101].

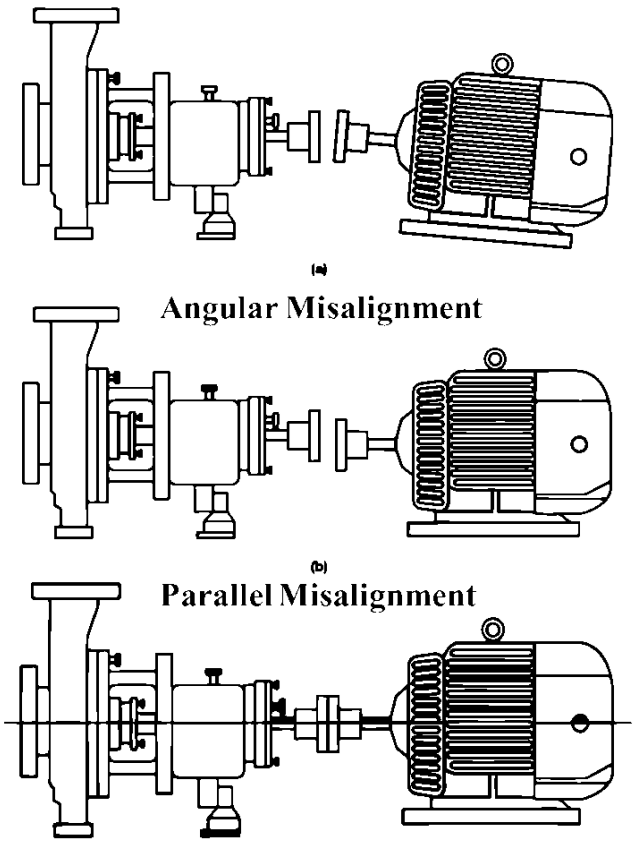

Figure 2.21 *Shaft Misalignment* [101].

There are two types of misalignment [101]:

- Parallel misalignment: This occurs when the axes of rotation of the two machines have the same orientation angle, but are vertically separated from each other.
- Angular misalignment: This occurs when the axis of rotation of two machines is at a different angle.

2.9.3 Faults in the gears

A gear is made up of two intermeshing toothed wheels, enabling power to be transmitted between two closely spaced shafts with a constant speed ratio. Depending on the relative position of the two shafts, there are three classes of gear (Figure 2.22) [102]:

- Parallel gears: "The 2 shafts are parallel.".
- Concurrent gears "The two shafts are such that their extensions intersect.".
- Left-hand gears: "The 2 shafts occupy any relative position.".

Gear teeth can be spur, helical, or herringbone. The resulting forces are:

- Only radial on parallel, spur or herringbone gears
- mixed "radial and axial" on helical gears, bevel gears, and worm and wheel gears [102].

(a) **(b)** **(c)**

Figure 2.22 *Different types of gears: (a) Spur gear (b) Straight bevel gears (c) Worm gear set.*

Gears are motion transmission elements that can be affected by defects such as:

- Pitting of cut teeth.
- Spalling of the teeth.
- Cracks.
- Fractures at the end of cracks.
- Seizures leading to major deterioration.

The main faults occurring on a pair of gears in a simple reduction gearbox are faults spread over the entire toothing and faults localised on part of the toothing.

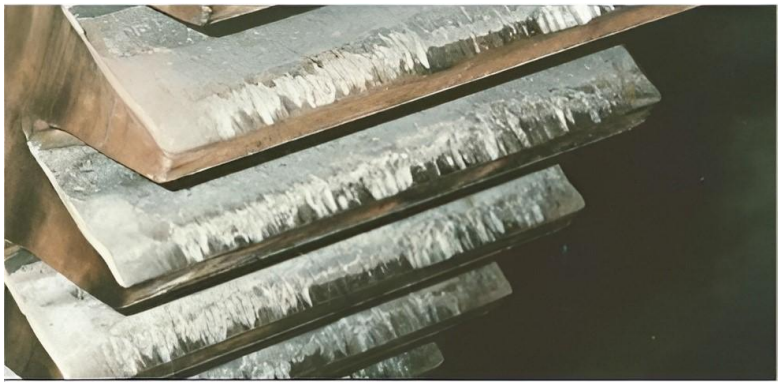

Figure 2.23 *Real gear seizure fault* [103].

Figure 2.24 *Real gear crack defects* [103].

More generally, surface damage to gears is the result of various phenomena that may occur during the operation of the system [102].

2.10 Conclusion

In conclusion, this chapter focuses on the critical area of fault analysis in induction motors, highlighting its significant role in safeguarding the essential machinery that powers industrial operations. The chapter begins with an introduction emphasising the robustness and versatility of induction motors in contemporary industrial settings, acknowledging their indispensable contribution to various machinery.

The subsequent exploration delves into the diverse categories of malfunctions that can affect induction motors, elucidating their potential consequences for both operational efficiency and safety. The chapter categorises these faults into specific types, such as rotor broken bars, mass unbalance, stator faults, single phasing, crawling, bearing faults, and other mechanical and electrical issues. Each fault category is thoroughly examined, providing insights into their origins, consequences, and specific manifestations.

For instance, the discussion on rotor mass unbalance explores various aspects, including unbalanced static mass rotors, two unbalanced rotors, and dynamic unbalanced rotors, elucidating their impact on motor performance. Similarly, stator faults, single phasing, crawling, bearing faults, and other faults are detailed with a focus on their causes and effects.

The comprehensive coverage of fault analysis in this chapter underscores its importance in ensuring the efficient and reliable operation of induction motors. By understanding the language of motor faults, the research emphasises the significance of pre-emptive action to mitigate potential negative impacts on industrial operations. This proactive approach is vital for prolonging the lifespan of induction motors, enhancing their performance, and creating a safer industrial environment.

The subsequent chapter, as indicated in the table of contents, is poised to delve into the study of detection techniques using signal processing and artificial intelligence methods. This transition suggests a forward-looking exploration of advanced methodologies to detect and address induction motor faults, complementing the foundational understanding established in this chapter.

Chapter 3 Integration of Signal Processing Methods and Artificial Intelligence for Faults Diagnosis

3.1 Introduction

This chapter emphasizes the importance of utilizing cutting-edge technologies such as signal processing and artificial intelligence to detect and diagnose faults in industrial and technical systems. Modern technologies may not always be compatible with the complexity of traditional methods, resulting in system malfunctions. By utilizing thermal imaging, acoustic signals, and vibrations, the integration of AI and machine learning algorithms holds great promise in enhancing fault detection. With their enhanced precision and ability to detect patterns, predictive models have the capability to anticipate failures and enhance the system's reliability.

3.2 Classification of methods for developing an industrial diagnostic system

The fault diagnosis strategies used in industry are many and varied [104]. Their basic principle is based on a comparison between the data observed during the operation of the machine and the knowledge acquired about its normal behaviour and its behaviour in the event of a fault [105].

The choice of one diagnostic method over another depends on two main criteria: a priori knowledge and knowledge derived from observations.

A priori knowledge can be acquired either by analysing the history of the system under study and extracting the relevant indicators for identifying the operating modes ("fault-free operating mode and faulty operating mode") or by expert analysis linking the various operating modes to their causes and symptoms. The knowledge derived from observations is generally acquired directly using sensors, where the transformation and analysis of all the information gathered at a given time are necessary to identify the system's operating mode. We can make a non-exhaustive classification of the main diagnostic methods encountered in the literature along two main lines: model-based approaches and model-free approaches. For more details, we refer readers to the following works: [106], [107], [108].

3.2.1 Model-based diagnostic methods

These approaches are based on comparing the observed behaviour of the system with the predicted behaviour of the established qualitative and/or quantitative model [109].

The presence of a discrepancy in this comparison means that a failure has been detected, as shown in Figure 3.1.

Two branches of methods can be distinguished according to the type of model to be established: quantitative methods and qualitative methods.

Diagnostic methods based on quantitative models are based on estimating the operating state using mathematical models simulating the behaviour of the system. If the difference between these models and the system variables exceeds a certain threshold, a fault is detected. After the detection phase, a residual is generated and compared with all known fault signatures to isolate and locate the fault. Among the various diagnostic methods using mathematical

models are the observer-based method [110], [111], the parity space method [112], and the parametric estimation method [106].

Diagnostic methods based on qualitative models make it possible to abstract the behaviour of the process to a certain degree of abstraction through symbolic (non-mathematical) models describing the continuous state space of the system in a qualitative manner [113]. Qualitative methods can be classified according to the level of abstraction considered for the system to be diagnosed, such as continuous systems [114] discrete-event systems [115], or dynamic hybrid systems [116], [117].

The separation between quantitative and qualitative methods does not imply that these two aspects are disjointed, because in reality, these two types of methods can coexist within the same diagnostic strategy.

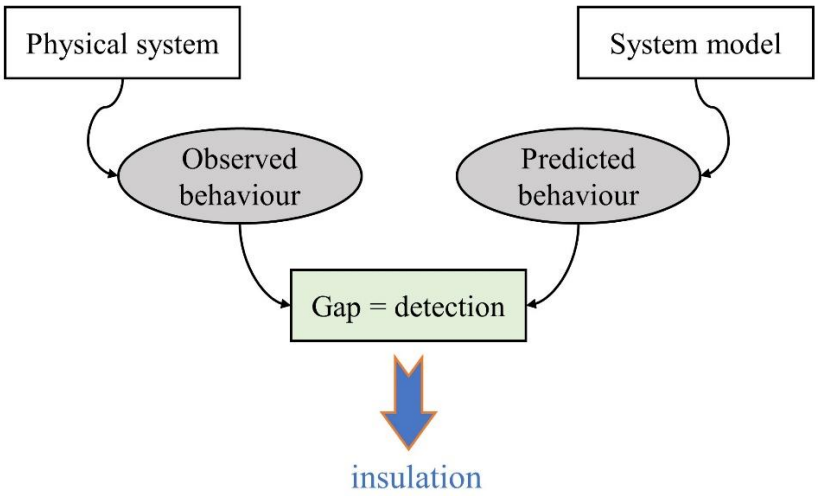

Figure 3.1 *Principle of model-based diagnostic methods.*

3.2.2 Diagnostic methods without models

In some industrial applications, it is difficult or even impossible to generate physical models representative of the operation of a system and its various components because of the increased complexity of the system to be diagnosed. Typically, these diagnostic methods exploit information from sensors installed on the machine without having to use the mathematical model simulating the system's behaviour. Model-free diagnostic strategies include artificial intelligence techniques such as expert systems [118] and pattern recognition methods [119].

Our work in this thesis focuses on the diagnosis of faults affecting the bearings of asynchronous motors, where AI techniques are the appropriate tools for performing this task by exploiting the information generated using sensors without the need for modelling, which is difficult to develop in this complex case. The diagnostic process involves several stages: data acquisition, extraction, and selection of relevant indicators, which are then taken as input to a classifier in order to identify and locate faults. The various steps involved in developing this diagnostic approach are detailed in the following sections.

3.3 Acquisition chains and information sources

The first task in fault diagnosis is the process of acquiring data from multiple sources, considered to be the physical foundation of preventive maintenance. Extracting information about a system is necessary to understand its condition, describe its behaviour, and predict any early faults so that corrective action can be taken.

The essential mechanism for data acquisition is the sensor, which is an element sensitive to a physical quantity that it transforms into an electrical quantity (a voltage or a current). It is often integrated into an acquisition chain, enabling the measured quantity to be conditioned so that the measurement (or output signal) gives an optimised estimate of the value of the measure, as shown in Figure 3.2.

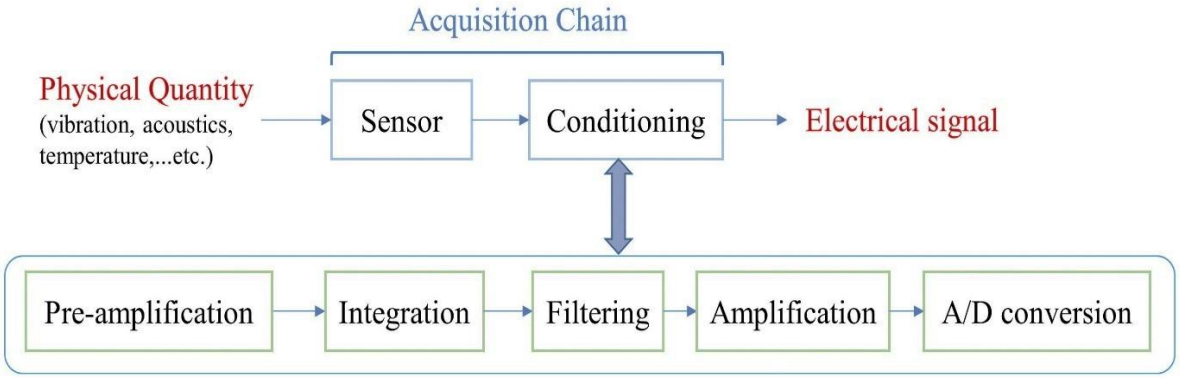

Figure 3.2 *Data acquisition chain.*

Whatever the data source, the sensor-conditioner association determines the characteristics of the output signal, where the various components of the acquisition chain must enable the measurement, processing, and restitution of the measurement with the characteristics necessary for the application, such as speed (the reaction time of a sensor), resolution (the smallest variation that needs to be measured), accuracy (the veracity of the measurement result in percentage), immunity to interference, etc.

The selection of appropriate data sources is key to the effectiveness of condition-based preventive maintenance, and a comprehensive data acquisition system can directly improve the capability and performance of diagnosing and prognosticating faults affecting rotating machinery. This selection is made according to several parameters, such as [120]:

- Installation cost parameters,
- parameters relating to machine dynamics and kinematics,
- environmental and space parameters,
- the criticality level of the application.

The types of data sources that can be used for predictive maintenance are listed below:

3.3.1 Vibration analysis

Vibration analysis is generally presented as the most effective method of condition-based maintenance, particularly for rotating machines, since these machines produce vibrations that are specific in their behaviour and character [121], [122], [123], [124], [125].

A new rotating machine has a relatively regular vibration signal during normal operation, but as it ages, degradation due to the wear of one or more of its components will alter the characteristics of the signal. The integrity of the machine can be assessed by a detailed comparison of new and old vibration spectra; that is, each fault in a machine will produce vibrations with distinctive vibrational characteristics, and these can be captured and compared with reference ones in order to perform fault diagnosis. It is well known that the vibration signal carries information about the structural resonances and other components of the machine, so it can give information about the operating conditions and efficiency of the machine. Consequently, monitoring methods based on vibration analysis have been the subject of intensive research over the last few decades.

Vital characteristic information from vibration signals can be obtained by employing various signal processing techniques. Industrial vibration analysis techniques use vibration sensors with different frequency ranges, depending on the machine being monitored. These sensors are usually placed at critical points where the local load is greatest, such as wheel axles, gearbox bearings, generator bearings, and the main bearing. Various sensors are used to measure vibration signals from machines, including displacement sensors (proximometers) operating in the low-frequency range, velocity sensors (velocimeters) operating in the medium-frequency range, acceleration sensors (accelerometers) in a high-frequency range…etc.

3.3.2 Lubricant analysis

Lubricants are widely used in almost all moving parts of rotating machinery to reduce friction and wear, as well as for cooling purposes. Oil analysis is the analysis of the compositional properties and the contaminants of a lubricant. It is a routine activity used to determine:

- The presence of contamination: different types of contamination due to foreign particles coming from the machine's environment can affect the equipment in different ways. For example, the presence of air and water can affect the fluid required for surface separation. The presence of atmospheric and process chemicals can cause surface abrasion.
- The presence of wear debris: Surface wear is considered to be the main threat to the long-term performance of equipment. Machine condition can be assessed by measuring debris in the lubricant.
- Lubricant properties: assesses the condition of the lubricant that could affect drain intervals.

Lubricant analysis programmes are designed to provide information about the condition of the oil and the condition of the machine [126]. There are a wide range of tests used to provide

this type of information. The following are specific examples of how lubricant properties, machine wear, and contamination can be tested.

- Viscosity: is the most important property of a lubricant; it is what enables it to form the protective layer needed to separate moving surfaces.
- Water measurement: water is a common contaminant with potentially devastating effects, including rusting, increased wear rates, and loss of additive functionality.
- Neutralisation index: measures a change in acid concentration in a lubricant that indicates oxidation or corrosion.
- Spectroscopy: helps monitor for metal contaminants and allows analysts to look for species of molecules that do not belong in the oil.

The use of lubricant analysis is inadequate as part of a strategy for diagnosing early faults affecting rotating machinery because of the difficulty of locating and isolating the faulty component, and the slowness of the analyses can reduce the possibilities of follow-up in situations or circumstances of rapidly progressing damage.

3.3.3 Acoustic emission

The surface vibration of a rotating machine is often the most important factor in generating the machine's acoustic signal, which means that there is a close relationship between acoustic and vibration signals. The fundamental difference is that vibration transducers are rigidly mounted on the component concerned and record local motion, whereas acoustic transducers summarise sound from many sources throughout the machine. This technique is not suitable for on-line testing because the acoustic signals are contaminated by the background noise of the machine if used in on-line conditions.

Acoustic emission (AE) is a non-destructive examination method and is widely used for the early detection of faults in rotating machinery because its sensitivity is higher than that of normal accelerometers and it can detect low-energy vibration signals [127], [128], [129].

EA is the generation of high-frequency elastic waves (in the approximate range of 100 kHz to 1000 kHz) due to the rapid release of accumulated strain energy from a localised source in a material, such as a fracture or crack. The energy released by the change in condition passes through the material and causes elastic vibrations.

3.3.4 Thermography

Thermography, also known as thermal or infrared inspection, is one of the most common non-destructive testing or inspection methods and is considered to be a rapid observation approach for monitoring the general condition of a rotating machine. It has been widely used because it allows the condition of machines to be inspected and any faults detected without having to disconnect the equipment from normal operation [130], [131], [132].

A thermal camera is capable of capturing the infrared radiation emitted by an object. It consists of an array of thermal sensors and can create a thermal image based on the pattern of

radiation detected, called a "thermogram.". The higher the temperature, the more radiation is emitted, and this is presented as image pixels with a higher intensity value on the thermogram.

Thermal images are generally in grayscale, but pseudo-colour can be assigned using different colour palettes to help users identify objects with different temperatures [133].

Most faults that can affect the operation of a machine will generate excessive heat in the vicinity of the fault area. These thermal anomalies can be easily captured by a thermal imaging camera and appear as a hot spot on the thermogram. By analysing the thermogram, it is possible to assess the condition of the equipment and identify any signs of failure.

3.4 Vibration signal processing tools adapted to the search for faults

3.4.1 Statistical indicators

When one or more faults occur in one or more components of a rotating machine, the vibration signals change in the time domain. The distribution and amplitude of these signals vary with different fault conditions, and it is very difficult to discriminate between normal and faulty motor vibration signals, especially in the case of bearing faults where there are many pulses in the vibration waveform.

Changes or variations in vibration signals for different faults cannot be predicted or separated by looking directly at these signals due to the presence of irrelevant information or high noise due to several harmonic interferences existing in the machine environment, especially in the case of an early-stage fault appearance. That is, the alteration of the vibration signals is too small to be detected. Therefore, comparing the raw signals in the time domain of faulty and healthy motors is not effective in determining whether the component is behaving normally or showing signs of failure.

The temporal analysis of vibration signals is generally based on the extraction and monitoring of several statistical characteristics that are more or less effective and suitable for observing certain failures more than others. The application of these techniques provides initial information from the signals but needs to be followed up, assisted, and completed by more in-depth investigations as part of the diagnosis. Table 3.1 summarises these main temporal descriptors.

In order to reveal the important information from the temporal signals, a signal processing process is required, which converts the raw signals into an appropriate condensed form.

Table 3.1 *The most commonly used statistical indicators with their mathematical definitions.*

Statistical parameter	Formule mathématique
RMS	$RMS = \sqrt{\left(\frac{1}{N}\right)\sum_{i=0}^{N}(x_i - x)^2}$ *3.1*
Peak	$Peak = Sup_{1<i<N}\lvert x_i\rvert$ *3.2*
Peak factor	$Peak\ factor = \frac{Peak}{RMS}$ *3.3*
Kurtosis	$Ku = \frac{\frac{1}{N}\sum_{n=0}^{N}(x(n) - x)^4}{\left[\frac{1}{N}\sum_{n=0}^{N}(x(n) - x)^2\right]^2}$ *3.4*
Skewness	$SK = \frac{\frac{1}{N}\sum_{n=0}^{N}(x(n) - x)^3}{\left[\frac{1}{N}\sum_{n=0}^{N}(x(n) - x)^2\right]^{3/2}}$ *3.5*

3.4.2 Spectral analysis

Frequency domain analysis techniques have the ability to divulge certain information based on frequency characteristics that are not easily observable in the time domain.

In practice, the Fourier transform (FT) is the appropriate mathematical tool for easily transforming the time-domain vibration signal into a frequency-domain representation. This method breaks down these complex signals into a multitude of elementary sinusoidal components and represents them in the form of an "amplitude-frequency" spectrum. Table 3.2 shows the most common faults affecting rotating machines and their characteristic frequencies.

There are two main types of FT: the discrete Fourier transform (DFT) and the continuous Fourier transform (CFT). The DFT is an important tool in the frequency analysis of discrete time signals '$x(n)$' and can be defined by equation (3.6):

$$\mathrm{X_{DFT}(k)} = \sum_{\mathrm{n=0}}^{\mathrm{N-1}} \mathrm{x(n)e^{-2\pi nk/N}},\ \ \mathrm{k} = 0.1, \dots, \mathrm{N}-1 \qquad 3.6$$

Or we could also write:

$$X_{DFT}(k) = \sum_{n=0}^{N-1} x(n) W_N^{nk},\ \ k = 0.1, \dots, N-1 \qquad 3.7$$

Where:

$$W_N = e^{-(j2\pi/N)} = cos\left(\frac{2\pi}{N}\right) - j\,sin\left(\frac{2\pi}{N}\right) \quad 3.8$$

The inverse of DFT, which transforms $X_{DFT}(k)$ into $x(n)$, can be expressed using the following equation:

$$x(n) = \frac{1}{N}\sum_{n=0}^{N-1} X_{DFT}(k) W_N^{nk}, \;\; n = 0.1, \dots, N-1 \quad 3.9$$

Table 3.2 *The typical frequencies of the main faults affecting rotating machines.*

Default	Characteristic frequency
Unbalanced	Rotation frequency (F_r)
Misalignment	F_r, $2F_r$, generally $2F_r$ is higher than F_r (axial vibrations are than radial vibrations)
Mounting fault	$0.5F_r$, F_r and several of their harmonics
Oil swirls	40-50% de F_r
Bearings	Frequencies corresponding to the passage of rolling elements given by the following equations: *Outer race defect:* $f_o = \frac{nf_r}{2}\left(1 - \frac{d}{D}cos\varphi\right)$ 3.10 *Inner race defect:* $f_i = \frac{nf_r}{2}\left(1 + \frac{d}{D}cos\varphi\right)$ 3.11 *Cage defect:* $f_c = \frac{f_r}{2}\left(1 - \frac{d}{D}cos\varphi\right)$ 3.12 *Rolling element defect:* $f_{re} = \frac{D}{2d}\left[1 - \left(\frac{d}{D}cos\varphi\right)^2\right]$ 3.13 n : the number of rolling elements, d : the rolling element diameter, D : the cage diameter, φ : the angles of the rolling elements, f_r: the rotational frequency of the bearing.
Belt	The belt rotation frequency is given by: $F_b = \frac{\pi D_1}{L} f_1 = \frac{\pi D_2}{L} f_2$ 3.14

	For wear in toothed belts: $F_t = NF_r \pm kF_b$ 3.15 D_1 : Diameter of pulley 1, D_2 : Diameter of pulley 2, L: Length of the belt, N: Number of teeth on the pulley $k = 0,1,2,3..$
Gears	Given by: $F_c = NF_r \pm kF_r$ 3.16 N: Number of teeth and $k = 0,1,2,3..$

3.4.3 Envelope analysis

The envelope of a vibration signal is calculated using the Hilbert transform (HT). This technique uses the modulation of the amplitude of the resonance frequency of one of the rotating machine's components by the appropriate characteristic fault frequency. HT is used to calculate the envelope of a signal $x(t)$ and is defined by the following mathematical expression:

$$HT[x(t)] = \bar{x}(t) = \frac{1}{\pi}\int_{-\infty}^{+\infty} \left(x(t)/(t-\tau)\right) d\tau \qquad 3.17$$

where $\bar{x}(t)$ is the imaginary part of the analytical signal $s(t)$ which is defined by the following formula:

$$s(t) = x(t) + j\bar{x}(t) \qquad 3.18$$

If we want to deduce the envelope of a vibration signal, called $y(t)$, we calculate the modulus of the analytical signal $y(t) = |s(t)|$ where the phase and instantaneous frequency of the signal are defined by the following formula:

$$\begin{cases} phase:\ \theta(t) = tan^{-1}\left(\bar{x}(t)/x(t)\right) \\ frequency:\quad f(t) = \dfrac{d\theta(t)}{dt} \end{cases} \qquad 3.19$$

3.4.4 Time-frequency analysis

3.4.4.1 Short-Term Fourier Transform (STFT)

Also known as the "sliding window Fourier transform" and proposed by Gabor in 1946 [134]. This method is based on the principle of the standard Fourier transform and was eventually developed to solve the shortcomings of the classical FFT in the analysis of real non-

stationary signals of short duration. In other words, the STFT is introduced to describe real signals in a way that allows the FFT to be adapted to the non-stationary framework (the FFT is a stationary tool). This consists of multiplying the source signal $x(t)$ by a function $g(t)$, called the "weighting window":

$$X(\tau,\omega) = \int_{-\infty}^{+\infty} x(t)\, g(t-\tau) e^{-2\pi\omega i} d\tau \qquad 3.20$$

where τ is the time location parameter of the weighting window g and the expression $[X(\tau,\omega)]^2$ represents the "spectrogram" in the time-frequency plane. According to Heisenberg's uncertainty principle, STFT suffers from a large resolution problem where the signal is estimated to be stationary for the duration of the window, and the window size has a direct influence on the time and frequency resolution. In other words, when the window size g is large, the frequency resolution is high but the time resolution is poor due to the loss of a large amount of time information, and vice versa.

3.4.4.2 Wavelet Transform (WT)

Because of the limitations of the Fourier and Gabor transforms (STFT), in the early 1980s, physicists and mathematicians introduced the wavelet transform, which decomposes the signal into both time and frequency and introduces a window whose size varies with frequency [135], [136].

The term wavelet refers to a function $\psi \in L^2(\Re)$ that oscillates on an interval of finite length, hence with a zero integral. Beyond this, the function decreases very quickly towards zero. It is normalised at $\psi = 1$ and satisfies the admissibility condition.

Proposed by Morlet in a series of articles published in the early 1980s [137], [138], [139]. The WT wavelet transform uses the wavelet basis function, unlike the sinusoidal functions used in Fourier analysis.

This method decomposes the vibration signal into a series of dilated or undilated wavelets that are localised in time, giving good temporal resolution at high frequencies and good frequency resolution at low frequencies.

The basic element of WT is the oscillating function $\psi_{a,b}(t)$, also known as the "mother wavelet", and it is characterised by a dilation coefficient b and a scaling coefficient a:

$$\psi_{a,b}(t) = \frac{1}{\sqrt{a}} \psi\left(\frac{t-b}{a}\right) \qquad 3.21$$

Its Fourier transform $\hat{\psi}(f) = 0$ if frequency $f < 0$.

Below are the wavelet families in Table 3.3, which remains a very interesting source of wavelet shapes.

Table 3.3 *Wavelet family [Matlab].*

Wavelet	Symbol
Haar	haar
Daubechies	db
Symlets	sym
Coiflets	coif
BiorSplines	bior
ReverseBior	rbio
Meyer	meyr
DMeyer	dmey
Gaussian	gaus
Mexican_hat	mexh
Morlet	morl
Complex Gaussian	cgau
Shannon	shan
Frequency B-Spline	fbsp
Complex Morlet	Cmor

3.4.4.2.1 Continuous wavelet transforms

The Continuous Wavelet Transform (CWT) is an implementation of the wavelet transform using arbitrary scales and practically arbitrary wavelets. The wavelets used are not orthogonal, and the data obtained by this transform are highly correlated [140], [141], [142].

In principle, the continuous wavelet transform works by directly using the definition of the wavelet transform, i.e., by calculating the convolution of the signal by the scaled wavelet.

In this way, we obtain for each scale a set of length N identical to that of the signal. Using M arbitrarily chosen scales, we obtain an $N \times M$ matrix directly representing the time-frequency plane. The algorithm used for this calculation can be based on direct convolution or convolution by multiplication in Fourier space (also known as the fast wavelet transform).

The choice of wavelet used for the time-frequency decomposition is the most important point. This has an influence on the time and frequency resolution of the result. We cannot modify the characteristics of the wavelet transform in this way (low frequencies have good frequency resolution but poor time resolution; high frequencies have good time resolution and poor frequency resolution), but we can increase the total frequency resolution or the total time resolution. This is directly proportional to the width of the wavelet used in real space and in Fourier space [141], [142].

The continuous wavelet transforms (CWT) of any signal $x(t)$ is expressed by:

$$CWT(a,b) = \frac{1}{\sqrt{a}} \int_{-\infty}^{+\infty} X(t) * \psi * \left(\frac{t-b}{a}\right) dt \qquad 3.22$$

This transform is continuous with respect to the dilation, translation, and rotation parameters and possesses certain properties, including conservation of energy (like the Fourier

transform), meaning that there is no loss of information between the function and its transform, the linearity of the transform, and invariance by translation and rotation. It is displayed in the form of a time-frequency energy map by calculating the scalogram $|W_x(a,b)|^2$.

3.4.4.2.2 Discrete wavelet transforms

It is adapted in the case of a discrete set and is then called the discrete wavelet transform. The Discrete Wavelet Transform (DWT) is an implementation using a discrete set of wavelet scales and translations obeying certain rules. This transform decomposes the signal into a set of mutually orthogonal wavelets, which is the main difference with the continuous wavelet transform, or its implementation in discrete-time series, sometimes called the discrete-time continuous wavelet transform (DT-CWT) [141], [142].

The discrete wavelet transform (DWT) is the discretisation of the scaling and dilation coefficients in the CWT. Using 2^{n} and $n2^{m}$ instead of the parameters a and b, the DWT can be described as follows:

$$DWT(m,n) = 2^{-\frac{m}{2}} \int_{-\infty}^{+\infty} X(t) * \psi * \left(2^m(t-n)\right)dt \qquad 3.23$$

The major disadvantage of the wavelet transform is the problem of choosing the right mother wavelet when analysing the vibration signals from the sensors in the case of defects that evolve gradually. This has prompted researchers to develop a more advanced technique based on adaptive wavelets.

3.5 Diagnostics based on artificial intelligence methods

One of the first people to tackle the subject of artificial intelligence (AI) was John McCarthy, a researcher and professor at the famous Massachusetts Institute of Technology, Stanford University, and Princeton University. In 1971, he received the Turing Award for his research work and his many contributions to AI and the development of intelligent systems.

The term AI was first introduced by J. McCarthy in 1955, and the basic premise of this approach is to make computer programs that attempt to imitate human reasoning in order to make machines intelligent through science and engineering [143]. In this way, using mathematics such as Boolean logic and probability, we can make a programme intelligent so that it decides on the appropriate sequence of events or makes a final decision.

The set of components of the AI branches can be presented as a combination of:

- Logique : le potentiel de juger d'une situation spécifique à l'instant t + 1 grâce au traitement des informations acquises à un instant t par un ensemble de relations mathématiques logiques.
- Similarity recognition: using appropriate tools, the computer (the program) recognises similarities between two specific situations on the basis of monodimensional and even multidimensional shapes.
- Inference: this is logical deductive reasoning based on the program's knowledge.

– Search: thanks to the high computational power of computers, it is possible to estimate the most likely event from a large set of possible situations in a short space of time based on past actions.

These branches of AI have enabled us to design effective tools, such as evolutionary algorithms [144] and classification algorithms [145], [146], [147], [148], which are widely used in scientific research and industrial applications in various fields. Based on this fact, this study aims to exploit the potential of AI techniques and merge them with the CWTs techniques in the context of automating the fault diagnosis process.

This part of chapter will be devoted to the intelligent diagnosis approach, in which its various stages will be described, followed by a literature review summarising the main AI methods currently used in the interests of an effective maintenance strategy and guiding the work carried out in subsequent chapters.

3.5.1 Intelligent fault diagnosis strategy

As mentioned in the first chapter, there are two main approaches to fault diagnosis for rotating machines, namely model-based diagnosis and model-free diagnosis.

Model-based diagnosis is generally based on the principle of mathematical modelling of the system to be monitored, with the aim of describing its behaviour and also the various failure modes that can affect its operation. This approach can be more effective than model-free approaches only if a correct and accurate model is built to mimic the actual behaviour of the machine under normal operating conditions and even in the presence of one or more faults.

Building an explicit model is not always easy or even impossible, especially in the case of systems with complex structures. To overcome this drawback, model-free diagnostics, or, more precisely, "diagnostics based on external methods," have been developed. This approach attempts to bypass mathematical models directly by exploiting condition monitoring data collected by sensors from the various information sources discussed earlier in Section 3.3.

The major advantage of intelligent fault diagnosis is that its calculations can be carried out by programming and generally comprise three crucial stages:

1. Extraction of indicators containing fault signatures.
2. Selection and reduction of the dimensionality of the indicators.
3. Fault classification using classifiers.

3.5.1.1 Extraction of defect indicators

Data acquisition is the most basic stage, involving the collection and processing of signals by a sensor system. These collected signals contain both useful information and useless, noisy content due to severe conditions linked to the machine's environment.

The extraction of information relating to the health of the machine comes after the data acquisition stage. It consists of extracting a set of statistical parameters that can truly reflect the operating state of one or more components of the system being monitored. These extracted

parameters are also called health indices, and they should be indicators of any change or evolution over time in the machine's operating mode.

Several indicators can be calculated from signals from different information sources, such as temporal descriptors (discussed in Section 3.4.1), such as root mean square (RMS), skewness, crest factor, kurtosis, standard deviation, and so on [149], [150]. The FFT peaks, the frequency band energy, and the power spectrum are important characteristics of the frequency domain, as are the wavelet coefficients, which are considered to be time-frequency state descriptors widely used by researchers.

It is not always common to keep or maintain a large number of statistical indicators in the diagnostic task. Some of these parameters are very sensitive to the occurrence of a fault and may even indicate the presence of a fault at an early stage, while other descriptors may not be so sensitive and are considered to be disruptive, harmful, or redundant elements that degrade diagnostic performance in the classification phase.

The sensitivity of these indicators depends on both environmental and operational conditions.

When calculating characteristics that are insensitive to external factors, there will be a trade-off between sensitivity and fault detection capability [151]. It is very important to use advanced signal processing methods to reduce the noise contained in the signals before the information extraction stage, which improves the quality of the extracted state descriptors and makes the monitoring operation more efficient [152].

3.5.1.2 Indicator selection and transformation for dimensionality reduction

The size of the extracted indicators or data is one of the major problems associated with data representation. This problem has an explicit effect on storage capacity, the cost of calculation (the speed of the algorithm), and can even degrade the performance of fault prediction.

There are two main approaches dedicated to reducing the representation space of indicators, which allow us to overcome any undesirable impacts and eventually have a better understanding and visualisation of these data.

- **Approach 01: selection of indicators**

This is an approach based on the selection of a set of characteristics extracted from their complete set. In other words, this approach selects the most discriminating subset of indicators from the initial set of available indicators.

This improves the quality of the descriptors, eliminates irrelevant elements, and removes any possible redundancy, which helps to discriminate and characterise each of the classes studied in the application. Selection approaches fall into three main groups:

- **The filter approach:** is based on the use of statistical measures deduced from the initial indicators to filter out irrelevant or uninformative indicators. These measures include similarity, dependency, and correlation.

  Filter methods are characterised by their speed, their robustness to overlearning, and their low computational complexity compared with other methods. The major disadvantage of this approach is that it does not take into account the relationship between indicators and is geared much more towards selecting descriptors containing redundant information than complementary information.
- **The wrapper approach:** this is the most widely explored and used approach. It is based on supervised learning, incorporating machine learning (ML) algorithms to select the most informative indicators.

  The main objective of wrappers is to search the space of indicator subsets and take the decision to add or remove an indicator from the subset by calculating the estimated accuracy using a predefined learning algorithm.

  This means that they evaluate the quality of a set of features selected via a specific classifier. This approach is more expensive in terms of computing time than the filter approach, but it is more reliable and accurate.
- **Embedded approach:** the principle is to incorporate the feature selection task into the learning and classifier construction operations.

➢ **Approach 02: transformation of indicators**

This is an approach based on transforming indicators from their original space into a reduced representation space. This principle involves creating new sub-sets of non-physical or synthetic characteristics, moving from their original representation space to a new, lower-dimensional space without losing much information. This transformation eliminates disruptive or redundant elements from the original dataset, which can have an undesirable effect on diagnostic performance, such as unnecessarily increasing computation costs and reducing classification accuracy.

3.5.1.3 Fault classification

3.5.1.3.1 Conventional statistical training

The first difficulty encountered when developing a fault monitoring system using classical learning tools is the need to manually extract the relevant indicators that must contain the fault signatures. This means that achieving an effective diagnosis with the desired performance implicitly depends on the quality of the extracted descriptors. Unfortunately, the probability of having a set of indicators that are insensitive to faults, redundant, or incomplete is extremely high. Consequently, as much information as possible must be studied and extracted from the signals collected before a satisfactory description of the data can be found. After the task of selecting significant indicators, a feature vector is constructed to be used as an input to a precise model for learning and classification purposes.

Conventional learning methods that are widely used in the fault diagnosis task include SVMs and ANNs.

3.5.1.3.2 Support Vector Machine (SVM)

Support vector machines, also known as wide margin separators, deal with binary classification problems, where their basic context is to find the optimal separating hyperplane between two classes based on the maximised margin criterion, as illustrated in Figure 3.3. In addition, these algorithms use the kernel function to find a better-separating hyperplane by transforming the data from one space to another [153].

Let the training set of n examples be: (x_i, y_i) where $i \in [1, n]$, and $x_i \in \mathbb{R}$; x_i belongs to a class labelled by y_i ; such that: y_i must have only two values $+1$ or -1.

The optimisation problem consists in maximising the margin separating the classes [154], and it can be defined by the following mathematical formula:

$$min_{m,n}\left\{\frac{1}{2}\|\omega\|^2 + C\sum_{i=1}^{l}\xi_i\right\} \quad 3.24$$

$$under\ pressure : \begin{cases} y_i(\omega . X_i - b) \geq \xi_{i'} & i = 1, \dots l \\ \xi_i \geq 0 & i = 1, \dots l \end{cases} \quad 3.25$$

Where C denotes the penalty parameter and ξ the spring variable relaxing the constraints on the training vectors. Revising the optimisation problem in terms of the Lagrangian multiplier leads to equation 3.26:

$$maximise : \tilde{L}(\alpha) = \sum_{k=1}^{n}\alpha_k - \frac{1}{2}\sum_{i,j}\alpha_i\alpha_j y_i y_j \alpha_i x_i^T x_j \quad 3.26$$

$$under\ pressure : \begin{cases} \alpha_k \geq 0 \\ \sum_{k=1}^{n}\alpha_k\, y_k = 0 \ \ et \ \ k = 1,2, \dots n \end{cases} \quad 3.27$$

For non-linear cases, we introduce Kernel cores and the formula for the hyperplane will be defined by:

$$f(x) = sign\left(\sum_{k=1}^{n}\alpha_k\, y_k K(x_i, y_i) + b\right) \quad 3.28$$

$$such\ as: \begin{cases} \omega = \sum_{i=0}^{N}\alpha_i x_i y_i \\ y_i(\omega^T . x_i + b) - 1 = 0 \end{cases} \quad 3.29$$

where $K(x_i, y_i)$ represents the "Kernel" function, and α_i represents the Lagrange multiplier. The most commonly used Kernel functions include the polynomial function, the Gaussian radial basis function (RBF), and the sigmoid function.

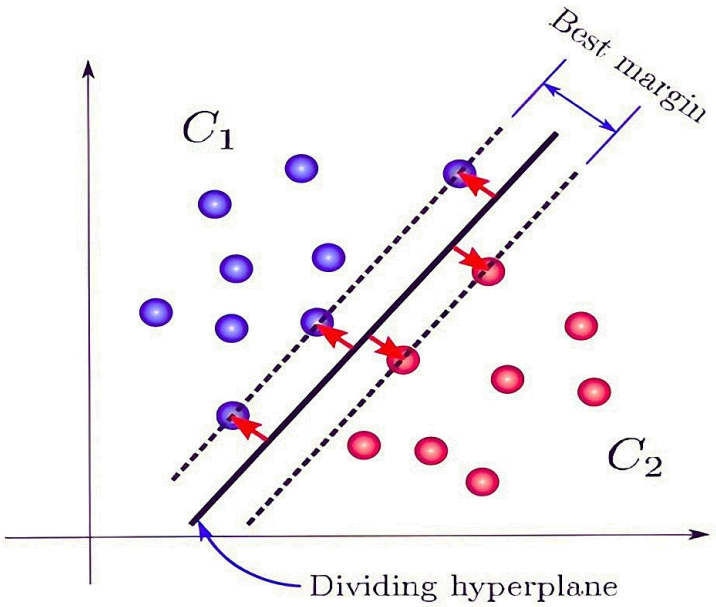

Figure 3.3 *An example of a separating hyperplane for a binary classification using the SVM tool.*

The SVM described above can only solve classification problems belonging to two class categories (positive or negative).

In reality, we often encounter multi-class problems, especially in applications related to monitoring the state of defective bearings. Therefore, the use of a multi-class SVM is a prerequisite. In recent years, two strategies have emerged to overcome this challenge. These two methods are detailed below:

- **One versus One (OVO) strategy**

This technique is used to solve multi-class classification problems using SVM algorithms. It is known as the "One-Versus-One method". This algorithm constructs $k(k-1)/2$ hyperplanes where each class is trained on a dataset spanning two classes.

Learning from the dataset of i^{th} and j^{th} classes, can be solved as a binary classification problem.

$$minimise: \frac{1}{2}\left\|\omega^{ij}\right\|^2 + C\sum_t \xi_t^{ij}\left(\omega^{ij}\right)^T \qquad 3.30$$

$$under\ pressure: \begin{cases} \left(\omega^{ij}\right)^T \phi(x_t) b^{ij} \geq 1 - \xi_t^{ij} \quad si \quad y_t = i, \\ \left(\omega^{ij}\right)^T \phi(x_t) b^{ij} \leq 1 - \xi_t^{ij} \quad si \quad y_t = j, \\ \xi_t^{ij} = 0, \quad j = 1, \ldots, l \end{cases} \qquad 3.31$$

Several methods are exploited to test the $k(k-1)/2$ classifiers constructed. After testing, the model choice decision is made using a strategy known as Win-Max:

$sign\left(\left(\omega^{ij}\right)^T \phi(x_t) b^{ij}\right)$, indicates that x is in the i^{th} class.

Then the vote for the i^{th} class is increased by one. Otherwise, it will be increased for the j^{th} class and x is predicted based on the class with the most votes. Figure 3.4 shows the MCSVM classification process with the OVO technique for a problem of N classes.

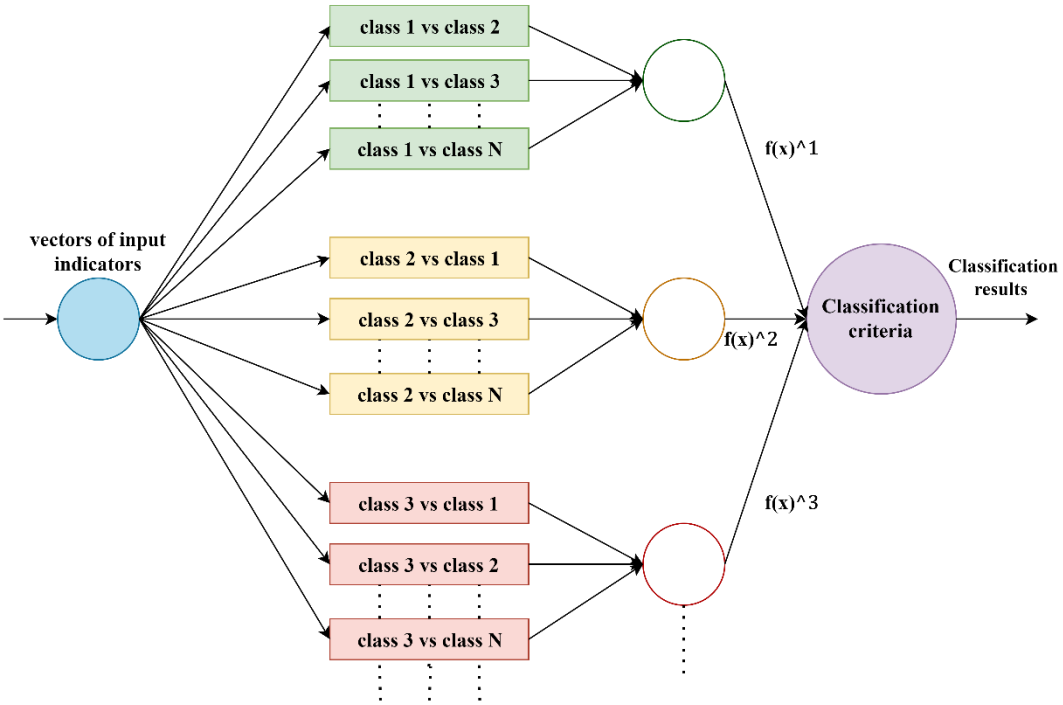

Figure 3.4 *MCSVM with the One-On-One (OVO) technique.*

- **One Against All (OVA) strategy**

This technique is called the "One-Versus-All method" and involves creating a number k of SVM models equal to the number of classes encountered in the problem.

The i^{th} SVM model is built by taking one class (labelled positive) and treating all other examples as another class (labelled negative). Then, the process is repeated for each class.

For a given training data set $l:\ (x1, y1), \ldots\ \ldots, (xl, yl)$, where $x_i \in \mathbb{R}^n$, $i = 1, \ldots, l$ and $y_i \in 1, \ldots, k$ is the class of x_i, the i^{th} SVM model can solve the problem below:

$$minimise: \frac{1}{2}\|\omega^{ij}\|^2 + C\sum_{i=1}^{l}\xi_t^i(\omega^i)^T \qquad 3.32$$

$$under\ pressure: \begin{cases} (\omega^i)^T\phi(x_j)b^i \geq 1-\xi_j^i & si \quad y = i, \\ (\omega^i)^T\phi(x_j)b^i \leq 1-\xi_j^i & si \quad y \neq j, \\ \xi_j^i = 0, \quad j = 1, \ldots, l \end{cases} \qquad 3.33$$

where C is the penalty parameter.

The model training data x_i, is mapped to a higher dimensional space by function ϕ. The minimisation of equation 3.32, maximises the margin $^2/_{\|\omega i\|}$ between two groups of data when the dataset is not linearly separable and the penalty parameter reduces the learning error.

Once the MCSVM model is designed and ready for use, the various test results (equal to the number of classes) are processed by applying a sum. Then, the final classification result is deduced by choosing the most probable solution. Figure 3.5 shows the resolution of a problem involving the classification of *N* classes by MCSVM using the OVA technique.

Multi-class SVM is a supervised learning algorithm that is widely used to monitor the health of rotating machinery. Generally, this method takes as input the vector of significant characteristics to classify the various faults encountered in a specific problem. It has been used to classify various bearing faults in numerous studies [155], [156], [157], [158].

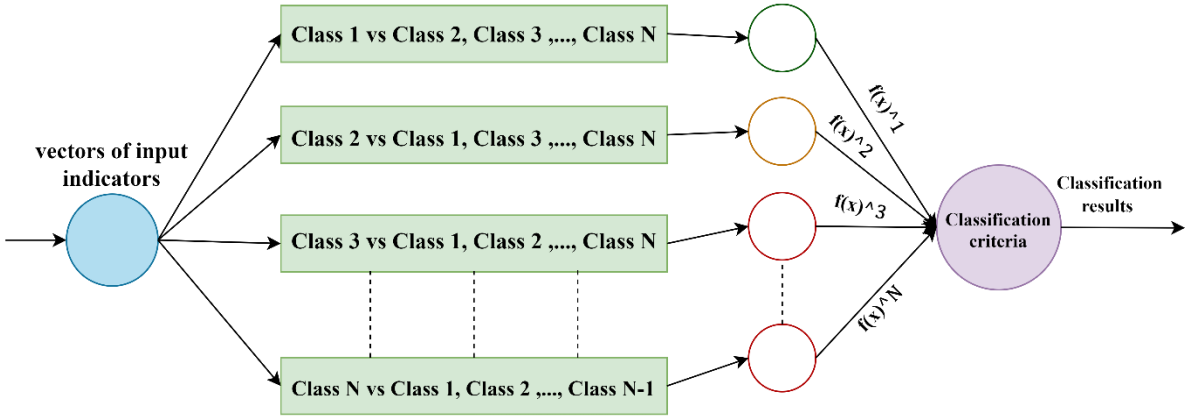

Figure 3.5 *MCSVM with the One Against All (OVA) technique.*

SVMs are commonly used in combination with other techniques to classify faults in induction machines [159], [160].

Recently, machine learning based approaches using techniques such as support vector machines (SVMs) have gained popularity for intelligent bearing fault diagnosis. Chen et al. [161] proposed using a multi-kernel SVM to classify three types of bearing defects - roller, inner race, and outer race defects. They achieved a classification accuracy of 94%.

Hwang [162] extensively compared various multiclass SVM formulations including one-vs-all (OVA), one-vs-one (OVO), and directed acyclic graph SVMs (DAG-SVMs) for bearing fault classification, finding DAG-SVMs to provide the best performance in most test cases.

More advanced variants like one-class SVMs have also been explored for their anomaly detection capabilities in condition monitoring applications. Rego et al. [163] applied a one-class SVM classifier with Gaussian kernels for fault detection of rolling element bearings, obtaining 96% accuracy for various bearing faults.

Expanding on these works, [164] develop a methodology using stationary wavelet packet transforms for feature extraction combined with one-class SVMs for multiclass classification of bearing defects under varying motor loads. In experimental evaluation with outer race, inner race and cage defects, they demonstrate 100% classification accuracy using the proposed approach with Symmlet kernel wavelet function, outperforming other SVM variants.

Additionally, the use of different SVM learning algorithms, such as cubic and Fine Gaussian SVM, has shown high accuracy in prediction time [165]. Therefore, SVMs are frequently used in fault detection and classification in induction machines due to their reliability and ability to improve the performance of classifiers.

3.5.1.3.3 Artificial Neural Network (ANN)

ANNs have been developed on the basis of a basic principle of information processing similar to that of the human brain. An ANN network consists of an input layer, one or more hidden layers, and an output layer. Each layer contains a number of neurons, which are considered to be computational units in the network (see Figure 3.7). The neuron receives inputs and multiplies each input by its weight. The multiplication results are then combined and transformed by an activation function to generate the neuron's output.

Let an ANN have M input neurons activated by an input vector x (of dimension M), and by $w_{i,j}^{0,1}$ the weight corresponding to the connection between neuron i of layer 0 and neuron j of layer l; the output Y_j^1 of each of the neurons of the first hidden layer will be expressed by equation 3.34:

$$Y_j^1 = f_j\left(\sum_{i=1}^{M} w_{i,j}^{0,1}\, x_i + b_j^1\right) \qquad 3.34$$

Where b_j^1 is the bias and f_j represents the activation function, which may be a sigmoid, hyperbolic tangent or piecewise linear function.

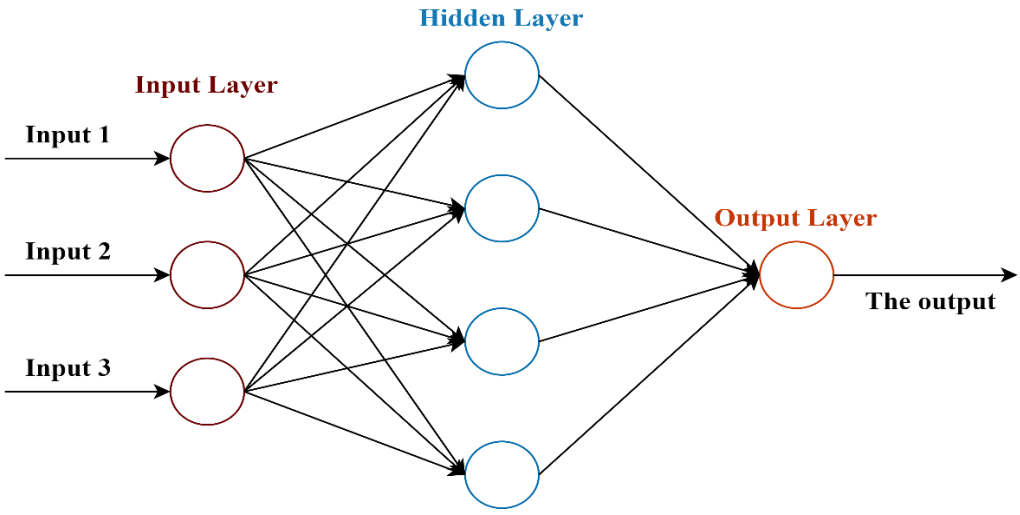

Figure 3.6 *An example of an artificial neural network.*

The same process expressed by equation 3.34 can be repeated for the other hidden layers or the output layer, such that each output of a layer l will be the input of the next layer $l + 1$.

The generalisation of equation 3.35 to all subsequent layers is defined as follows:

$$Y_j^{l+1} = f_j\left(\sum_{i=1}^{L} w_{i,}^{l,l+1} x_i^l + b_j^{l+1}\right) \qquad 3.35$$

where L is the number of neurons in layer l.

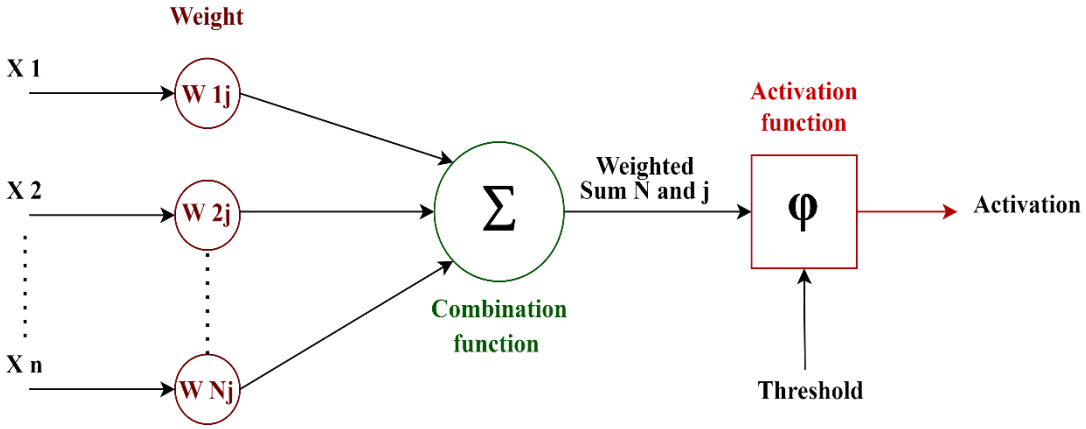

Figure 3.7 *Artificial neuron model.*

There are different types of artificial neural networks, for example: multilayer perceptrons (MLP), radial basis function networks (RBF), probabilistic neural networks (PNN), recurrent neural networks (RNN), etc.

The criteria that enable us to distinguish between these networks include the architecture of the network (for example, the type and number of layers), its level of complexity (such as the presence or absence of a feedback loop), etc.

3.5.1.3.4 Deep learning (DL)

As seen in the previous literature, conventional machine learning methods have shown significant effectiveness in fault diagnosis, but they have the disadvantage of limiting the learning capacity of the classifiers because they do not have the ability to process natural data (sensor data) in its raw form. This shows that these methods have difficulty learning or processing complicated non-linear relationships linked to the presence of a fault. As a result, the ability of classifiers to discriminate between classes is reduced, implying a high susceptibility to error in the classification phase. This generally depends on the extraction and selection phases of the relevant features, which require knowledge of signal processing techniques, considerable expertise, and in-depth knowledge in order to transform the raw data into an appropriate internal representation from which the classifier can effectively detect and classify defects.

Deep learning (DL) algorithms are part of the ML family and use deep architectures based on the layers used in ANNs, with the ability to automatically extract several sophisticated

indicators or hierarchical representations from raw data without the need for manual extraction or intervention by a domain expert.

The DL approach has the potential to overcome the shortcomings of conventional methods, making it possible to implement algorithms to create reliable monitoring and diagnostic systems for detecting faults affecting rotating machinery with high performance. This approach is increasingly rich, encompassing supervised and unsupervised learning algorithms, a variety of neural networks with different processing layers, and hierarchical probabilistic models.

Among the most powerful tools in the DL approach are convolutional neural networks (CNNs), which will be described in the next section.

3.5.1.3.5 Convolutional neural networks (CNN)

CNNs were first proposed by [166] for image processing and are considered to be a deep neural network model with an acyclic structure (feed-forward structure) whose weights and biases can be adjusted by learning.

These networks have powerful feature extraction capabilities thanks to their mesh-like structures designed for processing multidimensional data. This analysis quality can be summed up in three key properties: sparse connectivity (local receptive fields), a weight-sharing mechanism, and sub-sampling of the data dimension in the spatial domain, which considerably reduces the quantity of training parameters and avoids the risk of over-learning the algorithm.

A typical CNN architecture consists of three types of layers: the convolution layer, the subsampling layer, also known as the "clustering layer," and the fully connected layer.

- **The convolution layer (CL)**

is the basic building block of CNNs. This layer convolves the input indicator map with a heap of kernels in order to generate many new indicator maps as input to the next layer, where the results of the convolution operations are subjected to the activation function to obtain the output.

In general, the mathematical model of CL can be described by the following equation:

$$x_j^l = f\left(b_j^l + \sum_{i \in M_j} x_i^{l-1} * k_{ij}^l\right) \qquad 3.36$$

where $(*)$ defines the convolution operator, M_j illustrates the input map selection, l denotes the index of the l^{th} layer of the network, k is the kernel matrix (the convolution filter) of size $S \times S$, b is the bias, x represents the indicator map generated from the $(l-1)^{i^{th}}$ layer and f is the non-linear activation function.

The activation functions that are commonly used in CNN networks are the sigmoid function, the hyperbolic tangent and the rectified linear unit function (Relu), which has good

adaptability leading to low network density, which considerably improves the speed of calculation and effectively prevents gradient elimination.

The mathematical expressions defining the most common activation functions are shown in Table 3.4.

Table 3.4 *The activation functions most commonly used in CNN networks.*

Name of the function	Expressions
Relu	$f(x) = \begin{cases} x, & x \geq 0 \\ 0, & x < 0 \end{cases}$
Sigmoid	$f(x) = \frac{1}{1 + e^{-x}}$
Tanh	$f(x) = \frac{1 - e^{-2x}}{1 + e^{-2x}}$

- **The Subsampling Layer (SL)**

also known as the **Pooling Layer**, is located behind the Convolution Layer, where the input to the SL is the output of the CL. Its function is to progressively reduce the size and quantity of trainable parameters in a CNN. As a result, it reduces the computation for the higher layers and improves the computational capacity of the network.

The SL can be described mathematically by the following equation:

$$x_j^l = f\left(\beta_j^l down\left(x_j^{l-1}\right) + b_j^l\right) \qquad 3.37$$

where $\boldsymbol{down}(.)$ represents the subsampling function. This function sums each n block by n distinct in the input image such that the output image is n times smaller of the two spatial dimensions. Each output indicator map receives its own multiplicative bias β and additive bias b.

There are several pooling functions, such as: average, L2 norm, distance-weighted average of the central pixel, etc. However, the most commonly used function in CNNs is maximum pooling, or max-pooling, which selects the maximum of the restriction region as a new feature for later use in subsequent layers.

- **The Fully Connected Layer (FL)**

is a classical forward propagation neural network that is used in the classification stage of the CNN architecture. It generally uses the SoftMax function as the activation function in the output of the network.

The SoftMax function is defined by the following equation:

$$\sigma(z)_j = \frac{e^{zj}}{\sum_{k=1}^{K} e^{zk}} \quad , \quad For\ j = 1, \dots, K \qquad 3.38$$

In the FL layer, all the neurons between the layers are interconnected, as defined by equation 3.39 :

$$O(x) = f(W.X + b) \qquad 3.39$$

Where $f\ (*)$ is the activation function, X is the input of the fully connected layer, $O(X)$ is the output of FL, and W and b are the weights and biases, respectively.

The aim of FL is to collect all the features of the indicator sub-maps generated by the previous layer for classification. The final output is a one-dimensional vector, where each value of this $1D$ vector is a quantitative value of the n classification.

Convolutional neural networks (CNNs) have been the focus of significant research attention, proving highly effective in addressing pattern recognition and computer vision challenges [167]. Their application has been pivotal in the development of high-performance monitoring systems for diagnosing faults in rotating machines, especially bearing faults, highlighting their role in advancing diagnostic techniques. These advancements are crucial for the early detection of faults in motors, a key factor in ensuring the reliability and efficiency of machinery widely used across various industries. Recent studies leveraging CNNs have shown promising results in accurately identifying bearing faults, thereby preventing potential downtimes and extending the motors' service life. This integrated discussion combines insights into the methodologies, results, and contributions of innovative approaches to bearing fault diagnosis, reflecting the substantial impact of CNNs in this field.

Jiménez and MP [168] introduced a novel diagnostic methodology that combines maximal overlap discrete wavelet transform (MODWT) with a lightweight 1-D CNN architecture. This approach focuses on detecting both mechanical and electrical faults, including bearing defects, in adjustable speed drive (ASD)-powered induction motors. Their methodology demonstrated remarkable accuracy, exceeding 99%, in identifying single and combined faults under various operating conditions, emphasizing the efficiency of integrating MODWT with CNN for fault diagnosis.

In a parallel study, [169] explored a hybrid motor-current data-driven approach that leverages statistical features, genetic algorithms, and machine learning models to diagnose bearing faults. By optimizing feature selection through genetic algorithms and employing machine learning classifiers, their approach achieved an accuracy of over 97%. This study underlines the potential of combining genetic algorithms with machine learning to enhance diagnostic accuracy and reduce computational complexity.

Yilmaz [170] offered a comparative analysis of two fault detection techniques, namely the Park transform approach and the Concordia transform, for diagnosing bearing failures. Through experimental tests on a motor with artificially induced bearing damage, Yilmaz highlighted the effectiveness of these techniques in detecting and diagnosing bearing failures

in small- and medium-sized induction motors, providing valuable insights into their practical applications.

Further extending the diagnostic methodologies to acoustic signal analysis, A.Głowacz [171] and A.Głowacz with W.Glowacz, Z.Głowacz, and Kozik [172] both presented methods based on analysing acoustic signals for fault diagnosis. These studies developed feature extraction methods, such as SMOFS-22-MULTIEXPANDED and MSAF-20-MULTIEXPANDED, and utilized various classifiers to diagnose bearing, stator, and rotor faults. Their findings indicate that acoustic signal analysis, coupled with sophisticated feature extraction and classification techniques, can offer a viable solution for fault diagnosis in induction motors.

3.5.1.3.6 Other deep learning methods

Predictive maintenance (PdM) is a strategic approach that leverages data analysis tools and techniques to predict equipment failures before they occur, thereby reducing maintenance costs and downtime. With the advent of Industry 4.0, the integration of deep learning algorithms in PdM systems has shown significant promise in enhancing predictive accuracy and operational efficiency. This literature review discusses several pioneering studies that have utilized deep learning algorithms such as Long Short-Term Memory (LSTM) networks, Deep Belief Networks (DBNs), Autoencoders (AEs), and convolutional approaches to advance predictive maintenance methodologies [173], [174], [175], [176], [177].

Wu, Huang, and Sutherland [174] explored the interpretability of LSTM-RNN decisions in predictive maintenance through layer-wise relevance propagation (LRP). Their study demonstrates how LRP can provide insights into the decision-making process of LSTM-RNN models, particularly in bearing health monitoring applications. This approach not only enhances model transparency but also contributes to the improvement of model accuracy and efficiency in predictive maintenance.

Chen et al [176] introduced a novel approach, Cox proportional hazard deep learning (CoxPHDL), to address challenges such as data sparsity and censoring in maintenance data analysis. By integrating deep learning with reliability analysis, their method enhances the prediction of Time-Between-Failure (TBF), showcasing the potential of combining advanced machine learning techniques with traditional reliability models for predictive maintenance.

Hu, Zhang, and Liang [177] proposed an opportunistic predictive maintenance-decision (OPM) method that combines machinery prognostic and opportunistic maintenance models with a DBN-HAZOP model. Their method quantifies hazard and operability analysis through dynamic Bayesian networks, offering a comprehensive approach to predictive maintenance that accounts for component interactions and environmental factors.

Susto, Schirru, Pampuri, McLoone, and Beghi [175] presented a multiple classifier machine learning methodology for predictive maintenance. By employing a variety of classifiers with different prediction horizons, their methodology enables dynamic decision

rules for maintenance management, particularly in high-dimensional and censored data environments.

Hsu, Lu, and Yan [173] developed a temporal convolution-based LSTM network with an attention mechanism for remaining useful life (RUL) prediction. Their method outperforms traditional approaches by effectively extracting features from equipment sensor data and learning temporal dependencies among these features, demonstrating the efficacy of combining convolutional and recurrent neural network architectures in predictive maintenance applications.

3.6 Conclusion

In this chapter, we explored the integration of signal processing methods and artificial intelligence for fault diagnosis in industrial and technical systems. We delved into various diagnostic strategies, emphasizing the importance of combining traditional techniques with advanced technologies such as machine learning and deep learning to enhance fault detection and diagnosis.

The chapter highlighted the significance of data acquisition from multiple sources, including vibration analysis, lubricant analysis, acoustic emission, and thermography, as the foundation of preventive maintenance. We discussed the role of statistical indicators and spectral analysis in processing vibration signals to extract meaningful information for fault diagnosis.

Furthermore, we examined the application of artificial intelligence methods, particularly machine learning algorithms like Support Vector Machines (SVMs) and Artificial Neural Networks (ANNs), in developing intelligent fault diagnosis systems. The potential of deep learning approaches, including Convolutional Neural Networks (CNNs) and Long Short-Term Memory (LSTM) networks, was also explored to automate the fault diagnosis process and improve predictive maintenance.

In conclusion, the integration of signal processing methods and artificial intelligence offers a promising avenue for developing more accurate and reliable fault diagnosis systems. By leveraging the strengths of both traditional and modern techniques, we can enhance the detection of faults and contribute to the overall reliability and efficiency of industrial and technical systems.

The next chapter, titled "Application to the Diagnosis of Bearing Faults in IM Based on CWT and CNN," will delve deeper into the practical implementation of these concepts, focusing on the diagnosis of bearing faults in induction motors using Continuous Wavelet Transform (CWT) and Convolutional Neural Networks (CNN).

Chapter 4 Applications to Failures Affecting Induction Motors

4.1 Introduction

Monitoring rotating machines requires expert knowledge of dynamics and kinematics, making early fault detection challenging. With industrial growth, automatic monitoring systems prioritize preventive maintenance. Integrating artificial intelligence into diagnostic systems offers a promising solution, particularly for bearing faults, which are crucial components in rotating machinery.

Indeed, research studies indicate that bearing faults are a major source of failures in electric motors. Das and Ray [178] highlight that bearing faults are the most common in induction motors and that various techniques have been developed to diagnose these faults. Significantly, Nandi [45] reported that 40 to 50% of all failures affecting electric motors are caused by bearing faults, highlighting the importance of monitoring the operational condition of bearings to maintain the reliability and productivity of machines. Gundewar and Kane [179] also estimated that the probability of bearing failure varies significantly, underscoring the variability and complexity of bearing faults in rotating machines. Kumar et al. [180] add that bearing faults can significantly increase the likelihood of failures unless adequate introspection is accomplished to detect these faults early and reduce downtime and operating costs.

This chapter is divided into two parts: The first part will see an experimental study on using vibration analysis for detecting mechanical degradation in induction motors. It highlights the effectiveness of vibration analysis in diagnosing faults with high accuracy and speed, which can be integrated into predictive maintenance programs using automation and artificial intelligence. The study employs Fast Fourier Transform (FFT) and Discrete Wavelet Transform (DWT) for signal analysis, demonstrating their utility in early fault detection.

With this in mind, in the second part we propose a method for diagnosing bearing faults based on the analysis of vibration signals collected from the MFPT data.

This part will be devoted to the novel approach for diagnosing bearing faults in induction motors using a combination of continuous wavelet transform (CWT) and convolutional neural networks (CNNs). The method involves using scalograms with various CWT types as input to the network, employing multiple epochs and batch sizes during the training and testing phases of bearing fault classification. The approach is evaluated using an extension of the SqueezeNet pre-trained model, demonstrating superior accuracy and computational efficiency in detecting bearing faults compared to traditional methods. The results, based on publicly available MFPT data, highlight the potential of this method in bearing fault diagnosis and open new avenues for research in this field.

4.2 Part 01: Vibration Analysis for Assessing Mechanical Problems in Induction Motors

4.2.1 Theoretical Context

Vibration analysis is a crucial technique in condition monitoring and fault diagnosis of rotating machinery, including induction motors. It involves the measurement and analysis of the vibration signals emitted by a machine to detect any anomalies that may indicate mechanical faults. Two commonly used methods in vibration analysis are the Fast Fourier Transform (FFT) and the Discrete Wavelet Transform (DWT), which have been effectively applied for fault detection in unbalanced rotor induction motors [181].

4.2.1.1 Fast Fourier Transform (FFT)

The Fast Fourier Transform (FFT) is a mathematical algorithm that transforms a time-domain signal into its frequency-domain representation. This transformation enables the identification of the various frequency components present in the vibration signal, which can be correlated with specific mechanical faults. For example, an increase in the amplitude at the rotational frequency of the motor may indicate an imbalance, while the presence of harmonics can suggest misalignment or bearing defects [182].

The occurrence of imbalance will lead to a vibration in a perpendicular plane, which includes a part of the spectrum that aligns with the rotational frequency f_r. The most notable part of this spectrum is the one with the base frequency corresponding to f_r, and it is typically represented by the largest peak at the lower amplitude harmonics [183], described by the equation:

$$f_{unbalance} = 1.f_r \tag{4.1}$$

When the machine structure is not adequately secured, it results in vibrations and noise. Often, the vibration spectrum of a machine with slackness shows prominent peaks at frequencies that are integer multiples of the rotational frequency. Additionally, there can be peaks at fractional harmonics of the rotational frequency, such as half the rotational frequency and its multiples [184], represented by the equation:

$$f_{loosening} = 1/2.f_r \tag{4.2}$$

4.2.1.2 Discrete Wavelet Transform (DWT)

The Discrete Wavelet Transform (DWT) is a sophisticated method for vibration analysis, exceptionally beneficial for assessing non-stationary signals. Unlike the Fourier Transform (FFT), which conducts a general frequency analysis, DWT presents a combined time-frequency depiction of the signal. This dual perspective allows for the identification of transient faults and specific shifts within the signal's behavior. DWT's ability to perform multi-resolution signal analysis through the function of frequency and time localization makes it an invaluable adjunct to FFT, offering a more nuanced examination of mechanical issues in induction motors [185]. Wavelet theory posits that any signal $S(s_1, s_2, \ldots s_n)$ can be

reconstructed as the sum of an approximation signal a_n at a particular level of decomposition n, and a series of detail signals d_j at the same level, using scales α and coefficients β. The functions ψ_i^n and ψ_i^j represent the decomposed function at level n and the wavelet function at level j, respectively. as encapsulated by the ensuing formula:

$$S(t) = \sum_i \alpha_i^n \psi_i^n(t) + \sum_{j=1}^{n} \sum_i \beta_i^j \psi_i^j(t) = a_n + d_n + \cdots + d_n \qquad 4.3$$

4.2.2 Experimental Context

The experimental study was conducted using a test bench specifically designed to simulate mechanical faults in induction motors, as shown in Figure 4.1. The test bench consists of a three-phase cage induction motor with the following specifications: power rating of 180 W, rotational speed of 2400 RPM, and a voltage rating of 220/380 V (Δ/Y configuration). The motor is coupled to a load to simulate real-world operating conditions. Vibration sensors are strategically placed on the motor housing to capture the vibration signals emanating from the motor during operation [186].

Figure 4.1 *Test Bench Configuration for Simulating Mechanical Faults in Induction Motors.*

4.2.3 Experimental Results and Discussion

4.2.3.1 FFT Approaches

Figure 4.2 depicts the vibration spectra of the motor in the healthy state and in the presence of combined faults: an unbalance fault in the shaft and a loosening fault. It is observed that the frequencies characterizing the repetitive shocks due to the faults clearly emerge (in red) at 20 Hz and 40 Hz when the motor speed is at 2400 rpm.

FFT vibration spectra of an induction motor in a healthy state (in blue) and with faults (in red), highlighting characteristic frequencies at 20 Hz and 40 Hz.

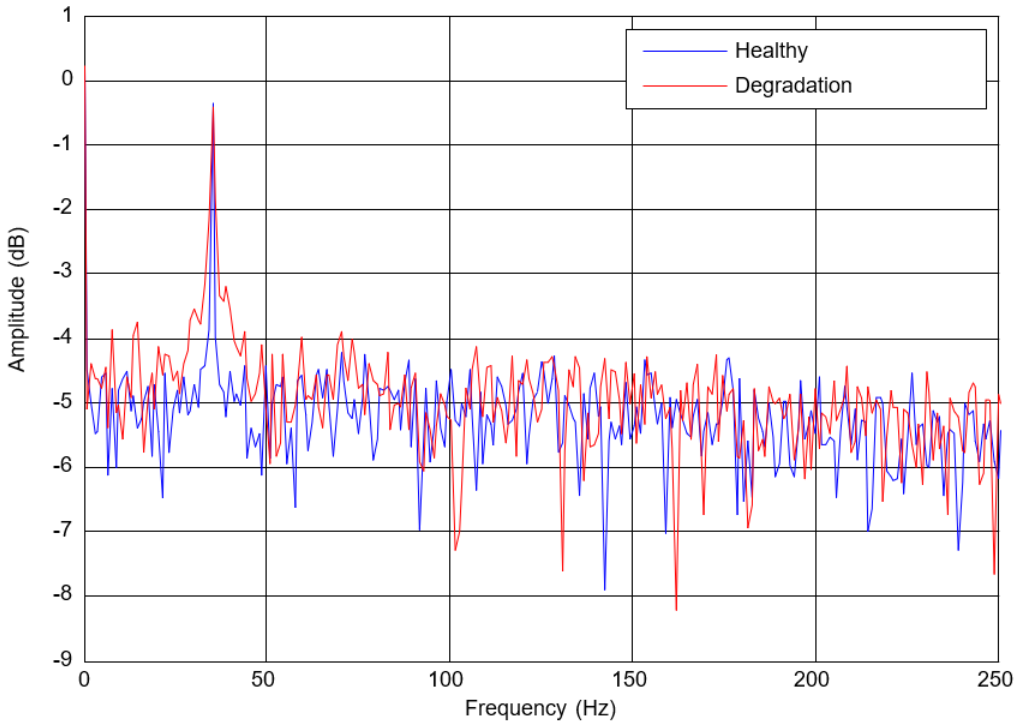

Figure 4.2 *FFT Vibration Spectra for Motor in Healthy and Faulty Conditions.*

The FFT analysis revealed significant differences in the frequency spectra of the motor in the healthy state compared to that with faults. In particular, the faults introduce distinct frequency components that can be clearly observed in the vibration spectrum. The peaks at 20 Hz and 40 Hz are indicative of the repetitive shocks associated with the unbalance and loosening faults. These results validate the FFT approach as an effective means to detect and diagnose mechanical faults in induction motors, offering a rapid and reliable method to anticipate potential failures.

4.2.4 DWT Approaches

The Discrete Wavelet Transform (DWT) was applied to the experimental signals to perform a time-frequency analysis. This technique is particularly effective for capturing transient behaviours in signals that may not be visible in the frequency domain alone [186].

4.2.4.1 Analysis of Healthy Motor Condition Using DWT:

Figure 4.3 illustrates the healthy motor condition signal decomposed using a 6-level DWT. The DWT analysis yielded several detail coefficients (D1 to D6), each corresponding to different frequency bands. For the healthy motor condition, the detail levels did not exhibit significant variations, aside from the initial oscillations that are characteristic of the motor's healthy operational state.

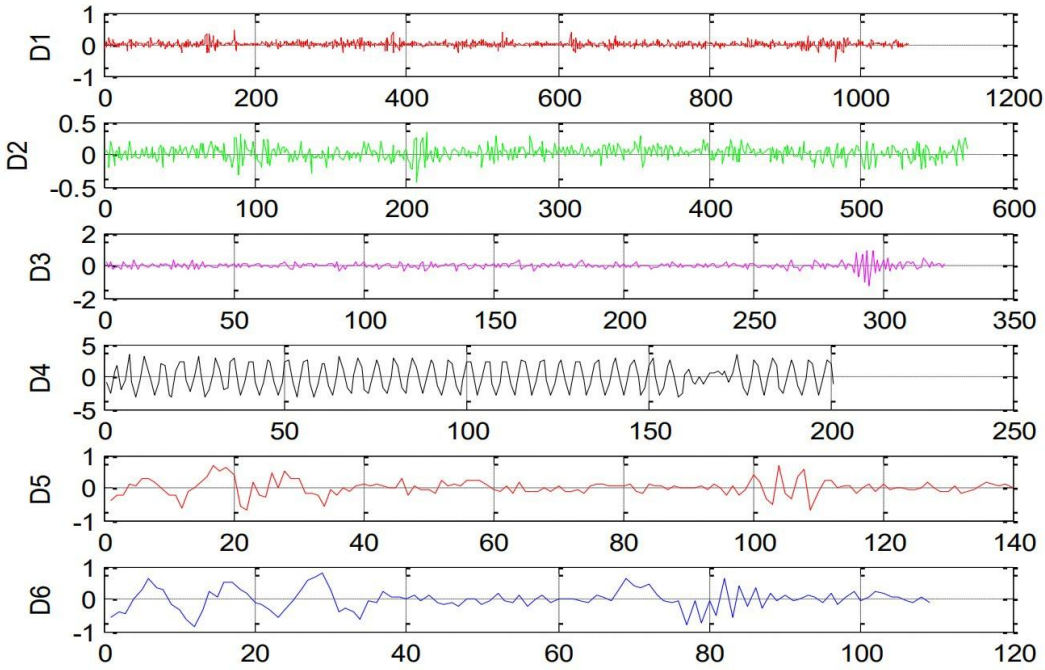

Figure 4.3 *6-Level DWT of Healthy Motor Signal.*

The lack of significant variations in the detail signals from the healthy motor's DWT analysis serves as a baseline for identifying anomalies. When faults are present, deviations from this baseline in the form of altered amplitudes or patterns in the detail coefficients can indicate specific mechanical issues. The DWT's multi-resolution analysis provides a diagnostic tool that is sensitive to both the magnitude and timing of such deviations, making it an indispensable part of the fault diagnosis process for induction motors.

The stability of the detail signals in the DWT analysis of the healthy motor also demonstrates the motor's lack of defects and the absence of transient behaviours that could suggest mechanical issues. This baseline is critical for comparative analyses when faults are introduced and for the development of automated diagnostic systems that can detect and predict mechanical failures in their early stages.

4.2.4.2 Analysis of Motor in Degraded Condition Using DWT:

When analysing the motor intentionally subjected to degradation, the Discrete Wavelet Transform provided insightful data. Figure 4.4 depicts the DWT results for the motor in a degraded state. Notably, there was a significant increase in the energy of the wavelet coefficients at the higher levels, specifically in the d3 and d4 detail signals. This increase was

observed when the motor operated at a lower speed of 2400 rpm, which is a condition often encountered in industrial settings.

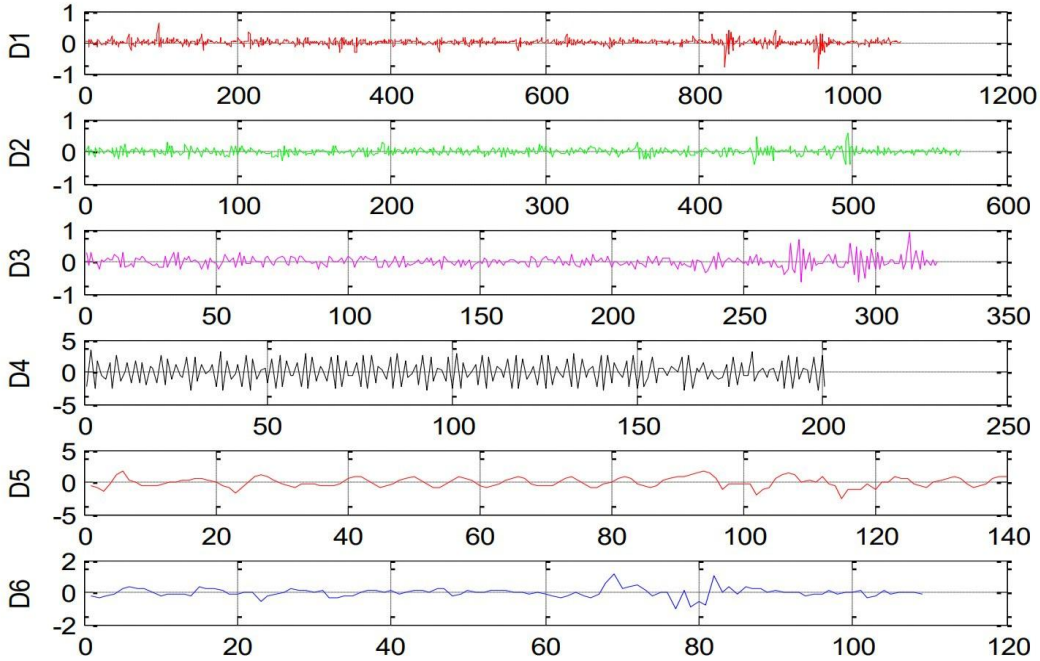

Figure 4.4 *DWT of Motor Vibration in Degraded State.*

The rise in energy levels within the d3 and d4 details signifies the motor's transition from a healthy to a degraded state. Such a change is indicative of the presence of faults and aligns with the expected behavior of mechanical degradations that impact motor performance. The oscillations within these specific DWT levels change in character, becoming more pronounced, which is not typically observed in the operation of a healthy motor.

This alteration in the signal's energy distribution across the wavelet detail levels provides a clear indication of degradation and can be used as a diagnostic feature for detecting and analysing mechanical faults. By comparing the DWT profiles of the motor in healthy and degraded conditions, it becomes possible to not only detect the occurrence of faults but also to infer their nature and potential impact on the motor's operation.

The ability of the DWT to capture these subtle changes at specific frequency bands demonstrates its advantage over traditional FFT analysis for certain types of mechanical faults, particularly those that manifest as non-stationary changes in the vibration signal. These findings reinforce the importance of employing a multi-faceted approach to vibration analysis, utilizing both FFT and DWT methodologies to ensure a comprehensive fault diagnosis.

4.3 Part 02: Fault diagnosis based on deep learning

4.3.1 Test bench for « MFPT »

The MFPT database is a valuable resource for predictive maintenance and diagnosis of rotating machinery, particularly rolling element bearings. It contains vibration records from bearings subjected to various health states and operating situations. The primary objective is to provide benchmark data for the development and validation of algorithms in this field. The dataset includes multiple sets of data, each corresponding to a certain type of failure and different operating situations. Vibration recordings are made using sensors placed on or near the bearings, allowing the capturing of vibration fluctuations based on the conditions [187].

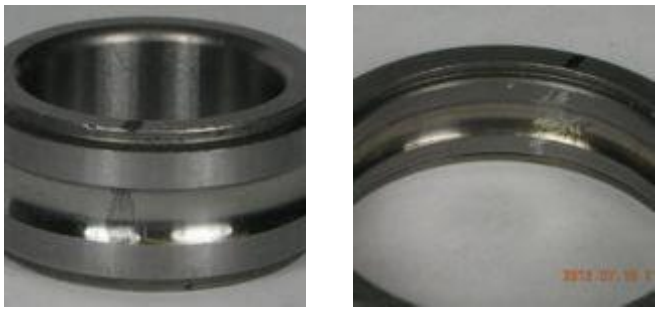

(a) (b)

Figure 4.5 *defective bearings: (a) Inner race defect (b) Outer race defect.*

The Bearing Fault Dataset is an invaluable resource for conducting research on bearing analysis. The dataset comprises data obtained from a bearing test rig, which consists of nominal bearing data, inner race faults observed under different loads shown in Figure 4.5 (a), outer race faults observed under different loads shown in Figure 4.5 (b) and three real-world defects. The test equipment utilized a NICE bearing with precise parameters: The roller diameter is 0.235 units. The pitch diameter is 1.245 units. The number of elements is 8, denoted as ne. The contact angle is zero.

The dataset consists of the following conditions: The experiment was conducted under three baseline conditions: a load of 270 lbs, an input shaft rate of 25 Hz, and a sampling rate of 97,656 samples per second, for a duration of 6 seconds. The three outer race fault conditions are as follows: a weight of 270 lbs, an input shaft rate of 25 Hz, and a sampling rate of 97,656 sps for a duration of 6 seconds.

The 7 fault conditions for the outer race are as follows: 25, 50, 100, 150, 200, 250, and 300 lbs of load. The input shaft rate is 25 Hz, and the sample rate is 48,828 sps for a duration of 3 seconds. It is important to note that the bearing resonance is less than 20 kHz. The inner race fault circumstances include load levels of 0, 50, 100, 150, 200, 250, and 300 lbs, an input shaft rate of 25 Hz, a sample rate of 48,828 samples per second, and a duration of 3 seconds.

Data, typically in matrix format, provide detailed information on operating conditions, failure kinds, and vibration measurements. They are widely used to develop and evaluate signal

processing techniques, classification algorithms, and machine learning models dedicated to the detection and diagnosis of bearing failures.

In summary, the MFPT database is a valuable resource for research and development in the field of predictive maintenance and diagnosis of rolling element bearing failures. It enables researchers and engineers to test and validate new methods and technologies in this essential sector of engineering.

4.3.2 Proposed approach

The present section provides a comprehensive exposition on the utilisation of a Convolutional Neural Network (CNN) combined with Continuous Wavelet Transform (CWT) for the purpose of diagnosing bearing faults in induction motors [82].

The chosen approach is based on its demonstrated proficiency in automated time-frequency analysis and feature extraction. This selection is expected to greatly improve the accuracy and efficiency of fault detection when compared to traditional diagnostic methods. The experimental protocol entails the collection of unprocessed vibration data from defective bearings, followed by the division of this data into smaller segments, and subsequently converting it into time-frequency images through the utilisation of different Continuous Wavelet Transforms (CWTs).

The images are subsequently transformed into 227×227-pixel RGB scalograms in order to undergo processing by a Convolutional Neural Network (CNN). The SqueezeNet model, which has been specifically modified and optimised for the purpose of analysing bearing fault data, is employed in the training and classification of these images.

The tools and materials utilised in this study encompass the SqueezeNet deep learning model, which is a widely recognised framework for image classification tasks, and the MATLAB software, a powerful computational tool commonly used in scientific research. The implementation of the Convolutional Neural Network (CNN) and Continuous Wavelet Transform (CWT) transformations is carried out within the MATLAB environment, allowing for efficient and accurate analysis of the data. The data employed for the purposes of training and testing in this study is sourced from the publicly accessible Machine Failure Prevention Technology (MFPT) datasets.

These datasets consist of a diverse range of bearing fault conditions. The incorporation of sophisticated signal processing and machine learning methodologies presents a resilient approach for addressing the intricate challenge of fault diagnosis in industrial motors.

This approach offers advantages in terms of processing time and classification accuracy compared to existing deep learning methods, as detailed in the following sections. Figure 4.6 illustrates the proposed methodology's flowchart.

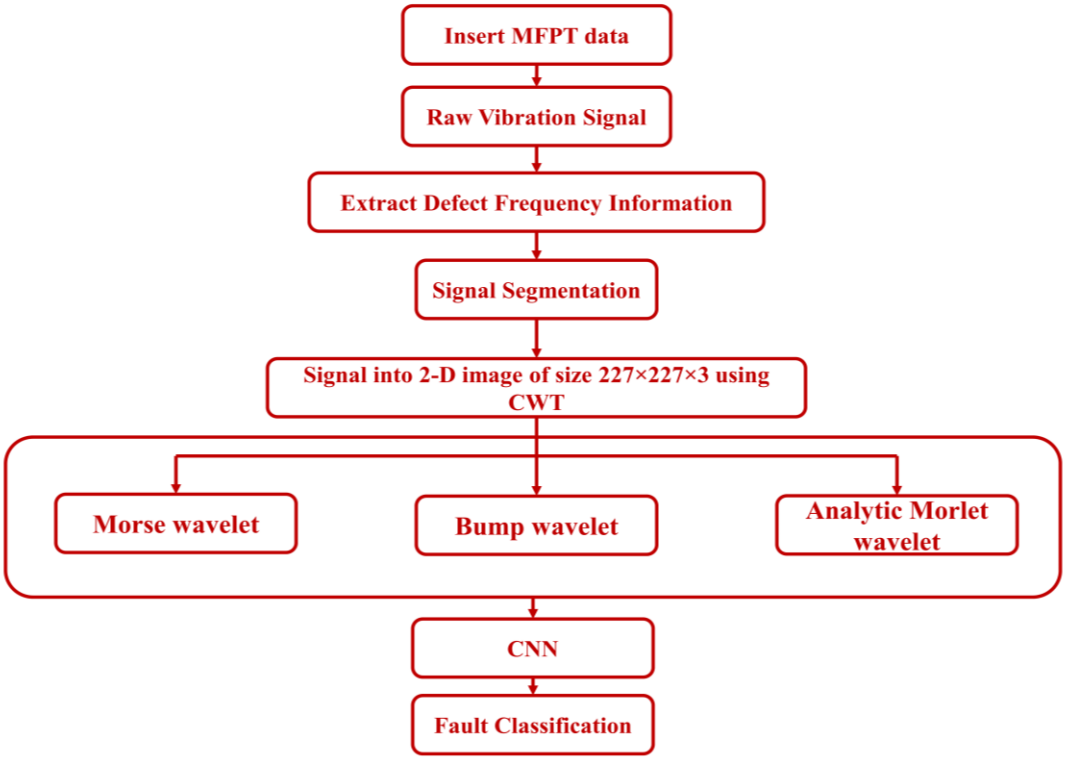

Figure 4.6 *Flowchart illustrating the proposed methodology for fault classification.*

4.3.3 Data processing

4.3.3.1 Signal processing

The present study focused on the analysis of vibration signals obtained from the Machinery Failure Prevention Technology (MFPT) dataset. This dataset was specifically designed to encompass a wide range of fault bearing conditions occurring within specified operational settings. The dataset comprises various types of faults, including outer-race-fault (ORF) conditions, inner-race-fault (IRF) conditions, and others. Each fault type is associated with specific load settings.

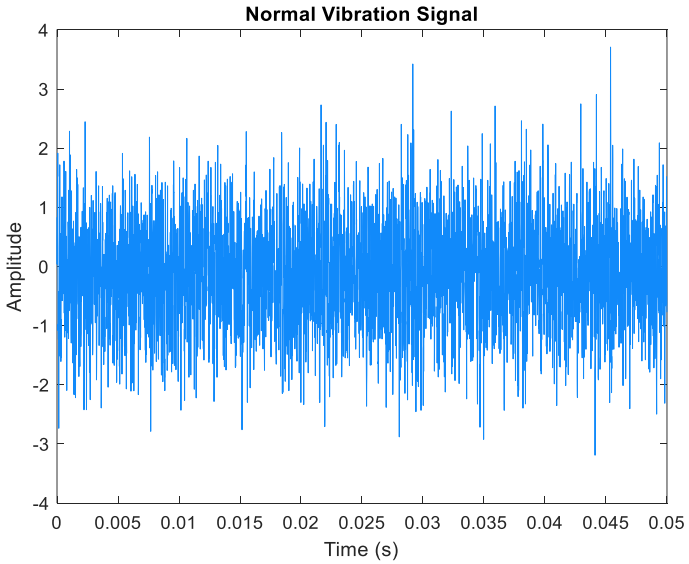

Figure 4.7 *Vibration signal under normal conditions.*

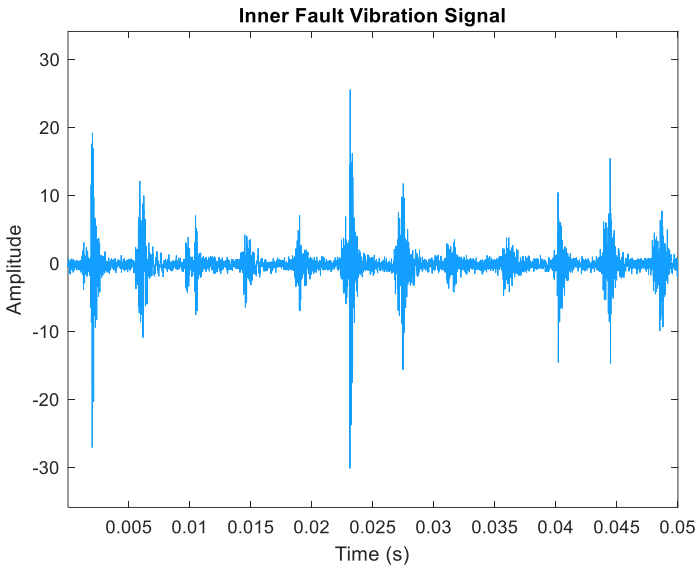

Figure 4.8 *Vibration signal under Inner-race bearing fault conditions.*

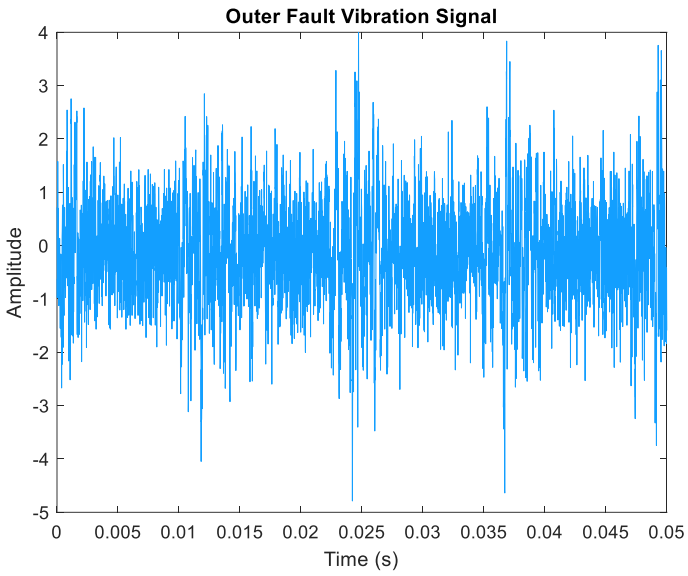

Figure 4.9 *Vibration signal under Outer-race bearing fault conditions.*

The diagnostic process for bearing faults requires a high level of sensitivity to data integrity when dealing with induction motors. The data points utilised in this specific analysis originate from the three defect datasets. The bearing data used in this study is composed of three files, each containing a total of 117 segments. Each segment consists of 5000 samples, resulting in a consistent length across all files. The dataset consisted of seven instances for both the inner and outer fault files. The inner fault file contained a total of 58 segments, while the outer fault file contained 117 segments.

Each segment of the raw data underwent transformation using the Continuous Wavelet Transform (CWT), producing a series of time-frequency images.

The conversion process yielded a total of 234 images representing the baseline set, 290 images capturing the inner-race signals, and 524 images showcasing the outer-race faults.

Consequently, this comprehensive dataset effectively showcases the distinctive features and visual representations of both the normal bearing and its various defects under different loading conditions.

The training set is instrumental in calibrating the CNN model, ensuring it learns the nuanced differences between normal and faulty conditions. The testing set then serves to validate the accuracy of the model, confirming its capacity to generalise and correctly classify new, unseen data. By incorporating all data points across the spectrum of fault conditions, we ensure a comprehensive understanding and robust detection capability, pivotal for the reliability and longevity of the induction motors.

Incorporating CWT in this manner provided a robust set of features for the CNN to identify, allowing for high-precision fault classification. The methods I employed here build directly on the established approach from my publication, Boudiaf et al. (2023), now further refined to meet the specific objectives and depth required for this thesis.

The transformation of 1D vibration data into a 2D scalogram with the three colour channels, RGB, signifying different frequency information encapsulated within the vibration signal. We map the normalised amplitude values onto the intensity across these colour channels, effectively translating the vibratory information into a format that a CNN can interpret.

Figure 4.11 illustrates the procedure for converting the 1D signal into a 2D scalogram. The normalised signal amplitude corresponds to the intensity and colour within the scalogram, creating a rich representation of the original vibration signal for subsequent analysis by the CNN. This step is critical because it preserves the signal's time-frequency characteristics within the image, which are critical for accurate fault classification.

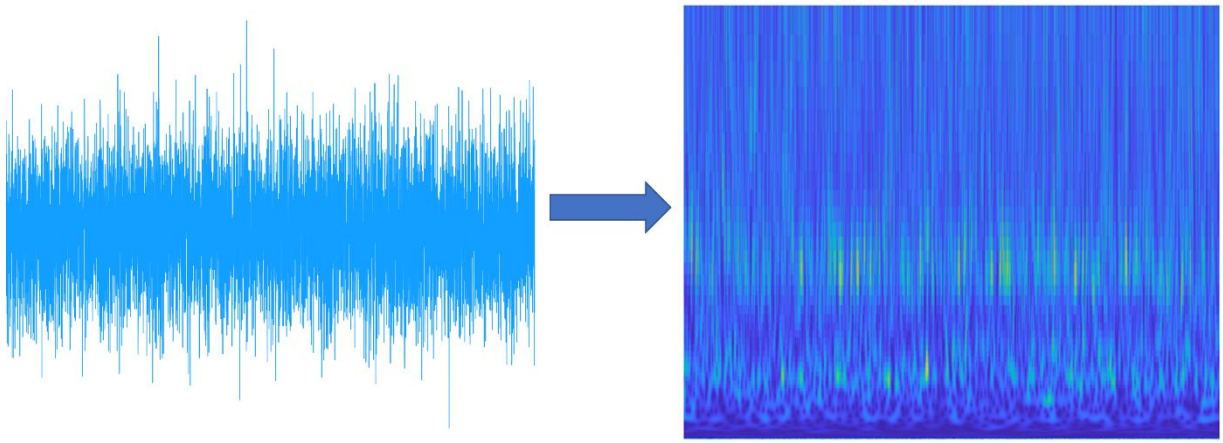

Figure 4.10 *Visualization of Normal Vibration Signal Conversion to Corresponding Scalogram.*

The count of unique peaks is a useful characteristic for distinguishing between inner race faults, outer race faults, and normal situations. Thus, a scalogram is a suitable option for categorising bearing defects. We obtained all the bearing signal data in this example from experiments conducted at a consistent shaft speed. In order to apply this example to bearing

signals at varying shaft speeds, it is necessary to normalise the data based on the shaft speed. Otherwise, the quantity of "pillars" in the scalogram will be incorrect.

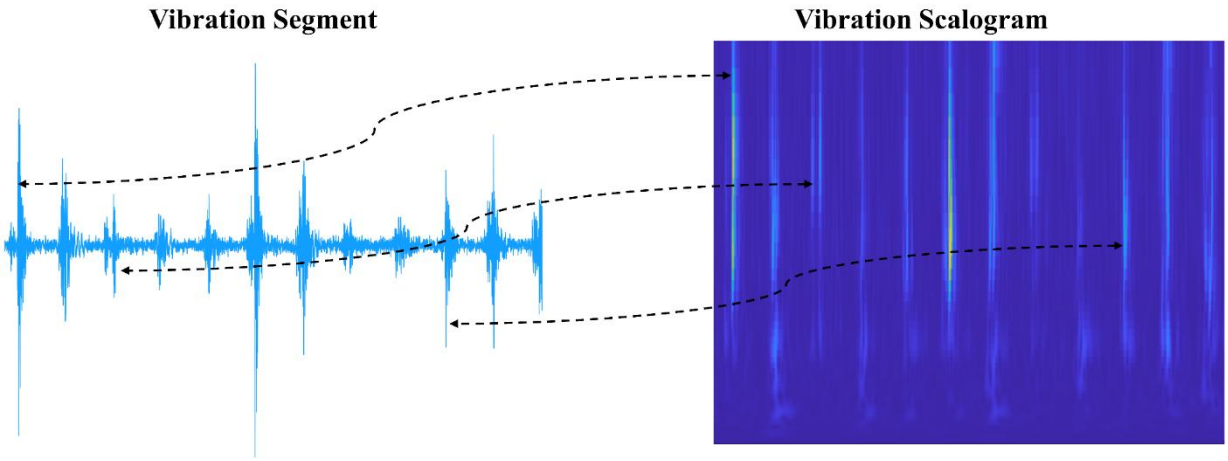

Figure 4.11 *Conversion process from 1D signal to 2D vibration image.*

Within the temporal interval, as depicted in the provided Figure 4.11, it can be observed that the vibration signal exhibits a total of 12 distinct impulses. This occurrence can be attributed to the fact that the bearing under investigation possesses a characteristic known as the Ball Pass Frequency Inner Race (BPFI), which has a frequency value of 118.875 Hz. the scalogram exhibits a total of 12 discernible peaks that correspond precisely to the impulses detected in the vibration signal.

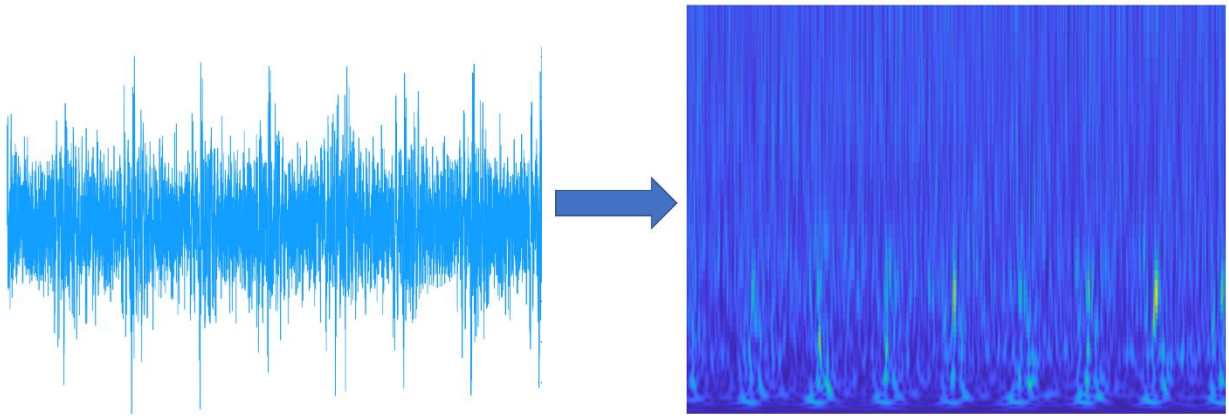

Figure 4.12 *Transformation of Vibration Signal to Scalogram for Outer Race Bearing Fault Analysis.*

Upon analysing the scalogram of the outer race fault, it is observed that there are a total of 8 distinct peaks within the initial 0.1 seconds. This finding aligns with the expected ball pass frequencies, indicating a consistent pattern. The to the relatively weaker impulses present in the time-domain signal compared to the inner race fault scenario, the scalogram exhibits less pronounced peaks that are less distinguishable from the background. The normal condition's scalogram lacks any identifiable, prominent, and distinct peaks.

The dataset consists of two sets: the training set and the testing set. The distribution of images between these sets is summarised in Table 4.1, with 80% of the images allocated to the training set and the remaining 20% allocated to the testing set.

The signals have been summarised in Table 4.1, providing the relevant information for each fault condition, including the type of fault, the length of the signals, and the number of segments used for training and testing purposes. The illustrative Figures 4.13, 4.14 and 4.15 correspond with these sets, showcasing the outputs of the three CWT types for the described conditions. Specifically, Figure 4.13 illustrates the Morse wavelet output, Figure 4.14 the Morlet wavelet, and Figure 4.15 the Bump wavelet. The subfigures for each category delineate the normal conditions (Figures 4.15(a)-4.15(b)), inner race faults (Figures 4.15(c)- 4.15(d)), and outer race faults (Figures 4.15(e)-4.15(f)).

Table 4.1 *Signal Types, Lengths, and Segment Numbers for Training and Testing Data with Various Fault Conditions.*

	Signals types	**Signal length**	**Number of segments**
Training	baseline_1	585936	117
	baseline_2	585936	117
	InnerRaceFault _various load 1	146484	58
	InnerRaceFault _various load 2	146484	58
	InnerRaceFault _various load 3	146484	58
	InnerRaceFault _various load 4	146484	58
	InnerRaceFault _various load 5	146484	58
	OuterRaceFault_1	585936	117
	OuterRaceFault_2	585936	117
	OuterRaceFault _various load 1	146484	58
	OuterRaceFault _various load 1	146484	58
	OuterRaceFault _various load 1	146484	58
	OuterRaceFault _various load 1	146484	58
	OuterRaceFault _various load 1	146484	58
Testing	baseline_3	585936	117
	InnerRaceFault _various load 6	146484	58
	InnerRaceFault _various load 7	146484	58
	OuterRaceFault_3	585936	117
	OuterRaceFault _various load 6	146484	58
	OuterRaceFault _various load 7	146484	58

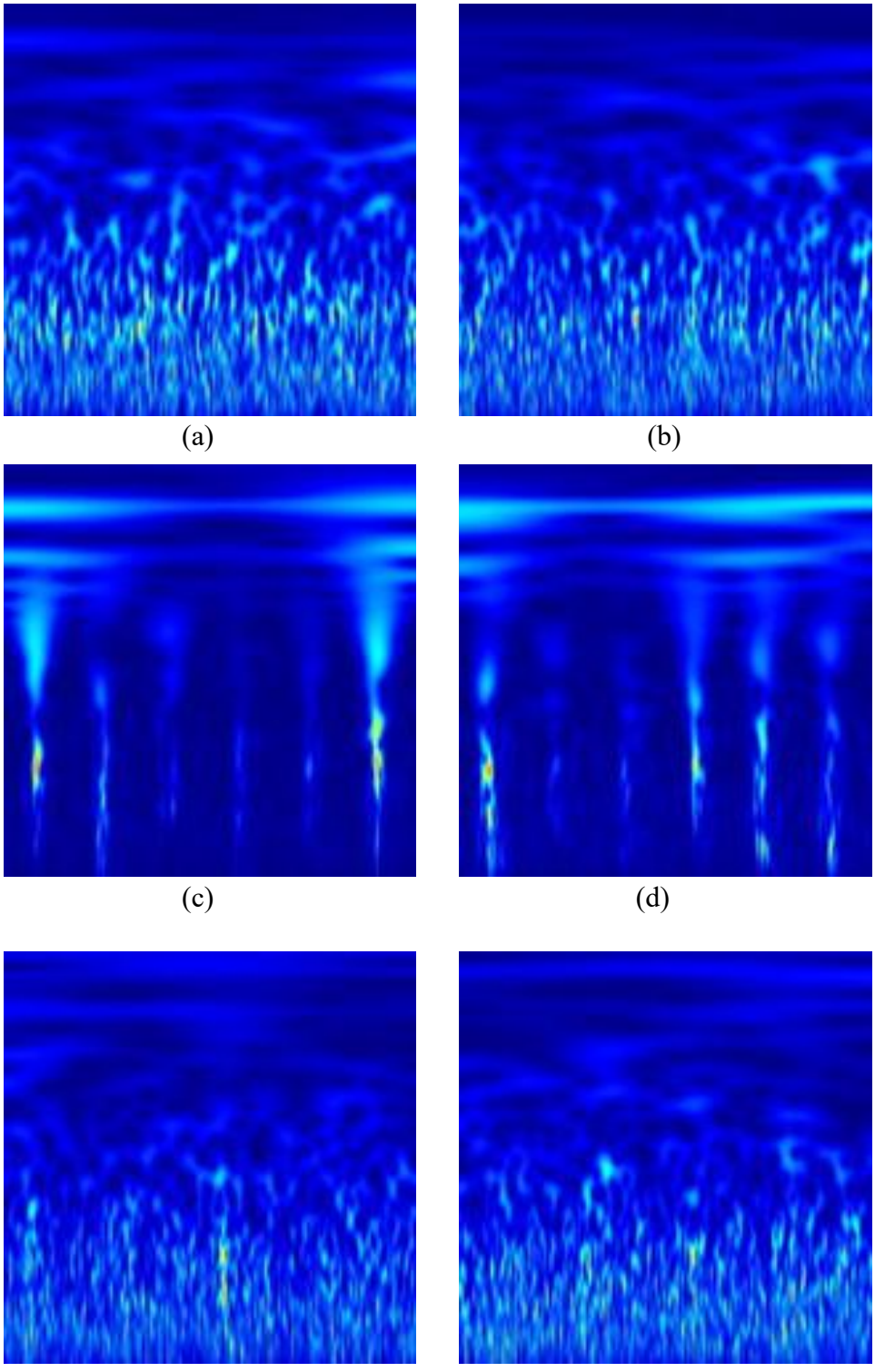

(a) (b)

(c) (d)

(e) (f)

Figure 4.13 *Morse Wavelet Output image (a)-(b) Normal (c)-(d) Inner race fault (e)-(f) Outer race fault.*

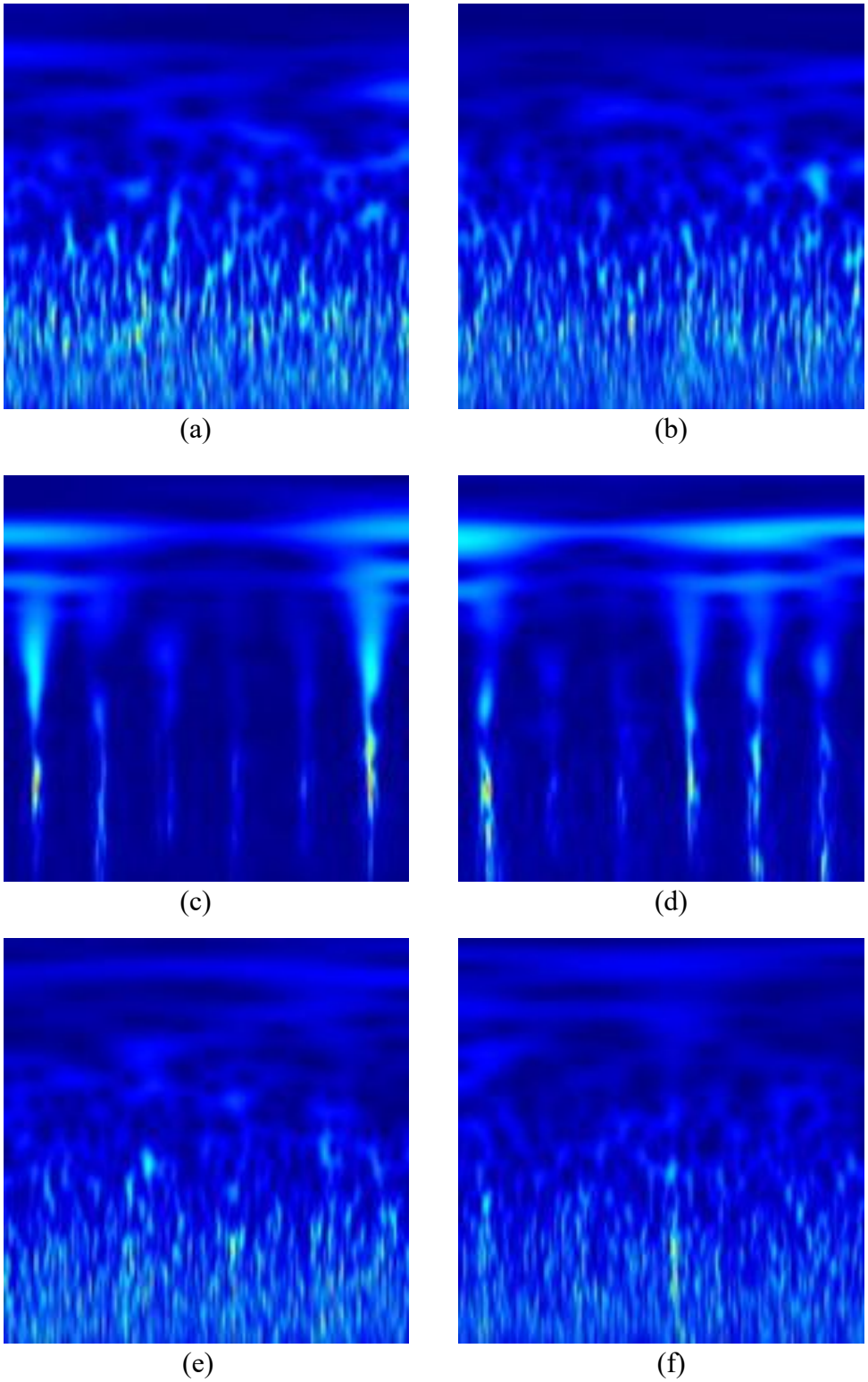

Figure 4.14 *Morlet Wavelet Output image (a)-(b) Normal (c)-(d) Inner race fault (e)-(f) Outer race fault.*

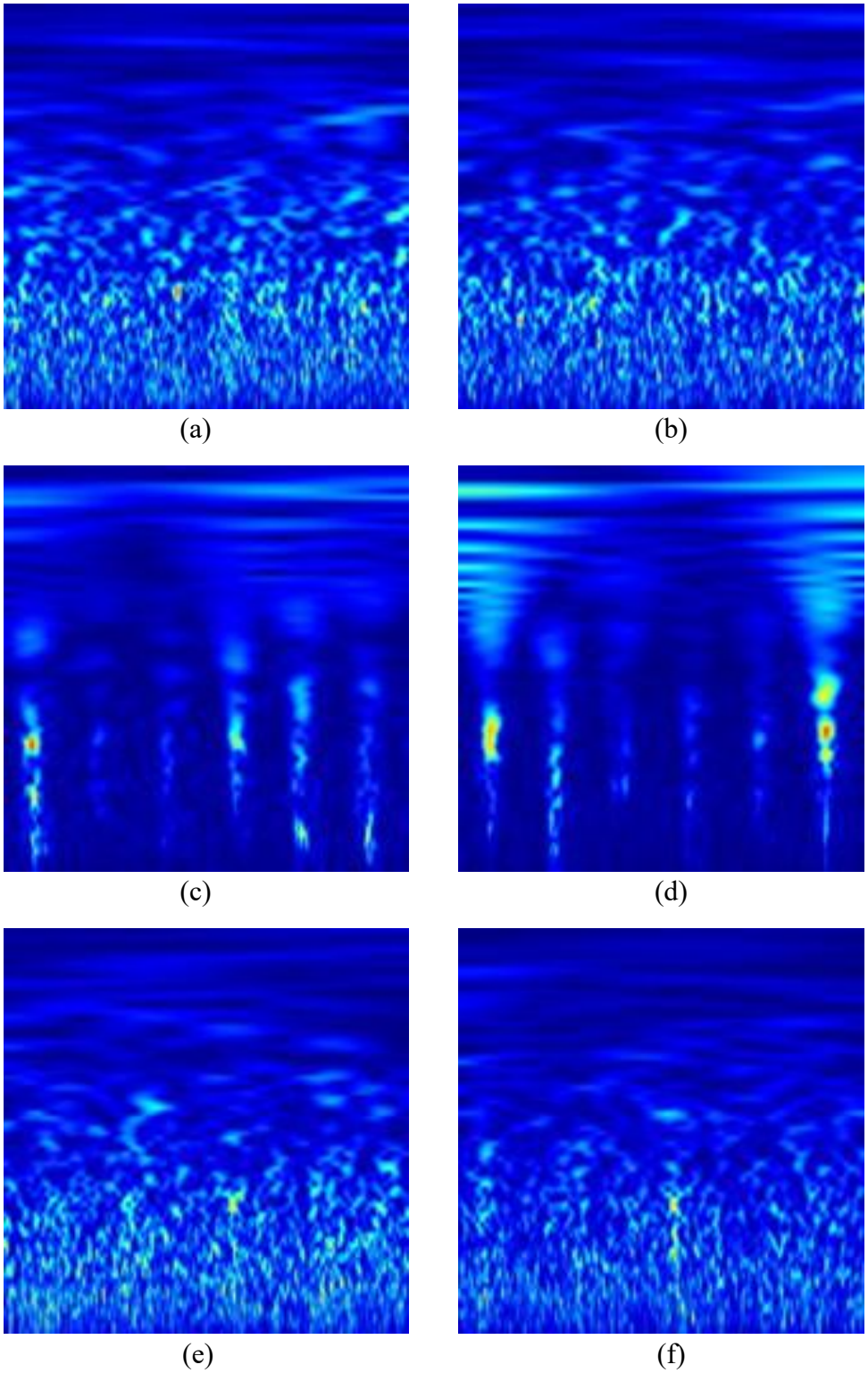

(a) (b) (c) (d) (e) (f)

Figure 4.15 *Bump Wavelet Output image (a)-(b) Normal (c)-(d) Inner race fault (e)-(f) Outer race fault.*

4.3.3.2 Enhancing Scalogram Classification with SqueezeNet Fine-Tuning and Transfer Learning

Ultimately, the pretrained SqueezeNet convolutional neural network is subjected to fine-tuning in order to effectively classify the scalograms. The SqueezeNet model has undergone training using a dataset consisting of over one million images. Through this training process, the model has acquired a comprehensive set of feature representations. Transfer learning, a commonly employed technique in the field of deep learning, finds frequent utilisation in various applications. Given that SqueezeNet has undergone prior training, it can be effectively employed to carry out a novel task. The process of fine-tuning a neural network through transfer learning is generally observed to be considerably more efficient and less complex compared to training a network from scratch with randomly initialised weights.

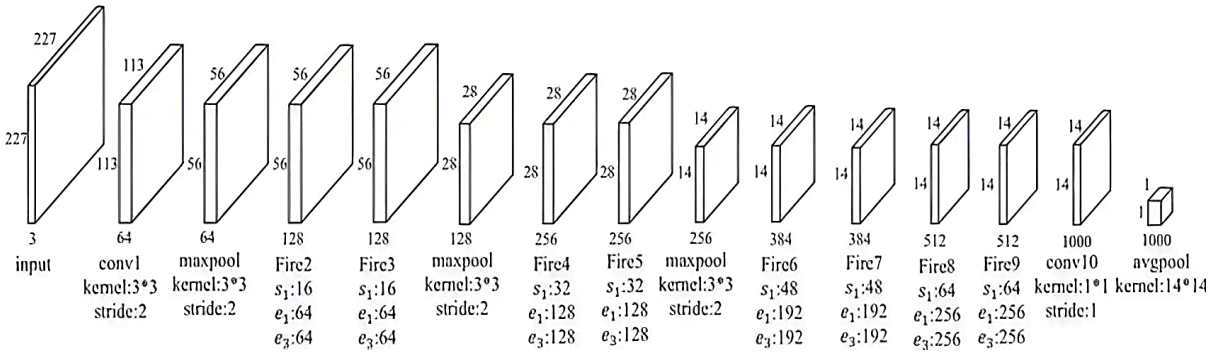

Figure 4.16 *The SqueezeNet architecture.*

In the critical phase of model training and fine-tuning, the SqueezeNet architecture, initially pre-trained on an extensive image dataset, was adapted for the specific task of bearing fault diagnosis through scalogram analysis. The training parameters were meticulously chosen to enhance model performance: a low learning rate of 0.0001 ensured gradual and stable convergence; the model underwent training for 8 epochs to optimise learning without overfitting; and a batch size of 32 struck a balance between computational efficiency and memory constraints.

The fine-tuning strategy involved two key stages. Initially, we frozen the model's early convolutional layers, which were responsible for capturing universal visual features like edges and textures. This ensured that the model's foundational capabilities remained intact while adapting to the nuances of vibration data analysis. We selectively unfroze deeper layers, which enabled the network to refine more complex features directly relevant to our specific diagnostic tasks. This selective re-training helped to tailor the SqueezeNet model more accurately to the characteristics of bearing faults depicted in the scalograms.

To combat the risk of overfitting, several regularisation techniques were employed. Dropout layers were integrated with a rate of 0.5 in the fully connected sections of the network during training, effectively randomising the learning process and enhancing the model's generalisation capabilities. Additionally, data augmentation techniques, including rotations and scaling of scalograms, were utilised to further robustify the model against variations in the input data.

MATLAB's Deep Learning Toolbox executed the entire training and fine-tuning process, providing a robust framework for managing the complexities of deep neural networks. A GPU-enabled ‘’ NVIDIA GeForce GTX 1650 Ti with total memory of 9979 MB’’ workstation accelerated the computations, crucially handling the extensive computational demands of training the deep learning model. The SqueezeNet model got a lot better at telling the difference between and classifying different kinds of bearing faults from scalogram data after going through this strict and structured training programme. This shows how useful it is to use advanced machine learning techniques in the diagnostic processes for industrial machinery.

4.3.4 Results and discussion

In this section, we will conduct a thorough comparison of the effectiveness and performance of different types of continuous wavelet transforms (CWT) commonly used in induction motor fault diagnosis. Our specific attention will be directed towards the Morse, Morlet, and Bump wavelets. We will specifically focus on the Morse; our evaluation benchmarks assess the efficacy of the evaluated methods in enhancing the fault diagnostic capabilities of convolutional neural networks (CNNs) [82].

After generating the images, they were divided into a ratio of 80:20 for training and testing. A total of 1048 images were utilised for training, and 466 instances were reserved for the testing set for each type of wavelet image. The performance of the model was assessed using various parameters, specifically accuracy and loss, as depicted in Figures 8 to 10 for the three distinct wavelet pictures. Furthermore, in order to enhance comprehension of the accurately and inaccurately identified instances, confusion matrices of CNN were presented in figures showcasing the outcomes for various wavelet pictures. More precisely, Figure 4.18 represents the Morse wavelet, Figure 4.20 shows the findings for the Morlet wavelet, and Figure 4.22 presents the outcomes for the Bump wavelet. This Figures provide a comprehensive analysis of the model's performance for each wavelet image type, offering significant insights into both accurately and inaccurately categorised examples.

Accuracy and loss are often employed measures to evaluate the performance of a model during both training and testing stages in deep learning. The loss metric quantifies the degree of similarity between the predicted values of the model and the actual values. On the other hand, the accuracy metric quantifies the frequency at which the model correctly predicts the class label of the input data. The accuracy metric of a deep learning model quantifies its performance in accurately identifying the input data. It is commonly expressed as a percentage, with larger values indicating superior performance. For instance, a 90% accuracy indicates that the model accurately predicted the class label for 9 out of every 10 input data points.

4.3.4.1 The Morse experience

The Morse wavelet of the continuous wavelet transform (CWT) converts the signal output into a scalogram, as shown in Figure 4.13. This transformation is critical for capturing the signal's inherent time-frequency information, which is important for the subsequent analysis. Following this conversion, the CNN model processes the data using the

hyperparameters outlined in Section 4.3.3.2. We designed the CNN model to efficiently extract features from the scalogram, enabling robust pattern recognition and classification that are essential for the study's objectives. Figure 4.17 illustrates the further analysis of the CNN model's performance in terms of accuracy and loss. This figure emphasises the model's effectiveness during the training and validation phases, providing insights into the model's convergence and the impact of the chosen hyperparameters.

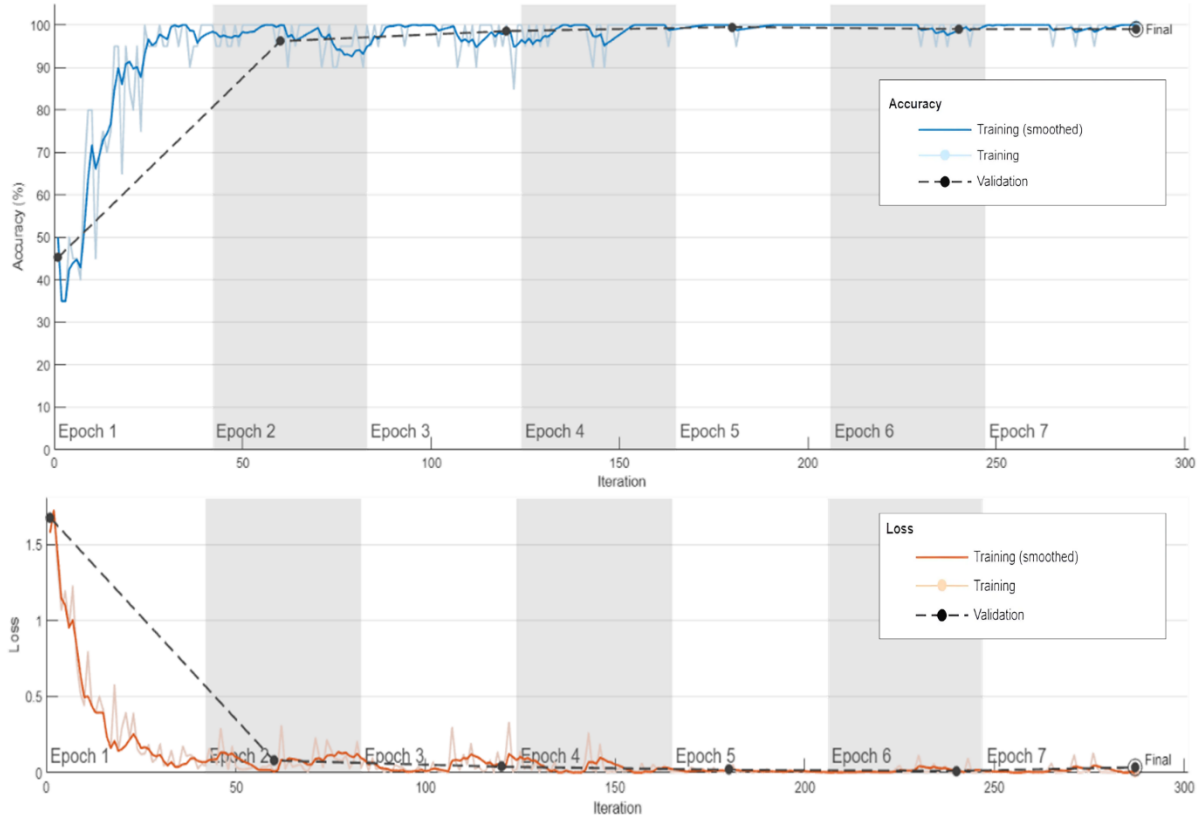

Figure 4.17 *Assessing Morse's performance by measuring accuracy and loss.*

Figure 4.17 appears to present the training progress of a convolutional neural network (CNN) over several epochs, as shown by two graphs tracking accuracy and loss.

In the accuracy graph, two lines represent the accuracy of the model over time, with one line representing the actual accuracy per iteration, and the other showing a smoothed version for better trend visualization. The training accuracy quickly increases in the initial epochs and then stabilises close to 100%, indicating that the model is effectively learning from the training data. The validation accuracy follows a similar upward trend but with some fluctuations, which is typical as the model tries to generalise from the training data to unseen validation data. The final validation accuracy appears to stabilise just below the training accuracy, suggesting a good fit without significant overfitting.

The loss graph similarly features two lines representing the actual and smoothed loss values during training. Both the training and validation losses decrease sharply in the initial epochs, which is expected as the model begins to learn from the data. The training loss continues to decline steadily, while the validation loss levels off and remains relatively constant

after the initial epochs. This suggests that the model is converging well, minimising the error in predictions as it learns.

The shading between epochs indicates the iterations within each epoch. Both accuracy and loss graphs display seven epochs in total, with the final epoch marked as the point where the training was concluded.

Overall, the graphs suggest that the CNN model trained effectively, achieving high accuracy while maintaining a low and stable loss, especially in the validation set, which indicates that the model is generalising well to new data.

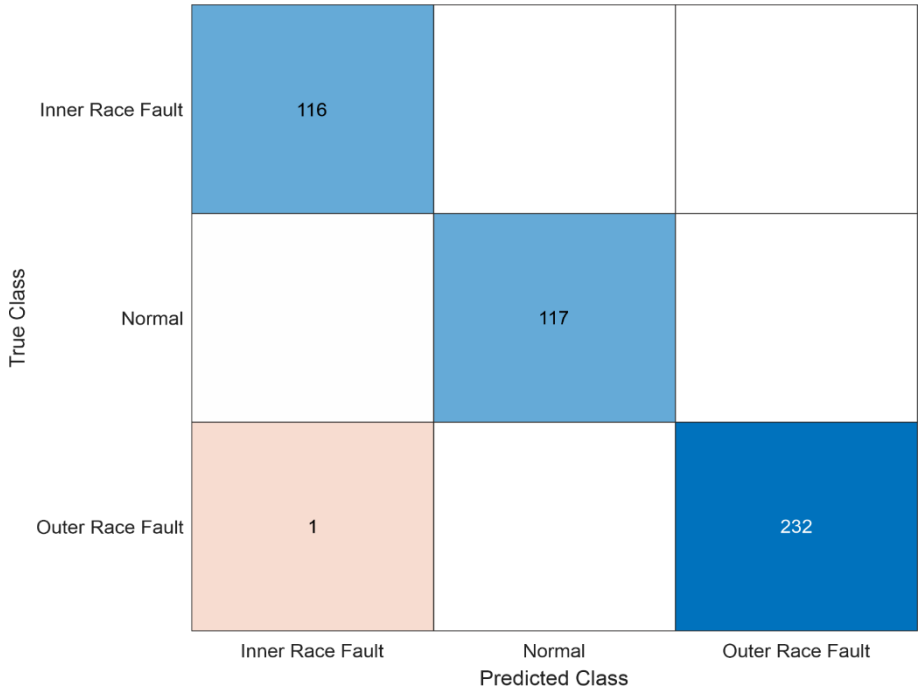

Figure 4.18 *CNN Confusion Matrix with Morse Wavelet for Fault Diagnosis.*

The confusion matrix for the Morse experiment offers a comprehensive view of the model's performance in classifying three different conditions: Inner Race Fault, Normal, and Outer Race Fault. The matrix reveals an impressive accuracy level, with the model correctly identifying 116 instances of Inner Race Fault, showing a high true positive rate for this fault type without any misclassifications into other categories. Similarly, the model accurately recognized 117 instances of the Normal condition, demonstrating its effective distinction between normal operations and fault states. In the case of Outer Race Fault, the model's robustness is further underscored by correctly predicting 232 instances, with only a single misclassification where an Outer Race Fault was mistakenly identified as an Inner Race Fault. This minimal error suggests a slight overlap in characteristics between these fault types under certain conditions, but the overall error rate remains negligible. The overwhelming concentration of correct predictions along the diagonal of the matrix indicates a strong alignment of predicted and actual classes, showcasing the model's capability to learn and predict effectively with high specificity and accuracy across the board. This excellent performance aligns with the high accuracy and low loss observed in Figure 4.17, confirming the model's practical effectiveness in fault detection applications.

4.3.4.2 The Morlet experience

In our research, the application of the Morlet wavelet through the Continuous Wavelet Transform (CWT) has been pivotal in translating signal output into a scalogram, as encapsulated in Figure 4.14. This Morlet-driven transformation is instrumental in extracting time-frequency information inherent in the signal, forming the basis for comprehensive analysis. Subsequently, the CNN model processes this transformed data, abiding by the hyperparameters specified in Section 4.3.3.2. The architecture of the CNN is intentionally tailored to maximise feature extraction from the Morlet scalogram, which is critical for the robust pattern recognition and classification at the heart of our objectives.

The performance of the CNN model, when evaluated through the lens of the Morlet wavelet, is illustrated in Figure 4.19. The figure highlights the model's performance metrics, specifically accuracy and loss during both training and validation phases. This portrayal is essential as it underscores the effectiveness of the CNN in deciphering the patterns encoded within the scalogram and reflects on the model's convergence. Furthermore, it provides an evaluation of the impact that the selected hyperparameters have on the model's learning and generalisation ability.

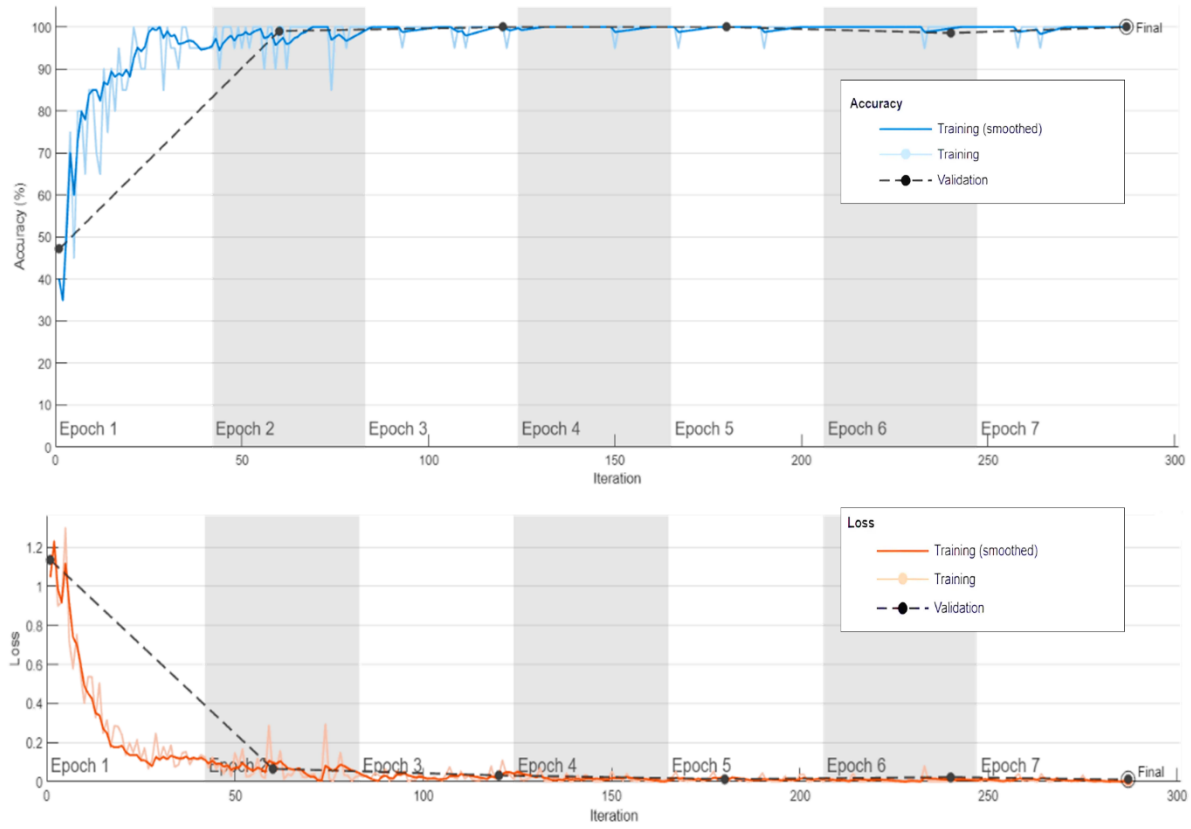

Figure 4.19 *Assessing Morlet's performance by measuring accuracy and loss.*

Figure 4.19 seems to provide a detailed view of the training and validation performance of a CNN model across multiple epochs, as measured by accuracy and loss metrics.

The top graph shows the model's accuracy. The blue line, representing the training accuracy, demonstrates a rapid increase in the initial epochs before plateauing, which suggests

quick learning in the early stages of training that becomes more gradual as the model starts to optimize and fine-tune. The smoothed version of this line shows a clearer upward trend without the noise from the raw data points. The dashed black line indicates validation accuracy, which also increases but with notable variability, hinting at how the model generalizes to new, unseen data. The final epoch shows that the validation accuracy is slightly lower than the training accuracy but remains high, suggesting that the model is well-tuned and not overfitted.

The bottom graph illustrates the loss during the training and validation phases. The orange line, representing training loss, declines sharply and then levels off, indicating that the model is effectively reducing error over time. The smoothed version of this line helps to visualize the overall declining trend in loss. The dashed black line shows the validation loss, which follows a similar downward trend, but with a slight upward shift towards the later epochs. This could be a sign of the model beginning to overfit to the training data, although the effect is minimal as the validation loss remains low.

Overall, the model appears to have a good balance between learning from the training data and generalizing to the validation data, with high accuracy and low loss by the final epoch. The slight divergence between training and validation metrics is common in machine learning and does not necessarily indicate a poorly performing model, especially when both accuracy and loss are within acceptable ranges.

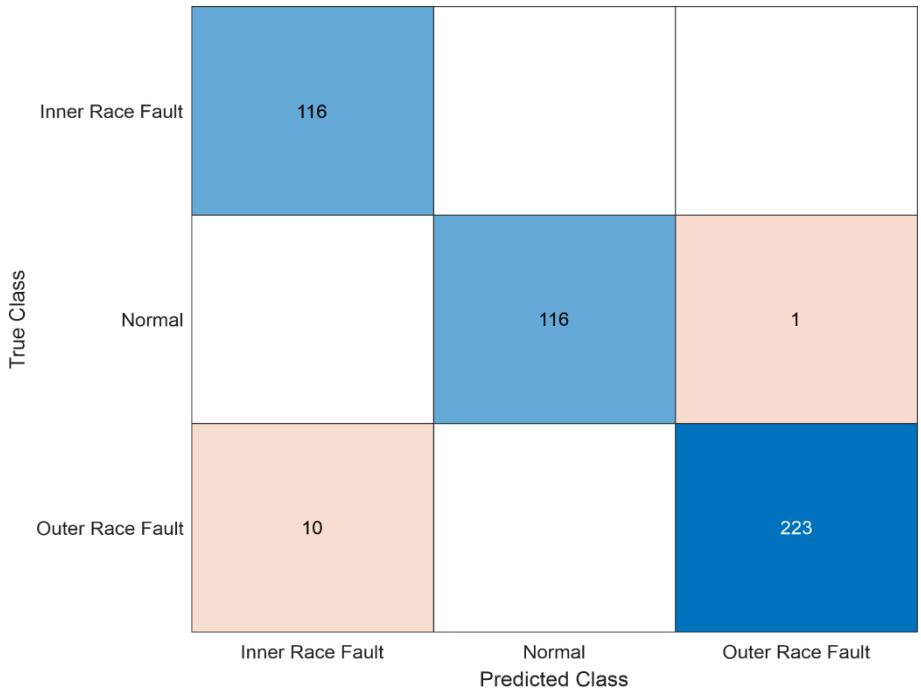

Figure 4.20 *CNN Confusion Matrix with Morlet Wavelet for Fault Diagnosis.*

In the Morlet experiment, the confusion matrix illustrates the model's performance across three categories, showing strong accuracy, especially in identifying Inner Race Fault and Normal conditions. The model correctly predicted 116 instances of Inner Race Fault and recognized 116 out of 117 Normal condition instances, with just one misclassified as Outer Race Fault, indicating high precision but a slight confusion under specific conditions. For Outer

Race Fault, the model successfully identified 223 instances but misclassified 10 as Inner Race Fault, pointing to an area where further tuning could enhance distinction between these fault types. The model's high accuracy in nearly all cases reflects its robust learning and general classification capabilities, making it a reliable tool for practical fault detection scenarios.

4.3.4.3 The bump experience

In the context of this study, the Bump wavelet via the Continuous Wavelet Transform (CWT) has been integral in transforming the signal output into a scalogram, as highlighted in earlier sections. The utilization of the Bump wavelet facilitates the extraction of nuanced time-frequency information from the signal, which is crucial for detailed analysis. Once transformed, this data is fed into the CNN model, adhering to the hyperparameters outlined in Section 4.3.3.2. The CNN's architecture is specifically designed to optimize feature extraction from the Bump scalogram, thereby enhancing pattern recognition and classification capabilities which are pivotal for achieving the objectives of this study.

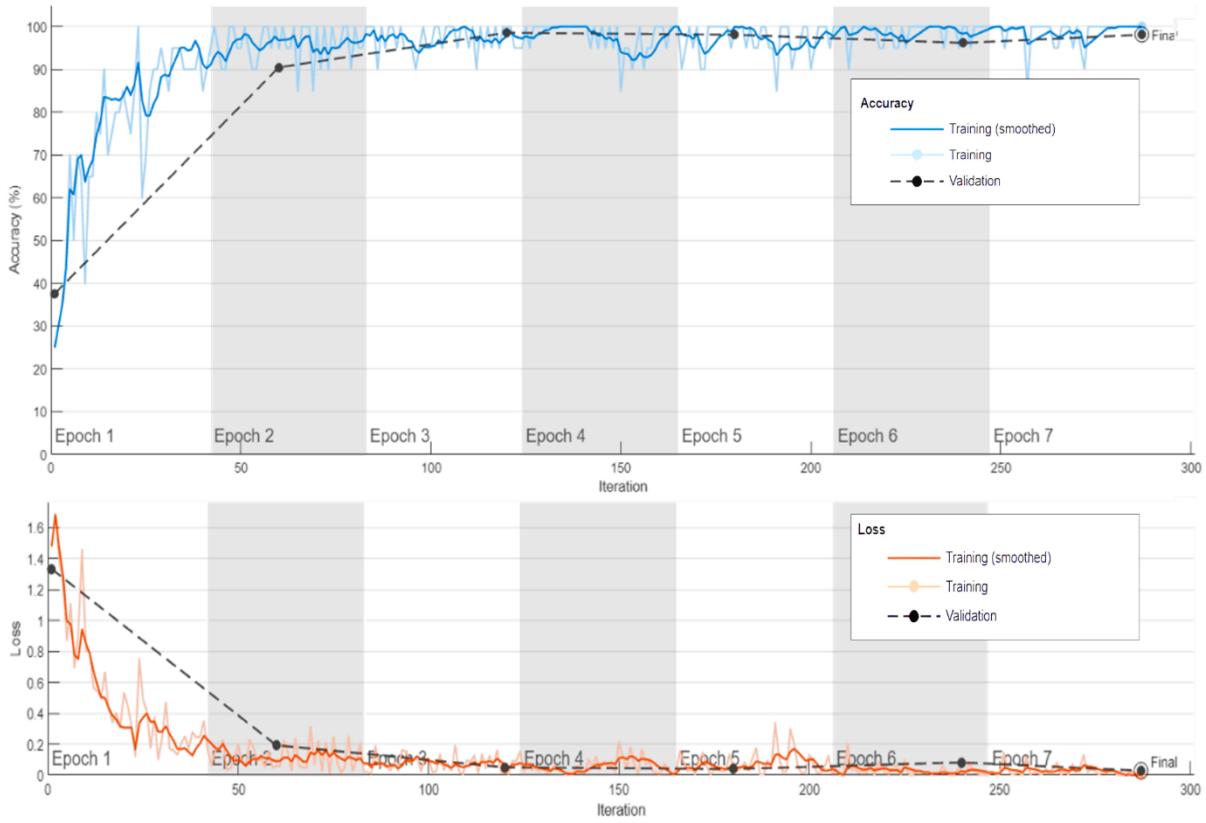

Figure 4.21 *Assessing Bump's performance by measuring accuracy and loss.*

Figure 4.21 illustrates the performance metrics of a convolutional neural network model across several epochs, focusing on accuracy and loss to indicate the model's effectiveness and efficiency. The accuracy graph in the top section reveals that both raw and smoothed training accuracy quickly climbs to over 90% by the third epoch and maintains a high level throughout the training. This rapid improvement and stability suggest effective learning from the training data. The validation accuracy also increases quickly, but exhibits more fluctuations, typical of testing against unseen data. However, it remains close to the training accuracy by the end of the training period, indicating good generalisation without significant overfitting.

The bottom section's loss graph shows a sharp initial decrease in the training loss, indicating the model's rapid improvement in predictive capability. This reduction in loss slows and stabilises as training progresses, showing diminishing returns from further learning. The validation loss follows a similar downward trend but with some variability, highlighting moments where the model's predictions are less consistent with the validation data. Nevertheless, the overall decrease and stabilisation of validation loss by the final epoch suggest that the model is also improving its accuracy on unseen data without considerable overfitting. Overall, Figure 4.21 depicts a successful training process where the CNN model quickly learns, achieves high accuracy, and maintains low and stable loss, indicating well-tuned performance capable of effective generalisation.

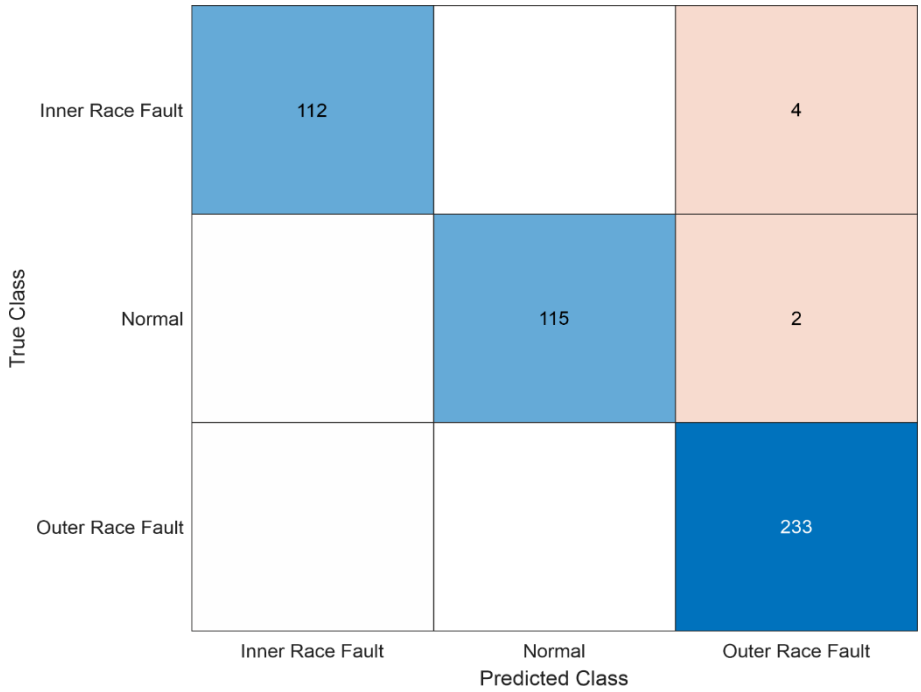

Figure 4.22 *CNN Confusion Matrix with Bump Wavelet for Fault Diagnosis.*

The confusion matrix for the Bump experiment reflects the model's classification performance for three conditions: Inner Race Fault, Normal, and Outer Race Fault. It shows how well the model can differentiate between these machine conditions with a notable degree of precision.

For Inner Race Fault, the model successfully identified 112 out of 116 instances correctly, with 4 instances misclassified as Outer Race Fault. This indicates a high level of accuracy in detecting this type of fault, though it suggests some minor confusion with the Outer Race Fault under certain scenarios.

The Normal condition saw an almost perfect classification, with 115 of 117 instances identified correctly. The two misclassifications involved one instance being wrongly classified as Inner Race Fault and another as Outer Race Fault, which demonstrates the model's strong capability in recognizing normal machine operation with minimal errors.

Outer Race Fault classification was highly accurate, with 233 out of 235 instances correctly identified. Only two instances were misclassified as Normal, underscoring the model's effectiveness in detecting this particular fault type with high reliability.

Overall, the Bump experiment's confusion matrix reveals that the model is highly effective in classifying different fault conditions with a small number of misclassifications. These results underscore the model's robustness and accuracy, making it a valuable tool for fault detection in practical settings, where precise fault diagnosis is critical for maintaining operational efficiency and preventing equipment failure.

4.4 Conclusion

This chapter presented advanced methodologies for diagnosing bearing faults in induction motors, combining traditional techniques like Fast Fourier Transform (FFT) and Discrete Wavelet Transform (DWT) with cutting-edge approaches using Continuous Wavelet Transform (CWT) and Convolutional Neural Networks (CNNs). The integration of CWT and CNNs, particularly using the SqueezeNet model, demonstrated superior accuracy and computational efficiency compared to traditional methods. This novel approach was thoroughly evaluated using the Machine Failure Prevention Technology (MFPT) dataset, showcasing its potential in revolutionizing bearing fault diagnosis.

The findings from this chapter open new avenues for research and application in the field of predictive maintenance and fault diagnosis. They underscore the importance of leveraging both machine learning and traditional signal processing techniques to enhance diagnostic capabilities in industrial settings.

General Conclusion

The main focus of this thesis is on the intersection of advanced diagnostics and predictive maintenance techniques with real-world industrial applications. It is a big step forward in the comprehensive study of asynchronous induction motors. By using advanced signal processing techniques and artificial intelligence together, the research has not only set a new standard for motor diagnostics but also helped make these important parts more reliable and efficient in a wide range of industrial settings.

Our study introduced a novel diagnostic framework that leverages the robust capabilities of deep learning algorithms and vibration analysis techniques. We meticulously designed this framework to accommodate the inherent complexities of asynchronous induction motor operation, especially in noisy industrial environments. The utilisation of continuous wavelet transforms combined with convolutional neural networks has been a cornerstone of this research, enabling the extraction and learning of complex data patterns that traditional diagnostic methods could not address.

We rigorously conducted the validation of our diagnostic techniques using an expansive array of public datasets, supplemented by targeted real-world scenario testing. These experimental validations confirmed the high accuracy and reliability of our proposed methods, showcasing their potential to significantly improve fault detection rates compared to existing standards. The novel integration of AI in this domain not only improved accuracy, but also increased diagnostic adaptability across different types of motors and operational conditions.

The practical implications of this research are profound. Our findings, which improve the reliability and efficiency of induction motors, can help mitigate the impact of motor failures on production lines, potentially saving industries significant amounts in downtime and maintenance costs. Moreover, the ability to predict potential failures before they occur is instrumental in transitioning from reactive to proactive maintenance strategies, a shift that can dramatically improve the sustainability and efficiency of industrial operations.

This thesis lays a solid foundation for future research. Future studies could explore the scalability of the proposed techniques across other types of electric motors and more diverse industrial applications. Additionally, there is a promising avenue in the integration of these diagnostic methods into IoT-enabled devices for real-time monitoring and maintenance, which

could further revolutionise the industry by enabling smarter, more connected industrial systems.

In conclusion, this thesis not only advances the academic understanding and technical methodologies in the diagnostics of asynchronous induction motors but also aligns these advancements with the needs of modern industrial practices. It heralds a new era in predictive maintenance, where the integration of artificial intelligence and advanced signal processing techniques can lead to significant enhancements in both the performance and longevity of critical industrial machinery. The continued exploration and expansion of these techniques will undoubtedly play a pivotal role in shaping the future landscape of industrial maintenance and operational optimisation.

Throughout this research, we have addressed the primary challenges posed by the limitations of traditional diagnostic methods for asynchronous induction motors. This thesis' significant contributions include the following elements:

- The integration of advanced signal processing techniques and artificial intelligence (continuous wavelet transforms and convolutional neural networks) that operate autonomously without requiring expert intervention or manual feature extraction.
- Accurate and early fault diagnosis is effective under various operational conditions through the application of deep learning models capable of analysing complex vibrational data.
- The developed method demonstrates exceptional generalisation capability, enabling efficient classification of unknown data while enhancing the reliability of predictions.
- A significant reduction in the cost and time required to process and learn from large datasets of vibrational data from different types of industrial motors.

Future Directions

This research has identified several promising directions for future work:

- Future studies could also include applying the proposed methods to fault diagnostics for other rotating machinery, such as turbines and gear reducers.
- We are applying the proposed methods to data from new sources, such as acoustic and current data, and diagnosing new types of faults, particularly gear defects.

- The development of more sophisticated diagnostic systems based on deep learning techniques such as parallel learning and transfer learning is underway.
- We are conducting more extensive experiments related to industrial applications in order to move towards more effective predictive maintenance of rotating machinery.
- This research provides a successful study of automatic bearing fault diagnosis using the CWT-CNN combination.

The ideas in this thesis and the ones that will be studied in the future can be put together to make a complete set of tools for finding faults. This will be very helpful for people who work with and study monitoring machine condition through vibrational analysis.

Bibliography

[1] D. Gielen, F. Boshell, D. Saygin, M. D. Bazilian, N. Wagner, and R. Gorini, "The role of renewable energy in the global energy transformation," *Energy Strategy Reviews*, vol. 24, pp. 38–50, Apr. 2019, doi: 10.1016/J.ESR.2019.01.006.

[2] T. S. Kishore, E. R. Patro, V. Harish, and A. T. Haghighi, "A comprehensive study on the recent progress and trends in development of small hydropower projects," *Energies (Basel)*, vol. 14, no. 10, p. 2882, 2021.

[3] N. Gakkhar, M. K. Soni, and S. Jakhar, "Solar Energy Technologies and Water Potential for Distillation: A Pre-Feasibility Investigation for Rajasthan, India," in *Progress in Solar Energy Technologies and Applications*, 2019, pp. 39–82. doi: https://doi.org/10.1002/9781119555650.ch2.

[4] O. N. E. Agency, *Nuclear Energy Today*, no. n° 964. in Nuclear Energy Today. Nuclear Energy Agency, Organisation for Economic Co-operation and Development, 2003. [Online]. Available: https://books.google.dz/books?id=cWxPAAAAMAAJ

[5] E. Dahlquist, *Biomass as energy source: resources, systems and applications*. CRC Press, 2013.

[6] J. Yuan, "Introduction of ZEB Technology in Japan," in *Nearly Zero Energy Building (NZEB)*, D. Bienvenido-Huertas, Ed., Rijeka: IntechOpen, 2021, p. Ch. 8. doi: 10.5772/intechopen.101464.

[7] K. K. Jaiswal *et al.*, "Renewable and sustainable clean energy development and impact on social, economic, and environmental health," *Energy Nexus*, vol. 7, p. 100118, Sep. 2022, doi: 10.1016/J.NEXUS.2022.100118.

[8] B. Babatunde, *Towards Ensuring Energy Security in Africa*. 2024.

[9] J. F. Manwell, J. G. McGowan, and A. L. Rogers, *Wind energy explained: theory, design and application*. John Wiley & Sons, 2010.

[10] N. Vaezi, P. Tavakoli, and S. K. H. Sani, "Elimination of Pitch Signal Fluctuations Caused by Unbalanced Aerodynamic System in 100 kW Wind Turbine," in *2019 27th Iranian Conference on Electrical Engineering (ICEE)*, 2019, pp. 446–450. doi: 10.1109/IranianCEE.2019.8786525.

[11] "Air Pollution Control," *Environmental Engineering*, pp. 385–409, 2003, doi: 10.1016/B978-075067294-8/50020-8.

[12] I. Fedorova, "Alloy development for high Cr martensitic steel," 2018.

[13] P. A. Rasheed, S. K. Nayar, I. Barsoum, and A. Alfantazi, "Degradation of Concrete Structures in Nuclear Power Plants: A Review of the Major Causes and Possible

Preventive Measures," *Energies (Basel)*, vol. 15, no. 21, 2022, doi: 10.3390/en15218011.

[14] O. Z. Sharaf and M. F. Orhan, "An overview of fuel cell technology: Fundamentals and applications," *Renewable and Sustainable Energy Reviews*, vol. 32, pp. 810–853, Apr. 2014, doi: 10.1016/J.RSER.2014.01.012.

[15] R. O'hayre, S.-W. Cha, W. Colella, and F. B. Prinz, *Fuel cell fundamentals*. John Wiley & Sons, 2016.

[16] J.-M. Tarascon and M. Armand, "Issues and challenges facing rechargeable lithium batteries," *Nature*, vol. 414, no. 6861, pp. 359–367, 2001.

[17] K. W. Beard and T. B. Reddy, "Linden's handbook of batteries," *(No Title)*, 2019.

[18] M. Aykol, P. Herring, and A. Anapolsky, "Machine learning for continuous innovation in battery technologies," *Nat Rev Mater*, vol. 5, no. 10, pp. 725–727, 2020, doi: 10.1038/s41578-020-0216-y.

[19] H. Razik, "Models of Asynchronous Machines," in *Handbook of Asynchronous Machine with Variable Speed*, 2013, pp. 59–136. doi: https://doi.org/10.1002/9781118601037.ch3.

[20] R. Crowder, "Induction motors," *Electric Drives and Electromechanical Systems*, pp. 187–207, Jan. 2020, doi: 10.1016/B978-0-08-102884-1.00007-8.

[21] J. Bonal and G. Séguier, *ENTRAINEMENTS ELECTRIQUES A VITESSE VARIABLE.* in Entraînements électriques à vitesse variable. Tec & Doc Lavoisier, 1997. [Online]. Available: https://books.google.dz/books?id=dWSoPAAACAAJ

[22] H. Chen, Y. Zuo, K. T. Chau, W. Zhao, and C. H. T. Lee, "Modern electric machines and drives for wind power generation: A review of opportunities and challenges," *IET Renewable Power Generation*, vol. 15, no. 9, pp. 1864–1887, Jul. 2021, doi: https://doi.org/10.1049/rpg2.12114.

[23] R. Crowder, "7 - Induction motors," in *Electric Drives and Electromechanical Systems (Second Edition)*, Second Edition., R. Crowder, Ed., Butterworth-Heinemann, 2020, pp. 187–207. doi: https://doi.org/10.1016/B978-0-08-102884-1.00007-8.

[24] J. A. Antonino-Daviu, M. Riera-Guasp, J. Pons-Llinares, J. Roger-Folch, R. B. Pérez, and C. Charlton-Pérez, "Toward Condition Monitoring of Damper Windings in Synchronous Motors via EMD Analysis," *IEEE Transactions on Energy Conversion*, vol. 27, no. 2, pp. 432–439, 2012, doi: 10.1109/TEC.2012.2190292.

[25] W. le Roux, R. G. Harley, and T. G. Habetler, "Detecting Rotor Faults in Low Power Permanent Magnet Synchronous Machines," *IEEE Trans Power Electron*, vol. 22, no. 1, pp. 322–328, 2007, doi: 10.1109/TPEL.2006.886620.

[26] L. F. P. de Oliveira, F. J. de O. Morais, and L. T. Manera, "Development of an energy harvesting system based on a thermoelectric generator for use in online predictive maintenance systems of industrial electric motors," *Sustainable Energy Technologies and Assessments*, vol. 60, p. 103572, Dec. 2023, doi: 10.1016/J.SETA.2023.103572.

[27] M. Seera, C. P. Lim, S. Nahavandi, and C. K. Loo, "Condition monitoring of induction motors: A review and an application of an ensemble of hybrid intelligent models," *Expert Syst Appl*, vol. 41, no. 10, pp. 4891–4903, Aug. 2014, doi: 10.1016/J.ESWA.2014.02.028.

[28] G. Didier, "Modélisation et diagnostic de la machine asynchrone en présence de défaillances," *These de doctorat de l'université Henri Poincaré, Nancy-I*, 2004.

[29] A. M. Trzynadlowski, *The field orientation principle in control of induction motors*. Springer Science & Business Media, 2013.

[30] K. Arnold and M. Stewart, "Electrical Systems**Reviewed for the 1999 edition by Dinesh P. Patel of Paragon Engineering Services, Inc.," *Surface Production Operations: Design of Gas-Handling Systems and Facilities*, pp. 493–552, 1999, doi: 10.1016/B978-088415822-6/50018-0.

[31] R. R. R. Deshmukh, *Voltage harmonics analysis and efficiency of three-phase induction motor with change in coil pitch of the stator winding*. Cardiff University (United Kingdom), 2006.

[32] R. H. Romer, "What do '"voltmeters"'measure?: Faraday's law in a multiply connected region," *Am J Phys*, vol. 50, no. 12, pp. 1089–1093, 1982.

[33] T. H. Morgan, W. E. Brown, and A. J. Schumer, "Induction-motor characteristics at high slip," *Electrical Engineering*, vol. 59, no. 8, pp. 464–468, 1940.

[34] S. J. Salon, C. J. Slavik, M. J. DeBortoli, and G. Reyne, "ANALYSIS OF MAGNETIC VIBRATIONS IN ROTATING ELECTRIC MACHINES," *Finite Elements, Electromagnetics and Design*, pp. 116–178, 1995, doi: 10.1016/B978-044489563-9/50024-5.

[35] K. Arnold and M. Stewart, "Electrical Systems**Reviewed for the 1999 edition by Dinesh P. Patel of Paragon Engineering Services, Inc.," *Surface Production Operations: Design of Gas-Handling Systems and Facilities*, pp. 493–552, 1999, doi: 10.1016/B978-088415822-6/50018-0.

[36] S. Singh, P. Sharma, A. Varshney, and A. Kumar, "Speed Control of Multilevel Inverter-Based Induction Motor Using V/F Method," in *Proceedings of Fourth International Conference on Soft Computing for Problem Solving*, K. N. Das, K. Deep, M. Pant, J. C. Bansal, and A. Nagar, Eds., New Delhi: Springer India, 2015, pp. 231–243.

[37] H. M. Mzungu, A. B. Sebitosi, and M. A. Khan, "Comparison of standards for determining losses and efficiency of three-phase induction motors," in *2007 IEEE*

Power Engineering Society Conference and Exposition in Africa-PowerAfrica, IEEE, 2007, pp. 1–6.

[38] B. Ch SAI BABU and A. Pradesh, "ONLINE GATE COACHING CLASSES Lecture 8 of Electrical Machines Topic: Three phase induction motors."

[39] Allianz, "Présentation des avaries. Machines électriques tournantes," 1988.

[40] A. E. Fitzgerald, C. Kingsley, and S. D. Umans, *Electric machinery*. McGraw-Hill, 2003.

[41] B. K. Bose, "Power electronics and AC drives," *Englewood Cliffs*, 1986.

[42] J. Bonal and G. Séguier, *Entraînements électriques à vitesse variable: Rappels d'électronique de puissance et d'automatique, les variateurs électroniques de vitesse*. in Entraînements électriques à vitesse variable. Tec & doc-Lavoisier, 1999. [Online]. Available: https://books.google.dz/books?id=XvDFAAAACAAJ

[43] O. Ondel, "Diagnostic par reconnaissance des formes : application à un ensemble convertisseur - machine asynchrone. (Diagnosis by Pattern Recognition: application on a set inverter - induction machine)," 2006. [Online]. Available: https://api.semanticscholar.org/CorpusID:32144099

[44] S. Karmakar, S. Chattopadhyay, M. Mitra, and S. Sengupta, "Induction Motor and Faults," in *Induction Motor Fault Diagnosis: Approach through Current Signature Analysis*, S. Karmakar, S. Chattopadhyay, M. Mitra, and S. Sengupta, Eds., Singapore: Springer Singapore, 2016, pp. 7–28. doi: 10.1007/978-981-10-0624-1_2.

[45] S. Nandi, H. A. Toliyat, and X. Li, "Condition Monitoring and Fault Diagnosis of Electrical Motors—A Review," *IEEE Transactions on Energy Conversion*, vol. 20, no. 4, pp. 719–729, 2005, doi: 10.1109/TEC.2005.847955.

[46] O. V Thorsen and M. Dalva, "A survey of faults on induction motors in offshore oil industry, petrochemical industry, gas terminals, and oil refineries," *IEEE Trans Ind Appl*, vol. 31, no. 5, pp. 1186–1196, 1995, doi: 10.1109/28.464536.

[47] J. Cusido, J. Rosero Garcia, E. Aldabas, J. Ortega, and L. Romeral, *Fault detection techniques for induction motors*, vol. 2005. 2005. doi: 10.1109/CPE.2005.1547550.

[48] M. Reliability, "Report of Large Motor Reliability Survey of Industrial and Commercial Installations, Part I."

[49] O. Vaag Thorsen and M. Dalva, "Transportation A Survey of Faults on Induction Motors in Offshore Oil Industry, Petrochemical Industry, Gas Terminals, and Oil Refineries."

[50] G. Rayappan, V. Duraisamy, D. Somasundareswari, and I. Rajarajeswari, "Implementation of Wavelet Packet Transform for Detection and Analysis of Stator Faults in Induction Machine," *Circuits and Systems*, vol. 07, no. 10, pp. 3253–3259, 2016, doi: 10.4236/cs.2016.710277.

[51] IEEE Industry Applications Society. Power Systems Reliability Subcommittee. and IEEE Standards Board., *IEEE recommended practice for the design of reliable industrial and commercial power systems*. Institute of Electrical and Electronics Engineers, 1998.

[52] P. F. Albrecht, J. C. Appiarius, R. M. Mccoy, E. L. Owen, and D. K. Sharma, "Fig 1 Magnetic pull force and spring force versus eccentric ¡ty of rotor center Assessment of the Reliability of Motors in Utility Applications. Updated," 1986.

[53] S. K. Gundewar and P. V Kane, "Condition Monitoring and Fault Diagnosis of Induction Motor," *Journal of Vibration Engineering & Technologies*, vol. 9, no. 4, pp. 643–674, 2021, doi: 10.1007/s42417-020-00253-y.

[54] R. Ouhibi, S. Bouslama, and K. Laabidi, "Faults classification of asynchronous machine based on the probabilistic neural network (PNN)," in *2016 4th International Conference on Control Engineering & Information Technology (CEIT)*, 2016, pp. 1–7. doi: 10.1109/CEIT.2016.7929124.

[55] S. Sakhara, S. Saad, and L. Nacib, "Diagnosis and detection of short circuit in asynchronous motor using three-phase model," *International Journal of System Assurance Engineering and Management*, vol. 8, no. 2, pp. 308–317, 2017, doi: 10.1007/s13198-016-0435-1.

[56] A. Gandhi, T. Corrigan, and L. Parsa, "Recent Advances in Modeling and Online Detection of Stator Interturn Faults in Electrical Motors," *IEEE Transactions on Industrial Electronics*, vol. 58, no. 5, pp. 1564–1575, 2011, doi: 10.1109/TIE.2010.2089937.

[57] W. T. Thomson, "A review of on-line condition monitoring techniques for three-phase squirrel-cage induction motors-past present and future," in *Keynote address at IEEE symposium on diagnostics for electrical machines, power electronics and drives, Gijon, Spain*, 1999, pp. 3–18.

[58] A. H. Bonnett and C. Yung, "Increased Efficiency Versus Increased Reliability," *IEEE Industry Applications Magazine*, vol. 14, 2008, [Online]. Available: https://api.semanticscholar.org/CorpusID:18008055

[59] W. Abu Elhaija and Q. Abu Al-Haija, "A novel dataset and lightweight detection system for broken bars induction motors using optimizable neural networks," *Intelligent Systems with Applications*, vol. 17, p. 200167, Feb. 2023, doi: 10.1016/J.ISWA.2022.200167.

[60] M. F. Yakhni *et al.*, "Variable speed induction motors' fault detection based on transient motor current signatures analysis: A review," *Mech Syst Signal Process*, vol. 184, p. 109737, Feb. 2023, doi: 10.1016/J.YMSSP.2022.109737.

[61] B. Asad, T. Vaimann, A. Belahcen, A. Kallaste, A. Rassõlkin, and M. N. Iqbal, "The Cluster Computation-Based Hybrid FEM–Analytical Model of Induction Motor for Fault Diagnostics," *Applied Sciences*, vol. 10, no. 21, 2020, doi: 10.3390/app10217572.

[62] M. Valtierra-Rodriguez, J. R. Rivera-Guillen, J. A. Basurto-Hurtado, J. J. De-Santiago-Perez, D. Granados-Lieberman, and J. P. Amezquita-Sanchez, "Convolutional Neural Network and Motor Current Signature Analysis during the Transient State for Detection of Broken Rotor Bars in Induction Motors," *Sensors*, vol. 20, no. 13, 2020, doi: 10.3390/s20133721.

[63] Y. Wu, S. Sun, Q. An, and X. Lie, "Treatment Strategy Research on a Squirrel-Cage Induction Motor with Broken Rotor Bar Faults," *Sensors*, vol. 22, no. 12, 2022, doi: 10.3390/s22124345.

[64] M. Jagiela, M. Kaminski, and K. Macek-Kaminska, "Estimation of squirrel cage induction motor equivalent circuit parameters from characteristics predicted by the finite element model," in *Computer Field Models of Electromagnetic Devices*, IOS Press, 2010, pp. 440–447.

[65] A. Bouras, S. Bouras, and S. Kerfali, "Prediction of the mass unbalance of a variable speed induction motor by stator current multiple approaches," *Turkish Journal of Electrical Engineering and Computer Sciences*, vol. 26, no. 2, pp. 1056–1068, 2018, doi: 10.3906/elk-1702-58.

[66] H. Kim, J. Nerg, T. Choudhury, and J. Sopanen, "Rotordynamic Simulation Method of Induction Motors Including the Effects of Unbalanced Magnetic Pull," *IEEE Access*, vol. 8, pp. 21631–21643, 2021, doi: 10.1109/access.2020.2968915.

[67] A. Salah, D. Dorrell, and Y. Guo, "A Review of the Monitoring and Damping Unbalanced Magnetic Pull in Induction Machines Due to Rotor Eccentricity," *IEEE Trans Ind Appl*, vol. 55, pp. 2569–2580, 2019, doi: 10.1109/tia.2019.2892359.

[68] S. Ram, M. Upadhyay, and S. Ram, "A Review on Different Types of Faults in Induction Motor and Methods to Control Speed of Induction Motors," *Research Journal of Engineering Technology and Medical Sciences (ISSN: 2582-6212)*, vol. 5, no. 03, 2022.

[69] P. Donolo, G. Bossio, C. De Angelo, G. García, and M. Donolo, "Voltage unbalance and harmonic distortion effects on induction motor power, torque and vibrations," *Electric Power Systems Research*, vol. 140, pp. 866–873, Nov. 2016, doi: 10.1016/J.EPSR.2016.04.018.

[70] L. Smolík, Š. Dyk, and J. Rendl, "Role of dynamic unbalance in dynamics of turbocharger rotors," *Int J Mech Sci*, p., 2023, doi: 10.1016/j.ijmecsci.2023.108237.

[71] M. Tiwari, K. Gupta, and O. Prakash, "DYNAMIC RESPONSE OF AN UNBALANCED ROTOR SUPPORTED ON BALL BEARINGS," *J Sound Vib*, vol. 238, pp. 757–779, 2000, doi: 10.1006/jsvi.1999.3108.

[72] W. T. Thomson and M. Fenger, “Current signature analysis to detect induction motor faults,” *IEEE Industry Applications Magazine*, vol. 7, no. 4, pp. 26–34, 2001, doi: 10.1109/2943.930988.

[73] M. Ahmed, K. Imran, and S. JunaidAkhtar, “Detection of eccentricity faults in machine usingfrequency spectrum technique,” *International journal of computer and Electrical Engineering*, vol. 3, no. 1, p. 111, 2011.

[74] G. Didier, “Modélisation et diagnostic de la machine asynchrone en présence de défaillances,” 2004. [Online]. Available: http://www.theses.fr/2004NAN10163

[75] S. M. Al-Ameri *et al.*, “Application of Frequency Response Analysis Method to Detect Short-Circuit Faults in Three-Phase Induction Motors,” *Applied Sciences*, vol. 12, no. 4, 2022, doi: 10.3390/app12042046.

[76] W. T. T, “ON-LINE MCSA TO DIAGNOSE SHORTl3D TURNS IN LOW VOLTAGE STATOR WINDINGS OF 3-PHASE INDUCTION MOTORS PRIOR TO FAILURE.”

[77] W. H. Kersting, “Causes and effects of single-phasing induction motors,” in *Rural Electric Power Conference, 2004*, 2004, pp. A4-1. doi: 10.1109/REPCON.2004.1307038.

[78] S. Chattopadhyay, S. Karmakar, M. Mitra, and S. Sengupta, “Assessment of crawling of an induction motor by stator current Concordia analysis,” *Electron Lett*, vol. 48, pp. 841–842, 2012, doi: 10.1049/el.2011.4008.

[79] B. J. Hamrock and W. J. Anderson, “NASA Reference Publication Rolling-Element Bearings,” 1105.

[80] P. Pennacchi, P. Borghesani, R. Ricci, and S. Chatterton, “An experimental based assessment of the deviation of the bearing characteristic frequencies,” *Science & Engineering Faculty*, 2011, [Online]. Available: https://api.semanticscholar.org/CorpusID:107691760

[81] A. Rai and S. H. Upadhyay, “A review on signal processing techniques utilized in the fault diagnosis of rolling element bearings,” *Tribol Int*, vol. 96, pp. 289–306, 2016, doi: https://doi.org/10.1016/j.triboint.2015.12.037.

[82] R. Boudiaf, B. Abdelkarim, and H. Issam, “Bearing fault diagnosis in induction motor using continuous wavelet transform and convolutional neural networks,” *International Journal of Power Electronics and Drive Systems (IJPEDS)*, vol. 15, no. 1, pp. 591–602, 2024.

[83] A. M. Al-Ghamd and D. Mba, “A comparative experimental study on the use of acoustic emission and vibration analysis for bearing defect identification and estimation of defect size,” *Mech Syst Signal Process*, vol. 20, no. 7, pp. 1537–1571, 2006, doi: https://doi.org/10.1016/j.ymssp.2004.10.013.

[84] S. Al-Dossary, R. I. R. Hamzah, and D. Mba, “Observations of changes in acoustic emission waveform for varying seeded defect sizes in a rolling element bearing,” *Applied Acoustics*, vol. 70, no. 1, pp. 58–81, 2009, doi: https://doi.org/10.1016/j.apacoust.2008.01.005.

[85] D. S. and K. J. G. and K. Y. C. and C. B. K. Kim Byeong Su and Gu, “Rolling element bearing fault detection using acoustic emission signal analyzed by envelope analysis with discrete wavelet transform,” in *Engineering Asset Lifecycle Management*, C. and K. A. and M. J. Kiritsis Dimitris and Emmanouilidis, Ed., London: Springer London, 2010, pp. 596–602.

[86] F. Hemmati, “Rolling element bearing condition monitoring using acoustic emission technique and advanced signal processing,” 2012. [Online]. Available: https://open.library.ubc.ca/collections/24/items/1.0073166

[87] E. Y. Kim, A. C. C. Tan, J. Mathew, and B. S. Yang, “Condition monitoring of low speed bearings: A comparative study of the ultrasound technique versus vibration measurements,” *Australian Journal of Mechanical Engineering*, vol. 5, pp. 177–189, 2008, [Online]. Available: https://api.semanticscholar.org/CorpusID:6199119

[88] J. Lineham, “Ultrasonic probes for inspecting bearings,” *World Pumps*, vol. 2008, no. 503, pp. 34–36, 2008, doi: https://doi.org/10.1016/S0262-1762(08)70252-9.

[89] V. Hegde and G. S. Maruthi, “Experimental investigation on detection of air gap eccentricity in induction motors by current and vibration signature analysis using non-invasive sensors,” *Energy Procedia*, vol. 14, pp. 1047–1052, 2012, doi: https://doi.org/10.1016/j.egypro.2011.12.1053.

[90] V. F. Pires, M. Kadivonga, J. F. Martins, and A. J. Pires, “Motor square current signature analysis for induction motor rotor diagnosis,” *Measurement*, vol. 46, no. 2, pp. 942–948, 2013, doi: https://doi.org/10.1016/j.measurement.2012.10.008.

[91] R. R. Schoen, T. G. Habetler, F. Kamran, and R. G. Bartfield, “Motor bearing damage detection using stator current monitoring,” *IEEE Trans Ind Appl*, vol. 31, no. 6, pp. 1274–1279, 1995, doi: 10.1109/28.475697.

[92] Z. Peng and N. Kessissoglou, “An integrated approach to fault diagnosis of machinery using wear debris and vibration analysis,” *Wear*, vol. 255, no. 7, pp. 1221–1232, 2003, doi: https://doi.org/10.1016/S0043-1648(03)00098-X.

[93] T. J. Harvey, R. J. K. Wood, and H. E. G. Powrie, “Electrostatic wear monitoring of rolling element bearings,” *Wear*, vol. 263, no. 7, pp. 1492–1501, 2007, doi: https://doi.org/10.1016/j.wear.2006.12.073.

[94] L. Wang, Y. Yan, Y. Hu, and X. Qian, “Intelligent condition monitoring of rotating machinery through electrostatic sensing and signal analysis,” in *2013 IEEE International Conference on Smart Instrumentation, Measurement and Applications (ICSIMA)*, 2013, pp. 1–4. doi: 10.1109/ICSIMA.2013.6717951.

[95] "Vibration Signals from Rotating and Reciprocating Machines," in *Vibration–based Condition Monitoring*, John Wiley & Sons, Ltd, 2021, ch. 2, pp. 25–61. doi: https://doi.org/10.1002/9781119477631.ch2.

[96] V. N. Patel, N. Tandon, and R. K. Pandey, "Vibration Studies of Dynamically Loaded Deep Groove Ball Bearings in Presence of Local Defects on Races," *Procedia Eng*, vol. 64, pp. 1582–1591, 2013, doi: https://doi.org/10.1016/j.proeng.2013.09.240.

[97] F. Cong, J. Chen, G. Dong, and M. Pecht, "Vibration model of rolling element bearings in a rotor-bearing system for fault diagnosis," *J Sound Vib*, vol. 332, no. 8, pp. 2081–2097, 2013, doi: https://doi.org/10.1016/j.jsv.2012.11.029.

[98] J. Mathew and R. J. Alfredson, "The condition monitoring of rolling element bearings using vibration analysis," *Journal of Vibration and Acoustics-transactions of The Asme*, vol. 106, pp. 447–453, 1984, [Online]. Available: https://api.semanticscholar.org/CorpusID:108773698

[99] J. Antoni, "Cyclic spectral analysis in practice," *Mech Syst Signal Process*, vol. 21, no. 2, pp. 597–630, 2007, doi: https://doi.org/10.1016/j.ymssp.2006.08.007.

[100] R. Casimir, "Diagnostic des défauts des machines asynchrones par reconnaissance des formes," Ecole Centrale de Lyon, 2003. [Online]. Available: https://theses.hal.science/tel-00139706

[101] M. Ohring, "Mechanical Properties of Thin Films," *Materials Science of Thin Films*, pp. 711–781, 2002, doi: 10.1016/B978-012524975-1/50015-X.

[102] S. K. Gundewar and P. V. Kane, "Condition Monitoring and Fault Diagnosis of Induction Motor," Jun. 01, 2021, *Springer*. doi: 10.1007/s42417-020-00253-y.

[103] J. Kerber, "Akustische Untersuchung fehlerhafter Verzahnungen bei Fahrzeuggetrieben."

[104] G. Zwingelstein, *Diagnostic des défaillances : théorie et pratique pour les systèmes industriels*. Hermès, 1995.

[105] M. Combacau, "Commande et surveillance des systèmes a évéments discrets complexes : application aux ateliers flexibles," 1991.

[106] A. S. Willsky, "A survey of design methods for failure detection in dynamic systems," *Automatica*, vol. 12, no. 6, pp. 601–611, 1976.

[107] R. Zemouri, "Contribution à la surveillance des systèmes de production à l'aide des réseaux de neurones dynamiques : Application à la e-maintenance," 2003.

[108] M. Basseville, "Detecting changes in signals and systems—a survey," *Automatica*, vol. 24, no. 3, pp. 309–326, 1988.

[109] M. Combacau, P. Berrut, F. Charbonnaud, and A. Khatab, “Réflexions sur la terminologie : Surveillance-supervision,” *Groupement pour la recherche en Produtique, Systèmes de Production Sûrs de Fonctionnement*, 2000.

[110] H. L. Jones, “Failure detection in linear systems,” 1973.

[111] R. V. Beard, “Failure accomodation in linear systems through self-reorganization,” 1971.

[112] J. Gertler and D. Singer, “A new structural framework for parity equation-based failure detection and isolation,” *Automatica*, vol. 26, no. 2, pp. 381–388, 1990.

[113] L. Travé-Massuyès, P. Dague, and F. Guerrin, *Le raisonnement qualitatif pour les sciences de l’ingénieur*. Hermès science publications, 1997.

[114] P. J. Mosterman, “Diagnosis of physical systems with hybrid models using parametrized causality,” in *Hybrid Systems: Computation and Control: 4th International Workshop, HSCC 2001 Rome, Italy, March 28–30, 2001 Proceedings 4*, Springer, 2001, pp. 447–458.

[115] M. Sampath, R. Sengupta, S. Lafortune, K. Sinnamohideen, and D. Teneketzis, “Diagnosability of discrete-event systems,” *IEEE Trans Automat Contr*, vol. 40, no. 9, pp. 1555–1575, 1995.

[116] P. Bhowal, D. Sarkar, S. Mukhopadhyay, and A. Basu, “Fault diagnosis in discrete time hybrid systems–a case study,” *Inf Sci (N Y)*, vol. 177, no. 5, pp. 1290–1308, 2007.

[117] A. K. Samantaray and B. O. Bouamama, “Diagnostic and Bicausal Bond Graphs for FDI,” *Model-based Process Supervision: A Bond Graph Approach*, pp. 271–314, 2008.

[118] J. Brunet, D. Jaume, M. Labarrère, A. Rault, and M. Verge, “Détection et diagnostic de pannes: approche par modélisation,” *Hermès Sciences publication*, 1990.

[119] B. Dubuisson, “Diagnostic et reconnaissance des formes, Traité des nouvelles Technonlogies, série Diagnostic et Maintenance,” *Hermes (Wiesb)*, 1990.

[120] F. Zeng, Y. Li, Y. Jiang, and G. Song, “An online transfer learning-based remaining useful life prediction method of ball bearings,” *Measurement*, vol. 176, p. 109201, 2021, doi: https://doi.org/10.1016/j.measurement.2021.109201.

[121] L. Ciabattoni, F. Ferracuti, A. Freddi, and A. Monteriu, “Statistical spectral analysis for fault diagnosis of rotating machines,” *IEEE Transactions on Industrial Electronics*, vol. 65, no. 5, pp. 4301–4310, 2017.

[122] X. Liang, M. J. Zuo, and Z. Feng, “Dynamic modeling of gearbox faults: A review,” *Mech Syst Signal Process*, vol. 98, pp. 852–876, 2018.

[123] P. D. Samuel and D. J. Pines, “A review of vibration-based techniques for helicopter transmission diagnostics,” *J Sound Vib*, vol. 282, no. 1–2, pp. 475–508, 2005.

[124] Z. Feng and M. J. Zuo, "Vibration signal models for fault diagnosis of planetary gearboxes," *J Sound Vib*, vol. 331, no. 22, pp. 4919–4939, 2012.

[125] X. Wang, S. Si, Y. Wei, and Y. Li, "The optimized multi-scale permutation entropy and its application in compound fault diagnosis of rotating machinery," *Entropy*, vol. 21, no. 2, p. 170, 2019.

[126] L. Márton and F. van der Linden, "Temperature dependent friction estimation: Application to lubricant health monitoring," *Mechatronics*, vol. 22, no. 8, pp. 1078–1084, 2012.

[127] J. Liang and Z. Yang, "A novel wavelet transform–empirical mode decomposition based sample entropy and SVD approach for acoustic signal fault diagnosis," in *Advances in Swarm and Computational Intelligence: 6th International Conference, ICSI 2015 held in conjunction with the Second BRICS Congress, CCI 2015, Beijing, China, June 25-28, 2015, Proceedings, Part III 6*, Springer, 2015, pp. 232–241.

[128] T. S. Mohammed, M. Rasheed, M. Al-Ani, Q. Al-Shayea, and F. Alnaimi, "Fault diagnosis of rotating machine based on audio signal recognition system: an efficient approach," *Int. J. Simul. Syst. Sci. Technol*, vol. 21, pp. 1–8, 2020.

[129] Y. He and X. Zhang, "Approximate entropy analysis of the acoustic emission from defects in rolling element bearings," *J Vib Acoust*, vol. 134, no. 6, p. 061012, 2012.

[130] O. Janssens *et al.*, "Thermal image based fault diagnosis for rotating machinery," *Infrared Phys Technol*, vol. 73, pp. 78–87, 2015.

[131] A. M. D. Younus and B.-S. Yang, "Intelligent fault diagnosis of rotating machinery using infrared thermal image," *Expert Syst Appl*, vol. 39, no. 2, pp. 2082–2091, 2012.

[132] E. Resendiz-Ochoa, R. A. Osornio-Rios, J. P. Benitez-Rangel, L. A. Morales-Hernandez, and R. de J. Romero-Troncoso, "Segmentation in thermography images for bearing defect analysis in induction motors," in *2017 IEEE 11th International Symposium on Diagnostics for Electrical Machines, Power Electronics and Drives (SDEMPED)*, IEEE, 2017, pp. 572–577.

[133] M. Vollmer, "Infrared thermal imaging," in *Computer Vision: A Reference Guide*, Springer, 2021, pp. 666–670.

[134] D. Gabor, "Theory of communication. Part 1: The analysis of information," *Journal of the Institution of Electrical Engineers-part III: radio and communication engineering*, vol. 93, no. 26, pp. 429–441, 1946.

[135] I. P. Tsoumas, G. Georgoulas, E. D. Mitronikas, and A. N. Safacas, "Asynchronous machine rotor fault diagnosis technique using complex wavelets," *IEEE Transactions on Energy Conversion*, vol. 23, no. 2, pp. 444–459, 2008.

[136] R. Yan, R. X. Gao, and X. Chen, "Wavelets for fault diagnosis of rotary machines: A review with applications," *Signal Processing*, vol. 96, pp. 1–15, 2014.

[137] J. Morlet, G. Arens, E. Fourgeau, and D. Glard, “Wave propagation and sampling theory—Part I: Complex signal and scattering in multilayered media,” *Geophysics*, vol. 47, no. 2, pp. 203–221, 1982.

[138] J. Morlet, G. Arens, E. Fourgeau, and D. Giard, “Wave propagation and sampling theory; Part II, Sampling theory and complex waves,” *Geophysics*, vol. 47, no. 2, pp. 222–236, 1982.

[139] A. Grossmann and J. Morlet, “Decomposition of Hardy functions into square integrable wavelets of constant shape,” *SIAM journal on mathematical analysis*, vol. 15, no. 4, pp. 723–736, 1984.

[140] F. Truchetet, *Ondelettes pour le signal numérique*. Hermes Paris, 1998.

[141] S. G. Chang, B. Yu, and M. Vetterli, “Spatially adaptive wavelet thresholding with context modeling for image denoising,” *IEEE Transactions on image Processing*, vol. 9, no. 9, pp. 1522–1531, 2000.

[142] S. G. Chang, B. Yu, and M. Vetterli, “Adaptive wavelet thresholding for image denoising and compression,” *IEEE transactions on image processing*, vol. 9, no. 9, pp. 1532–1546, 2000.

[143] J. McCarthy, “4.2 Asset price inflation,",” *Boom & Bust: A Look at Economic Bubbles*, p. 207, 2015.

[144] Y. Yuan, H. Xu, and B. Wang, “An improved NSGA-III procedure for evolutionary many-objective optimization,” in *Proceedings of the 2014 annual conference on genetic and evolutionary computation*, 2014, pp. 661–668.

[145] A. Glowacz and Z. Glowacz, “Diagnostics of stator faults of the single-phase induction motor using thermal images, MoASoS and selected classifiers,” *Measurement*, vol. 93, pp. 86–93, 2016.

[146] M. R. Mehrjou *et al.*, “Wavelet-Based Analysis of MCSA for Fault Detection in Electrical Machine,” in *Wavelet Transform and Some of Its Real-World Applications*, D. Baleanu, Ed., Rijeka: IntechOpen, 2015, p. Ch. 5. doi: 10.5772/61532.

[147] C. S. Syan and G. Ramsoobag, “Empirical Mode Decomposition for Fault Diagnosis of Multi-Component Systems,” in *2018 Annual Reliability and Maintainability Symposium (RAMS)*, 2018, pp. 1–7. doi: 10.1109/RAM.2018.8463000.

[148] H. Liu, L. Li, and J. Ma, “Rolling Bearing Fault Diagnosis Based on STFT-Deep Learning and Sound Signals,” *Shock and Vibration*, vol. 2016, p. 6127479, 2016, doi: 10.1155/2016/6127479.

[149] B. R. Nayana and P. Geethanjali, “Effective time domain features for identification of bearing fault using LDA and NB classifiers,” *Int J Mech Product Eng Res Dev*, vol. 8, pp. 1135–1150, 2018.

[150] J. Chang, T. Li, and P. Li, “The selection of time domain characteristic parameters of rotating machinery fault diagnosis,” in *2010 International Conference on Logistics Systems and Intelligent Management (ICLSIM)*, IEEE, 2010, pp. 619–623.

[151] E. J. Cross, G. Manson, K. Worden, and S. G. Pierce, “Features for damage detection with insensitivity to environmental and operational variations,” *Proceedings of the Royal Society A: Mathematical, Physical and Engineering Sciences*, vol. 468, no. 2148, pp. 4098–4122, 2012.

[152] Y. Lei, D. Kong, J. Lin, and M. J. Zuo, “Fault detection of planetary gearboxes using new diagnostic parameters,” *Meas Sci Technol*, vol. 23, no. 5, p. 055605, 2012.

[153] V. Vapnik, *The nature of statistical learning theory*. Springer science & business media, 2013.

[154] Z. Wang and X. Xue, “Multi-class support vector machine,” *Support vector machines applications*, pp. 23–48, 2014.

[155] A. Kabla and K. Mokrani, “Bearing fault diagnosis using Hilbert-Huang transform (HHT) and support vector machine (SVM),” *Mechanics & Industry*, vol. 17, no. 3, p. 308, 2016.

[156] C. Rajeswari, B. Sathiyabhama, S. Devendiran, and K. Manivannan, “Bearing fault diagnosis using multiclass support vector machine with efficient feature selection methods,” *Int. J. Mech. Mechatronics Eng*, 2015.

[157] H. Keskes, A. Braham, and Z. Lachiri, “Broken rotor bar diagnosis in induction machines through stationary wavelet packet transform and multiclass wavelet SVM,” *Electric Power Systems Research*, vol. 97, pp. 151–157, 2013.

[158] P. Konar, J. Sil, and P. Chattopadhyay, “Knowledge extraction using data mining for multi-class fault diagnosis of induction motor,” *Neurocomputing*, vol. 166, pp. 14–25, 2015.

[159] P. Zitha and B. A. Thango, “On the Study of Induction Motor Fault Identification using Support Vector Machine Algorithms,” in *2023 31st Southern African Universities Power Engineering Conference (SAUPEC)*, 2023, pp. 1–5. doi: 10.1109/SAUPEC57889.2023.10057836.

[160] K. Yatsugi, E. P. Shrinathan, Y. Mizuno, and H. Nakamura, “Support Vector Machine Aided Diagnosis of Concurrent Multiple Faults in Induction Motor,” in *2023 IEEE International Conference on Industrial Technology (ICIT)*, 2023, pp. 1–6. doi: 10.1109/ICIT58465.2023.10143119.

[161] F. Chen, B. Tang, T. Song, and L. Li, “Multi-fault diagnosis study on roller bearing based on multi-kernel support vector machine with chaotic particle swarm optimization,” *Measurement*, vol. 47, pp. 576–590, 2014.

[162] H. H. Kim and J. Y. Choi, "Hierarchical multi-class LAD based on OvA-binary tree using genetic algorithm," *Expert Syst Appl*, vol. 42, no. 21, pp. 8134–8145, 2015.

[163] D. Martínez-Rego, O. Fontenla-Romero, A. Alonso-Betanzos, and J. C. Principe, "Fault detection via recurrence time statistics and one-class classification," *Pattern Recognit Lett*, vol. 84, pp. 8–14, 2016.

[164] S. Zgarni and A. Braham, "Classification of Bearing Fault Detection Using Multiclass SVM: A Comparative Study," in *2018 15th International Multi-Conference on Systems, Signals & Devices (SSD)*, 2018, pp. 888–892. doi: 10.1109/SSD.2018.8570564.

[165] S. Walker, W. Khan, K. Katic, W. Maassen, and W. Zeiler, "Accuracy of different machine learning algorithms and added-value of predicting aggregated-level energy performance of commercial buildings," *Energy Build*, vol. 209, p. 109705, Feb. 2020, doi: 10.1016/J.ENBUILD.2019.109705.

[166] Y. LeCun *et al.*, "Handwritten digit recognition with a back-propagation network," *Adv Neural Inf Process Syst*, vol. 2, 1989.

[167] A. Krizhevsky, I. Sutskever, and G. E. Hinton, "Imagenet classification with deep convolutional neural networks," *Adv Neural Inf Process Syst*, vol. 25, 2012.

[168] M. Jiménez-Guarneros, C. Morales-Perez, and J. d. J. Rangel-Magdaleno, "Diagnostic of Combined Mechanical and Electrical Faults in ASD-Powered Induction Motor Using MODWT and a Lightweight 1-D CNN," *IEEE Trans Industr Inform*, vol. 18, no. 7, pp. 4688–4697, 2022, doi: 10.1109/TII.2021.3120975.

[169] R. N. Toma, A. E. Prosvirin, and J.-M. Kim, "Bearing Fault Diagnosis of Induction Motors Using a Genetic Algorithm and Machine Learning Classifiers," *Sensors*, vol. 20, no. 7, 2020, doi: 10.3390/s20071884.

[170] I. Y. Önel and M. E. H. Benbouzid, "Induction Motor Bearing Failure Detection and Diagnosis: Park and Concordia Transform Approaches Comparative Study," *IEEE/ASME Transactions on Mechatronics*, vol. 13, no. 2, pp. 257–262, 2008, doi: 10.1109/TMECH.2008.918535.

[171] A. Glowacz, "Fault diagnosis of single-phase induction motor based on acoustic signals," *Mech Syst Signal Process*, vol. 117, pp. 65–80, Feb. 2019, doi: 10.1016/J.YMSSP.2018.07.044.

[172] A. Glowacz, W. Glowacz, Z. Glowacz, and J. Kozik, "Early fault diagnosis of bearing and stator faults of the single-phase induction motor using acoustic signals," *Measurement*, vol. 113, pp. 1–9, Jan. 2018, doi: 10.1016/J.MEASUREMENT.2017.08.036.

[173] C.-Y. Hsu, Y.-W. Lu, and J.-H. Yan, "Temporal Convolution-Based Long-Short Term Memory Network With Attention Mechanism for Remaining Useful Life Prediction," *IEEE Transactions on Semiconductor Manufacturing*, vol. 35, no. 2, pp. 220–228, 2022, doi: 10.1109/TSM.2022.3164578.

[174] H. Wu, A. Huang, and J. W. Sutherland, “Layer-wise relevance propagation for interpreting LSTM-RNN decisions in predictive maintenance,” *The International Journal of Advanced Manufacturing Technology*, pp. 1–16, 2022.

[175] G. A. Susto, A. Schirru, S. Pampuri, S. McLoone, and A. Beghi, “Machine Learning for Predictive Maintenance: A Multiple Classifier Approach,” *IEEE Trans Industr Inform*, vol. 11, no. 3, pp. 812–820, 2015, doi: 10.1109/TII.2014.2349359.

[176] C. Chen *et al.*, “Predictive maintenance using cox proportional hazard deep learning,” *Advanced Engineering Informatics*, vol. 44, p. 101054, Apr. 2020, doi: 10.1016/J.AEI.2020.101054.

[177] J. Hu, L. Zhang, and W. Liang, “Opportunistic predictive maintenance for complex multi-component systems based on DBN-HAZOP model,” *Process Safety and Environmental Protection*, vol. 90, no. 5, pp. 376–388, Sep. 2012, doi: 10.1016/J.PSEP.2012.06.004.

[178] A. Das and S. Ray, “A Review on Diagnostic Techniques of Bearing Fault and its modeling in Induction Motor,” in *2020 IEEE Calcutta Conference (CALCON)*, 2020, pp. 502–505. doi: 10.1109/CALCON49167.2020.9106511.

[179] S. K. Gundewar and P. V Kane, “Condition Monitoring and Fault Diagnosis of Induction Motor,” *Journal of Vibration Engineering & Technologies*, vol. 9, no. 4, pp. 643–674, 2021, doi: 10.1007/s42417-020-00253-y.

[180] S. Kumar *et al.*, “A Comprehensive Review of Condition Based Prognostic Maintenance (CBPM) for Induction Motor,” *IEEE Access*, vol. 7, pp. 90690–90704, 2019, doi: 10.1109/ACCESS.2019.2926527.

[181] M. M. Rahman and M. N. Uddin, “Online unbalanced rotor fault detection of an IM drive based on both time and frequency domain analyses,” in *2015 IEEE Industry Applications Society Annual Meeting*, 2015, pp. 1–8. doi: 10.1109/IAS.2015.7356825.

[182] E. J. McCoy, “Fast F ourier Transform (FFT),” *Encyclopedia of Biostatistics*, vol. 4, 2005.

[183] Q. Chen, G. Liu, and B. Han, “Suppression of Imbalance Vibration in AMB-Rotor Systems Using Adaptive Frequency Estimator,” *IEEE Transactions on Industrial Electronics*, vol. 62, no. 12, pp. 7696–7705, 2015, doi: 10.1109/TIE.2015.2455022.

[184] K. Ren, B. Leng, C. Zhang, Q. Sun, and W. Tang, “The dynamic investigation of intrinsic vibration characteristics of a stranding machine by the finite element method,” *Front Phys*, vol. 11, 2023, [Online]. Available: https://www.frontiersin.org/articles/10.3389/fphy.2023.1159064

[185] B. Belkacemi, S. Saad, Z. Ghemari, F. Zaamouche, and A. Khazzane, “Detection of induction motor improper bearing lubrication by discrete wavelet transforms (DWT) decomposition,” *Instrum. Mes. Metrol*, vol. 19, no. 5, pp. 347–354, 2020.

[186] Rabah Boudiaf, Bouras Abdelkarim, and Issam Harida, “Vibration Analysis to Assess Mechanical Problems in Induction Motors,” in *1st International Symposium on INDUSTRIAL ENGINEERING, MAINTENANCE AND SAFETY*, Oran, Mar. 2022.

[187] MFPT Dataset, “Society for Machinery Failure Prevention Technology,” 2012.